

10-1-2013

Covariance in Multigroup and Few Group Reactor Physics Uncertainty Calculations

Curtis E. McEwan

McMaster University, cemcewan@yahoo.ca

Follow this and additional works at: <http://digitalcommons.mcmaster.ca/opendissertations>



Part of the [Nuclear Engineering Commons](#)

Recommended Citation

McEwan, Curtis E., "Covariance in Multigroup and Few Group Reactor Physics Uncertainty Calculations" (2013). *Open Access Dissertations and Theses*. Paper 8216.

This Thesis is brought to you for free and open access by the Open Dissertations and Theses at DigitalCommons@McMaster. It has been accepted for inclusion in Open Access Dissertations and Theses by an authorized administrator of DigitalCommons@McMaster. For more information, please contact scom@mcmaster.ca.

COVARIANCE IN REACTOR PHYSICS UNCERTAINTY CALCULATIONS

COVARIANCE IN MULTIGROUP AND FEW GROUP REACTOR PHYSICS
UNCERTAINTY CALCULATIONS

By CURTIS EDWARD MCEWAN, B.Eng.

A Thesis Submitted to the School of Graduate Studies in Partial Fulfilment of the
Requirements for the Degree of Master of Applied Science

McMaster University © Copyright by Curtis McEwan, August 2013

McMaster University, Master of Applied Science (2013) Hamilton, Ontario
(Engineering Physics)

TITLE: Covariance in Multigroup and Few Group Reactor Physics
Uncertainty Calculations

AUTHOR: Curtis Edward McEwan, B.Eng. (McMaster University)

SUPERVISOR: Professor D.R. Novog

NUMBER OF PAGES: xiii, 129

Abstract

Simulation plays a key role in nuclear reactor safety analysis and being able to assess the accuracy of results obtained by simulation increases their credibility. This thesis examines the propagation of nuclear data uncertainties through lattice level physics calculations. These input uncertainties are in the form of covariance matrices, which dictate the variance and covariance of specified nuclear data to one another. These covariances are available within certain nuclear data libraries, however they are generally only available at infinite dilution for a fixed temperature. The overall goal of this research is to examine the importance of various applications of covariance and their associated nuclear data libraries, and most importantly to examine the effects of dilution and self-shielding on the results.

One source of nuclear data and covariances are the TENDL libraries which are based on a reference ENDF data library and are in continuous energy. Each TENDL library was created by randomly perturbing the reference nuclear data at its most fundamental level according to its covariance. These perturbed nuclear data libraries in TENDL format were obtained and NJOY was used to produce cross sections in 69 groups for which the covariance was calculated at multiple temperatures and dilutions. Temperature was found to have little effect but covariances evaluated at various dilutions did differ significantly. Comparisons of the covariances calculated from TENDL with those in SCALE and ENDF/B-VII also revealed significant differences. The multigroup covariance library produced at this stage was then used in subsequent analyses, along with multigroup covariance libraries available elsewhere, in order to see the differences that arise from covariance library sources.

Monte Carlo analysis of a PWR pin cell was performed using the newly created covariance library, a specified reference set of nuclear data, and the lattice physics transport solver DRAGON. The Monte Carlo analysis was then repeated by systematically changing the input covariance matrix (for example using an alternative matrix like that included with the TSUNAMI package) or alternate input reference nuclear data. The uncertainty in k -infinite and the homogenized two group cross sections was assessed for each set of covariance data. It was found that the source of covariance data as well as dilution had a significant effect on the predicted uncertainty in the homogenized cell properties, but the dilution did not significantly affect the predicted uncertainty in k -infinite.

Acknowledgements

I would like to start by thanking my supervisor Dr. David Novog for his guidance throughout this work. I have learned a lot from him at both the graduate and undergraduate level and have had the opportunity to do several undergraduate research projects as well as a research term abroad during my graduate studies thanks to him.

I would also like to thank the Laboratoire de Physique Subatomique et de Cosmologie (LPSC) and Dr. Adrien Bidaud for the opportunity to work and study in Grenoble, France. I enjoyed my time there very much and benefitted from the guidance of Pouya Sabouri, who taught me a great deal about the processing of evaluated nuclear data libraries which was an important step in the completion of my thesis. For this I owe him many thanks.

The completion of this work was made possible thanks to funding from the Natural Sciences and Engineering Research Council of Canada (NSERC), the University Network of Excellence in Nuclear Engineering (UNENE), the Rhône-Alpes CMIRA scholarship, and the Eugene G. Bolotkin Scholarship. Financial support from these organizations is greatly appreciated by myself as well as many other graduate students and faculty.

On a personal level, I cannot thank my family and friends enough for their encouragement throughout my education. In particular I want to thank my parents, my sister, and Camille Desoubrie for all their love and support throughout the completion of this degree.

Table of Contents

ABSTRACT.....	III
ACKNOWLEDGEMENTS.....	IV
INTRODUCTION.....	1
1.1 General Uncertainty Propagation.....	1
1.2 Monte Carlo Method.....	2
1.2.1 Covariance and Covariance Decomposition.....	3
1.2.2 Calculation of Output Error.....	4
1.3 Sensitivity Based Methods.....	6
1.3.1 The One-At-A-Time Method.....	6
1.3.2 The Adjoint Method.....	7
1.4 Covariance Matrices.....	13
1.5 Reactor Physics Calculation Chain.....	13
1.6 Project Scope.....	15
TOOLS AND METHODOLOGY.....	16
2.1 Methodology Overview.....	16
2.2 ENDF/B.....	17
2.3 TENDL and TALYS.....	20
2.4 NJOY.....	21
2.4.1 MODER.....	22
2.4.2 RECONR.....	22
2.4.3 BROADR.....	24
2.4.4 PURR.....	26
2.4.5 THERMR.....	27
2.4.6 GROUPR.....	27
2.4.7 WIMSR.....	32
2.4.8 ERRORR.....	32

2.4.9 COVR	32
2.4.10 PLOTR.....	32
2.5 DINOSAUR	33
2.6 COCOAPUFFS	33
2.7 DRAGON.....	37
2.7.1 Progression of Calculations in DRAGON	38
2.7.2 Neutron Transport.....	39
2.8 Existing Tools for Uncertainty Analysis.....	41
2.9 Problem Statement and Methodology.....	43
ANALYSIS OF MULTIGROUP COVARIANCE.....	48
3.1 Covariances from Different Evaluations.....	48
3.2 Temperature Effect	51
3.3 Dilution Effect.....	52
ANALYSIS OF HOMOGENIZED FEW GROUP COVARIANCE.....	56
4.1 Input Covariance Matrix Effect	56
4.2 Dilution Effect.....	61
4.2.1 Effect of Dilution on the Fuel Only	67
CONCLUSIONS.....	69
5.1 Role of Reference Library.....	69
5.2 Role of Temperature	69
5.3 Role of Covariance Source	70
5.4 Role of Dilution	70
5.5 Contributions to Knowledge Statement	71
5.6 Future Work	71
5.7 Publications.....	72
BIBLIOGRAPHY	73
APPENDIX A – U238 COVARIANCE DATA IN 69 GROUPS	77
APPENDIX B – U235 COVARIANCE DATA IN 69 GROUPS	88

APPENDIX C – DILUTION DEPENDANCE OF U238 TENDL COVARIANCE IN 69 GROUPS.....	100
APPENDIX D – DILUTION DEPENDANCE OF U235 TENDL COVARIANCE IN 69 GROUPS.....	104
APPENDIX E – DILUTION DEPENDENCY OF 2 GROUP HOMOGENIZED CROSS SECTION COVARIANCE.....	108
APPENDIX F – EFFECT OF FLUX SOLUTION METHOD ON HOMOGENIZED 2 GROUP CROSS SECTION COVARIANCE.....	111
APPENDIX G – NJOY AND DRAGON INPUT FILES.....	114

List of Figures

Figure 1.1 – Methods of Uncertainty Propagation.....	2
Figure 1.2 – Monte Carlo Method of Uncertainty Propagation.....	3
Figure 1.3 – Reactor Physics Calculation Chain	15
Figure 2.1 – U235 Fission Cross Section Showing the Various Cross Section Regions	22
Figure 2.2 – ^{240}Pu (n, γ) Cross Section at 0K (solid line), 30 000K (dotted line) and 300 000K (dashed-dotted line) [18].....	26
Figure 2.3 – Self-Shielding of the Flux in the Presence of a Resonance Peak [14]	28
Figure 2.4 – Continuous Energy Cross Section and Corresponding Multigroup Cross Section (in 4 Groups) at Infinite Dilution	31
Figure 2.5 – Continuous Energy Cross Section and Corresponding Multigroup Cross Section (in 4 Groups) at a Dilution of 10 Barns	31
Figure 2.6 – Production of Multigroup Covariance Libraries at Multiple Value of Dilution Using NJOY and COCOAPUFFS	34
Figure 2.7 – U235 Inelastic Scattering Covariance as Calculated by COCOAPUFFS.....	35
Figure 2.8 – U235 Inelastic Scattering Covariance as Calculated by OpenOffice Calc	35
Figure 2.9 – U235 Cross-Covariance Between Fission and Elastic Scattering as Calculated by COCOAPUFFS.....	36
Figure 2.10 - U235 Cross-Covariance Between Fission and Elastic Scattering as Calculated by OpenOffice Calc	36
Figure 2.11 – 2 Group Homogenized Cross Section Covariance as Calculated by COCOAPUFFS.....	37
Figure 2.12 – 2 Group Homogenized Cross Section Covariance as Calculated by OpenOffice Calc	37
Figure 2.13 – Module Progression in a Typical DRAGON Lattice Cell Calculation	38
Figure 2.14 – Implementations of Monte Carlo Uncertainty Propagation Using DINOSAUR Alone (left) and the Modified Methodology Developed in This Work (right)	44
Figure 2.15 – Creation of a SCALE/TENDL Hybrid Covariance Library	45
Figure 2.16 – Creation of a SCALE-TENDL Finite Dilution Covariance Library from the SCALE-TENDL Infinite Dilution Covariance Library.....	46
Figure 2.17 – Depiction of the U238 Covariance Matrix in the SCALE-TENDL Hybrid Covariance Library at Infinite Dilution	46

Figure 2.18 – Depiction of the U238 Covariance Matrix in the SCALE-TENDL Hybrid Covariance Library at The Problem Dilution	47
Figure 3.1 – Calculated TENDL Covariance in 69 Groups for U238 Reaction MT 18 (fission)	49
Figure 3.2 – 44 Group SCALE Covariance Interpolated to 69 Groups Using ANGELO2 for U238 Reaction MT 18 (fission) [3]	49
Figure 3.3 – Calculated ENDF Covariance Using ERRORR in NJOY in 69 Groups for U238 Reaction MT 18 (Fission).....	50
Figure 3.4 - Absolute Change in Relative Covariance for U235 Between 293K and 1100K for MT 18 (above) and MT 102 (below).....	52
Figure 3.5 - Absolute Change in Relative Covariance for U238 MT 2 Between Infinite Dilution and 52 Barns (52b - ∞).....	54
Figure 3.6 – Absolute Change in Relative Covariance for U235 MT 2 Between Infinite Dilution and 800 Barns (800b - ∞).....	54
Figure 4.1 – Homogenous 2 Group Covariance from Perturbation of the 69 Group ENDF/B-VI Library Using Covariances from SCALE (left) and TENDL (right).....	58
Figure 4.2 - Homogenous 2 Group Covariance from Perturbation of the 69 Group ENDF/B-VII Library Using Covariance from SCALE (left) and TENDL (right).....	58
Figure 4.3 - Homogenous 2 Group Covariance from Perturbation of the 69 Group IAEA Library Using Covariance from SCALE (left) and TENDL (right).....	59
Figure 4.4 - Homogenous 2 Group Covariance from Perturbation of the 69 Group JEFF2.2 Library Using Covariances from SCALE (left) and TENDL (right)	59
Figure 4.5 Standard Deviation of K-Inf Resulting from Perturbations of Various Libraries Using SCALE and TENDL Covariances	61
Figure 4.6 - Homogenous 2 Group Covariance from Perturbation of the 69 Group ENDF/B-VI Library Using Infinite (left) and Finite (right) Dilution Covariance	63
Figure 4.7 - Homogenous 2 Group Covariance from Perturbation of the 69 Group ENDF/B-VII Library Using Infinite (left) and Finite (right) Dilution Covariance	63
Figure 4.8 - Homogenous 2 Group Covariance from Perturbation of the 69 Group IAEA Library Using Infinite (left) and Finite (right) Dilution Covariance.....	64
Figure 4.9 - Homogenous 2 Group Covariance from Perturbation of the 69 Group JEFF 2.2 Library Using Infinite (left) and Finite (right) Dilution Covariance	64
Figure 4.10 – Standard Deviation of K-Inf Resulting from Perturbations of Various Libraries Using Infinite and Finite Dilution Covariances	66
Figure 4.11 – 2 Group Homogenized Cross Section Covariance for Fuel Only Resulting from Perturbations with Infinite Dilution Covariances	68
Figure 4.12 - 2 Group Homogenized Cross Section Covariance for Fuel Only Resulting from Perturbations with Finite Dilution Covariances.....	68

Figure A.1 – 69 Group Covariance for Reaction MT 2 in TENDL.....	77
Figure A.2 – 69 Group Covariance for Reaction MT 2 in SCALE	78
Figure A.3 – 69 Group Covariance for Reaction MT 2 in ENDF/B-VII.....	78
Figure A.4 – 69 Group Covariance for Reaction MT 4 in TENDL.....	79
Figure A.5 – 69 Group Covariance for Reaction MT 4 in ENDF/B-VII.....	79
Figure A.6 – 69 Group Covariance for Reaction MT 16 in TENDL.....	80
Figure A.7 – 69 Covariance for Reaction MT 16 in SCALE	80
Figure A.8 – 69 Group Covariance for Reaction MT 16 in ENDF/B-VII.....	81
Figure A.9 – 69 Group Covariance for Reaction MT 18 in TENDL.....	82
Figure A.10 – 69 Group Covariance for Reaction MT 18 in SCALE	82
Figure A.11 – 69 Group Covariance for Reaction MT 18 in ENDF/B-VII*	83
Figure A.12 – 69 Group Covariance for Reaction MT 102 in TENDL.....	84
Figure A.13 – 69 Group Covariance for Reaction MT 102 in SCALE	84
Figure A.14 – 69 Group Covariance for Reaction MT 102 in ENDF/B-VII.....	85
Figure A.15 - 69 Group Covariance for Reaction MT 452 in TENDL	86
Figure A.16 – 69 Group Covariance for Reaction MT 452 in SCALE	86
Figure A.17 – 69 Group Covariance for Fission Spectrum in TENDL	87
Figure A.18 – 69 Group Covariance for Fission Spectrum in SCALE	87
Figure B.1 – 69 Group Covariance for Reaction MT 2 in TENDL.....	88
Figure B.2 – 69 Group Covariance for Reaction MT 2 in SCALE	89
Figure B.3 – 69 Group Covariance for Reaction MT 2 in ENDF/B-VII.....	89
Figure B.4 – 69 Group Covariance for Reaction MT 4 in TENDL.....	90
Figure B.5 – 69 Group Covariance for Reaction MT 4 in ENDF/B-VII.....	90
Figure B.6 – 69 Group Covariance for Reaction MT 16 in TENDL.....	91
Figure B.7 – 69 Group Covariance for Reaction MT 16 in SCALE	91
Figure B.8 – 69 Group Covariance for Reaction MT 16 in ENDF/B-VII.....	92
Figure B.9 – 69 Group Covariance for Reaction MT 18 in TENDL.....	93
Figure B.10 – 69 Group Covariance for Reaction MT 18 in SCALE	94
Figure B.11 – 69 Group Covariance for Reaction MT 18 in ENDF/B-VII.....	94
Figure B.12 – 69 Group Covariance for Reaction MT 102 in TENDL.....	95
Figure B.13 – 69 Group Covariance for Reaction MT 102 in SCALE	95
Figure B.14 – 69 Group Covariance for Reaction MT 102 in ENDF/B-VII.....	96
Figure B.15 – 69 Group Covariance for Reaction MT 107 in TENDL.....	97
Figure B.16 – 69 Group Covariance for Reaction MT 452 in TENDL.....	98
Figure B.17 – 69 Group Covariance for Reaction MT 452 in TENDL.....	98
Figure B.18 – 69 Group Covariance for Fission Spectrum in TENDL	99
Figure B.19 – 69 Group Covariance for Fission Spectrum in SCALE.....	99
Figure C.1 – 69 Group TENDL Covariance for Reaction MT 2 at Infinite Dilution	100
Figure C.2 – 69 Group TENDL Covariance for Reaction MT 2 at a Dilution of 52 Barns	101

Figure C.3 – 69 Group TENDL Covariance for Reaction MT 18 at Infinite Dilution	102
Figure C.4 – 69 Group TENDL Covariance for Reaction MT 18 at a Dilution of 52 Barns	102
Figure C.5 – 69 Group TENDL Covariance for Reaction MT 102 at Infinite Dilution	103
Figure C.6 – 69 Group TENDL Covariance for Reaction MT 102 at a Dilution of 52 Barns	103
Figure D.1 – 69 Group TENDL Covariance for Reaction MT 2 at Infinite Dilution	104
Figure D.2 – 69 Group TENDL Covariance for Reaction MT 2 at a Dilution of 800 Barns	105
Figure D.3 – 69 Group TENDL Covariance for Reaction MT 18 at a Dilution of 800 Barns	106
Figure D.4 – 69 Group TENDL Covariance for Reaction MT 18 at a Dilution of 800 Barns	106
Figure D.5 – 69 Group TENDL Covariance for Reaction MT 102 at Infinite Dilution	107
Figure D.6 – 69 Group TENDL Covariance for Reaction MT 102 at a Dilution of 800 Barns	107
Figure E.1 - Homogenous 2 Group Covariance from Perturbation of the ENDF/B-VI Library Using Infinite (left) and Finite (right) Dilution Covariance with Positive Covariances in Grey and Negative Covariances in Red	109
Figure E.2 - Homogenous 2 Group Covariance from Perturbation of the ENDF/B-VII Library Using Infinite (left) and Finite (right) Dilution Covariance with Positive Covariances in Grey and Negative Covariances in Red	109
Figure E.3 - Homogenous 2 Group Covariance from Perturbation of the IAEA Library Using Infinite (left) and Finite (right) Dilution Covariance with Positive Covariances in Grey and Negative Covariances in Red	110
Figure E.4 - Homogenous 2 Group Covariance from Perturbation of the JEF22 Library Using Infinite (left) and Finite (right) Dilution Covariance with Positive Covariances in Grey and Negative Covariances in Red	110
Figure F.1 – 2 Group Homogenized Cross Section Covariance Obtained by Perturbing the ENDF/B-VI Multigroup Library Using a Fixed K-Effective (left) and Fixed Buckling (right) Flux Solution	112
Figure F.2 - 2 Group Homogenized Cross Section Covariance Obtained by Perturbing the ENDF/B-VII Multigroup Library Using a Fixed K-Effective (left) and Fixed Buckling (right) Flux Solution	112
Figure F.3 - 2 Group Homogenized Cross Section Covariance Obtained by Perturbing the IAEA Multigroup Library Using a Fixed K-Effective (left) and Fixed Buckling (right) Flux Solution.....	113

Figure F.4 - 2 Group Homogenized Cross Section Covariance Obtained by Perturbing the JEFF 2.2 Multigroup Library Using a Fixed K-Effective (left) and Fixed Buckling (right) Flux Solution.....	113
Figure G.1 – TMI1 PWR Pin Cell Specifications [15]	123

List of Tables

Table 2.1 – ENDF/B Sublibraries	19
Table 2.2 – File Types in ENDF/B	19
Table 2.3 – Common Reactions in ENDF/B	20
Table 2.4 –Employed Modules of NJOY and their Function	21
Table 2.5 – Interpolation Schemes Used in ENDF/B and NJOY	23
Table 2.6 – Commonly Used Modules for Lattice Physics Calculations in DRAGON	39
Table 2.7 – Contributions by Term to the Neutron Transport Equation.....	40
Table 2.8 – Tools Currently Available for Lattice Physics Uncertainty Analysis	42
Table 3.1 – Maximum Relative Change in Covariance Between 293K and 1100K	51
Table 3.2 - Maximum Relative Change With Dilution.....	55
Table 4.1 – Calculated Problem Dilutions and Chosen Covariance Dilution.....	62

Chapter 1

Introduction

A measurement is an attempt to evaluate a parameter by quantifying it according to a known scale. The use of a common scale allows for multiple parameters to be easily compared. However, a measurement is often of limited use if nothing is known about its uncertainty. Any measured value will have some uncertainty that can be due to the instrument used to measure it and how it was measured among other things. Moreover, any value that is calculated using a measured value will acquire its own uncertainty due to the uncertain nature of the measured parameter or parameters used in the calculation. If such calculations involve modelling, assumptions, simplifications and numerical methods, then the calculations may contain further uncertainty.

Knowledge of the uncertainty in calculated and measured parameters is of paramount importance to nuclear reactor safety analysis. To ensure compliance with regulations, one must be able to demonstrate with a certain confidence that a parameter and its range of uncertainty lie within safety margins. In nuclear reactor physics simulations, the calculation of important safety parameters such as power and reactivity may involve the use of thousands of measured values (such as nuclear interaction cross sections and data) each with their own uncertainties. The question then becomes, given the uncertainty in a set of input parameters, how can the uncertainty in a set of output parameters be evaluated? In other words, how do all the uncertainties in the input parameters interact and combine as they are used to perform calculations and what is the effect on the output?

1.1 General Uncertainty Propagation

If we have a function $g = f(x_1, x_2, x_3, \dots, x_n)$, the uncertainty in the function g can be expressed as [1]:

$$\delta g = \left(\frac{\partial g}{\partial x_1} \right) (\delta x_1) + \left(\frac{\partial g}{\partial x_2} \right) (\delta x_2) + \dots + \left(\frac{\partial g}{\partial x_n} \right) (\delta x_n) \quad (1.1)$$

Where $\delta x_1, \delta x_2, \dots, \delta x_n$ are the absolute uncertainties in the parameters x_1, x_2, \dots, x_n respectively. This is simple enough when the partial derivatives of

the function are known but for many practical applications, the partial derivatives between each input and output are often time-consuming and difficult to evaluate analytically. To overcome this problem, there are three main methods of uncertainty propagation that can be used to find the uncertainty in a set of output parameters due to uncertainty in the set of input parameters. These methods can be generally categorized into two approaches: Monte Carlo based and sensitivity based.

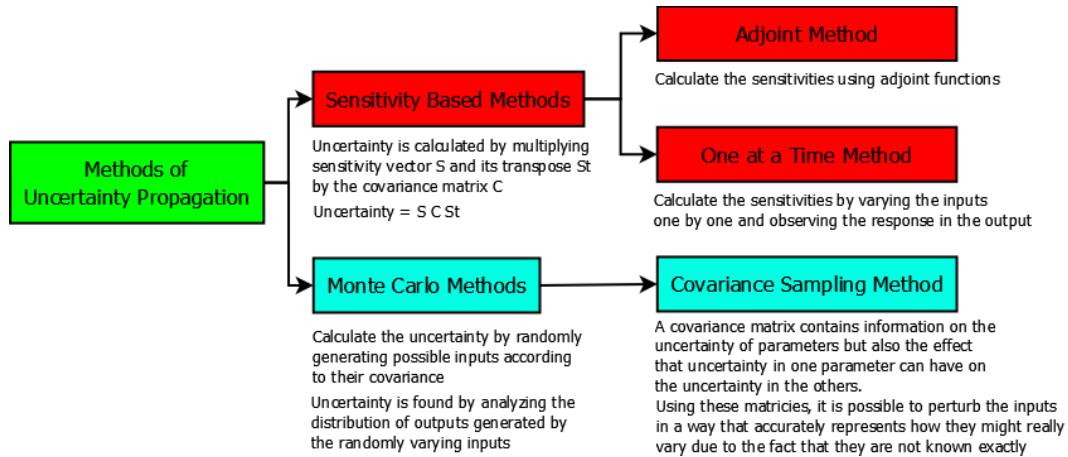


Figure 1.1 – Methods of Uncertainty Propagation

1.2 Monte Carlo Method

The Monte Carlo method determines the uncertainty in the output by randomly sampling a value for each input parameter according to a user defined distribution and the covariance matrix for the input parameters. This process is repeated a large number of times in order to obtain a distribution of results for each output parameter, which in turn can be used to quantify their uncertainty. Because the choice of each input distribution is subjective, the calculated uncertainty has the potential to depend heavily on the chosen distribution [2]. This effect was investigated during the development of the Monte Carlo propagation module of the code DINOSAUR at McMaster University, it was found that no statistically significant differences occurred in the calculated uncertainty when parameters were sampled according to a normal distribution versus a uniform distribution [3]. The covariance matrix used can also have a significant effect on the results as was shown in a comparison of the k -effective, reaction rates, and isotope number densities over burnup obtained using the SCALE6.1/COVA and ENDF/B-VII.1 covariance matrices [4]. The Monte Carlo process is briefly summarized in Figure 1.2 below.

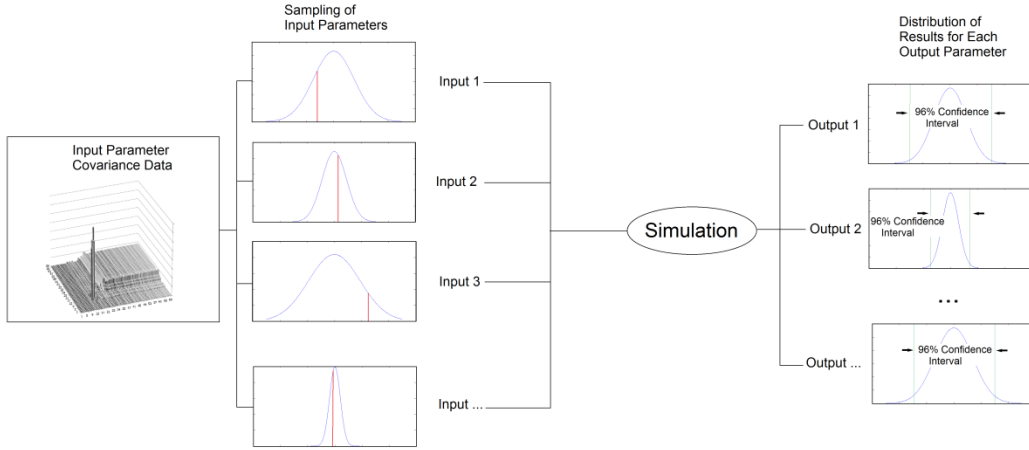


Figure 1.2 – Monte Carlo Method of Uncertainty Propagation

1.2.1 Covariance and Covariance Decomposition

Covariance is a measure of how likely two parameters are to deviate from their reference condition in a consistent direction. Mathematically the absolute covariance between two parameters x and y can be expressed as:

$$COV(x, y) = \frac{1}{N-1} \sum_{i=1}^N (x_i - \bar{x})(y_i - \bar{y}) \quad (1.2)$$

Covariance matrices Σ are normally stored as relative covariances Σ_r which are calculated as follows:

$$\Sigma_r(x, y) = \frac{\Sigma(x, y)}{(\bar{x} \cdot \bar{y})} \quad (1.3)$$

Where \bar{x} and \bar{y} are the average values of x and y respectively and $\Sigma(x, y)$ is the absolute covariance between x and y . A set of random dependent variables can be generated using a vector of random independent numbers with average 0 and mean 1 using the formula:

$$G(\mu, \Sigma) = \Sigma^{\frac{1}{2}} G(0, 1) + \mu \quad (1.4)$$

Where $G(\mu, \Sigma)$ is a vector of random dependent variables with covariance Σ , $G(0, 1)$ is a vector of random independent variables, and μ is a vector of average values. The square root of the covariance matrix can be calculated by decomposing the matrix into a product of eigenvalues and eigenvectors and taking the square root of the diagonal matrix (which is simply a matter of taking the square root of each of the diagonal entries).

$$\Sigma = V D V^T \quad (1.5)$$

$$\Sigma^{\frac{1}{2}} = V D^{\frac{1}{2}} V^T \quad (1.6)$$

Where V is an eigenvector and D is a diagonal matrix of corresponding eigenvalues.

Note that the covariance matrix Σ is a set of absolute covariances. As mentioned above, covariances are normally given as relative covariances so to use Equation (1.4) we would have to first multiply each entry in the relative covariance matrix by the averages of the two parameters between which the covariance was calculated for that particular entry [see equation (1.3)]. The set of dependent variables generated would thus depend on the average values used and the decomposition process would need to be repeated if the perturbations were to be performed for a different set of average values. In other words, the process would need to be repeated each time a new library is to be perturbed because it will contain values that differ from the previous library. To get around this problem, we can instead generate a vector of perturbation factors which are essentially just a vector of dependent variables with covariance $\Sigma = \Sigma_r$ where all of the average values are equal to 1.

$$P(1, \Sigma) = \Sigma_r^{\frac{1}{2}} G(0,1) + [1.0, 1.0, 1.0, \dots, 1.0]^T \quad (1.7)$$

The set of perturbation factors can then be stored and multiplied by a vector of average values as needed in order to create a vector of random dependent variables centered on those average values.

$$G(\mu, \Sigma) = P(1, \Sigma)^T \mu \quad (1.8)$$

This process avoids the time consuming procedure of decomposing the covariance matrix each time it needs to be applied to a new set of average values and is implemented in the Monte Carlo uncertainty propagation code DINOSAUR [3] (see section 2.5 for details on the DINOSAUR code).

1.2.2 Calculation of Output Error

Once a set of perturbed input parameters has been generated, they are used in place of the original values and a simulation is run. This process can be repeated as many times as desired to achieve a distribution of output results, for which the resultant accuracy improves with each successive new set of random independent variables. The accuracy in the calculated uncertainty from n simulations can be found using the standard deviation estimator approach [4].

$$\frac{\sigma_{KnS}}{\sigma} = \frac{K_n \sqrt{V_n}}{\sqrt{n-1}} \quad (1.9)$$

$$= \sqrt{\frac{n-1}{2}} \cdot e^{[\ln \Gamma(\frac{n-1}{2})] - [\ln \Gamma(\frac{n}{2})]} \sqrt{2 \left[\frac{n-1}{2} - \frac{\Gamma^2(\frac{n}{2})}{\Gamma^2(\frac{n-1}{2})} \right]} \quad (1.10)$$

Where σ_{KnS}/σ is the relative uncertainty in the standard deviation. Note that when $n > 10$, Equation (1.9) can be simplified to Equation (1.11) below since the product $K_n \sqrt{V_n}$ will converge to $\frac{1}{\sqrt{2}}$.

$$\frac{\sigma_{KnS}}{\sigma} = \frac{1}{\sqrt{2(n-1)}} \quad (1.11)$$

Thus running 1000 simulations would yield an output whose standard deviation was accurate to about 2.2%¹.

An alternative approach to determine the accuracy of the predicted uncertainty is to view the set of outputs resulting from perturbation of the inputs as a population with an unknown but continuous distribution. In this case, the problem can be solved using order statistics [5]. Order statistics involves the ordering of a set of values from smallest to largest. The limiting maximum and minimum value in the set can then be predicted with a certain confidence. When applied to uncertainty analysis, this permits an uncertainty range to be established from the set of outputs (regardless of the distribution, assuming it is continuous) resulting from perturbation of the inputs. One method of implementing order statistics to assess the accuracy of the predicted uncertainty is the use of Wilks' Formula [6] to predict the number of simulations required to ensure that P , the proportion of a single variable of interest that lies between two boundaries with average a , is between L_1 and L_2 with a confidence η .

$$\eta = \int_{L_1}^{L_2} g(P) dP \quad (1.12)$$

$$= \int_{L_1}^{L_2} \frac{\Gamma(n+1)}{\Gamma[a(n+1)] \cdot \Gamma[(1-a)(n+1)]} P^{a(n+1)-1} (1-P)^{(1-a)(n+1)-1} dP \quad (1.13)$$

¹ 2.2% is the standard deviation of the calculated error so this figure would have a 68.27% confidence.

To find the minimum number of samples required to establish a confidence interval that contains a fraction κ of all the output data points with a confidence η , Wilks' formula can be simplified and rearranged into an equation for n (the minimum number of samples required).

$$n = \frac{\ln(1 - \eta)}{\ln(\kappa)} \quad (1.14)$$

1.3 Sensitivity Based Methods

The sensitivity based methods include the One-At-a-Time (OAT) method, and the adjoint method. The goal of both of these methods is to determine the sensitivities between input and output parameters. The uncertainty can then be calculated using the sandwich rule [7].

$$\Delta^2 x = S \Sigma S^T \quad (1.15)$$

Where S is a vector of partial derivatives between each input parameter and the output parameter x , and Σ is the (absolute) covariance matrix.

The sensitivity based methods have the advantage of being able to show the individual contributions of each input parameter to the final output uncertainty. This is very valuable since it permits an understanding of which variables are the most sensitive (or insensitive) and can in turn be used to reduce the output uncertainty because it identifies the most important contributors.

1.3.1 The One-At-A-Time Method

The OAT method is the most simple but also the most computationally expensive option. A simulation is first performed with all the parameters at their expectation values. One of the parameters is perturbed slightly and the simulation is performed again to observe the change in the output. The parameter is then returned to its initial value, another parameter is perturbed slightly, and the simulation is run again to observe the change in output with respect to the initial (unperturbed) simulation. The process is repeated until each parameter of interest has been perturbed and the change in the output as a result of each perturbation has been noted. The partial derivative between the output and each input can then simply be approximated as:

$$\frac{\partial f(p)}{\partial p} \approx \frac{f(p + \delta p) - f(p)}{\delta p} \quad (1.16)$$

This approximation becomes better and better as δp approaches zero but smaller and smaller changes in the input parameter p also elicit a smaller and smaller response in $f(p)$ so there is a tradeoff. One must choose a perturbation size that is as small as possible but still gives a large enough response in the output to avoid truncation errors when calculating the partial derivative. Note that this partial derivative is only valid in the vicinity of the reference value used to calculate it and will not, in general, be the same for a reference value that differs significantly from the original.

The dimensionless sensitivity is often used in place of the partial derivatives to show the relationship between input and output parameters and is defined as follows:

$$S_{f,p} = \frac{p}{f(p)} \frac{\partial f(p)}{\partial p} \quad (1.17)$$

1.3.2 The Adjoint Method

It is clear that the OAT method becomes more and more computationally expensive as the number of input parameters increases since a new simulation must be performed to observe the effect of each input parameter. There are also limits to how small a perturbation can be used to obtain the local sensitivity while avoiding truncation errors. This problem can be avoided by the use of the Adjoint Sensitivity Analysis Procedure (ASAP) proposed by Cacuci [8]. A detailed derivation of this method is beyond the scope of this work but a demonstration of how this method can be applied to perform uncertainty analysis on a simple problem is given as an example to the reader [8]. An explanation of how the adjoint method is applied in Classical Perturbation Theory (CPT) and Generalized Perturbation Theory (GPT) follows the example.

Suppose we are faced with the system of equations represented in matrix form below.

$$Ax = b \quad (1.18)$$

$$\begin{pmatrix} A_{11} & \cdots & A_{1n} \\ \vdots & \ddots & \vdots \\ A_{n1} & \cdots & A_{nn} \end{pmatrix} \begin{bmatrix} x_1 \\ \vdots \\ x_n \end{bmatrix} = \begin{bmatrix} b_1 \\ \vdots \\ b_n \end{bmatrix} \quad (1.19)$$

We will also suppose that the values in matrix A and vector b have been determined experimentally and so they have some uncertainty. The solution we

calculate is thus the solution to what is called the “base-case system” and is represented as follows:

$$A^0 x^0 = b^0 \quad (1.20)$$

Now we will imagine that we are measuring x using a detector which produces a response R that is directly proportional to x .

$$R = cx \quad (1.21)$$

However recall that we can only measure the nominal solution x^0 since we do not know the exact values of A and b . Thus equation (1.21) becomes:

$$R^0 = c^0 x^0 \quad (1.22)$$

The uncertainties in the parameters A , b , and c , are represented by δA , δb , and δc respectively so our system of equations and responses becomes:

$$(A^0 + \delta A)(x^0 + \delta x) = (b^0 + \delta b) \quad (1.23)$$

$$(R^0 + \delta R) = (c^0 + \delta c)(x^0 + \delta x) \quad (1.24)$$

We are looking for the local sensitivities about R^0 between R and each of the input parameters A , b , and c at their nominal values of A^0 , b^0 , and c^0 respectively. It is worthwhile at this point to emphasize the use of the word “local sensitivities” instead of just “sensitivities” since the sensitivities calculated using this method are only valid locally about the values A^0 , b^0 , and c^0 and will not, in general, be the same when calculated about a different set of nominal values.

Recall that we are looking for the sensitivities between input and output parameters which are calculated using equation (1.17) and can be approximated with the help of equation (1.16). We start by solving for the response function:

$$(A^0 + \delta A)(x^0 + \delta x) = (b^0 + \delta b)$$

$$(x^0 + \delta x) = (A^0 + \delta A)^{-1}(b^0 + \delta b) \quad (1.25)$$

$$(R^0 + \delta R) = (c^0 + \delta c)(x^0 + \delta x)$$

$$(R^0 + \delta R) = (c^0 + \delta c)(A^0 + \delta A)^{-1}(b^0 + \delta b)$$

$$\delta R = (c^0 + \delta c)(A^0 + \delta A)^{-1}(b^0 + \delta b) - R^0 \quad (1.26)$$

Now we can invoke equation (1.16) for each input parameter, we will start with A . Note that the calculation is performed for each entry in A individually and is thus represented as A_{ij} for the i^{th} row and j^{th} column of A . The term $R_{A_{ij}}^0$ is adopted to reinforce that we are only considering the effect of uncertainty in A on R .

$$\begin{aligned}\frac{\partial R}{\partial A_{ij}} &\approx \frac{R(A_{ij}^0 + \delta A_{ij}) - R(A_{ij}^0)}{(A_{ij}^0 + \delta A_{ij}) - A_{ij}^0} \\ &= \frac{(R_{A_{ij}}^0 + \delta R_{A_{ij}}^0) - R_{A_{ij}}^0}{\delta A_{ij}} = \frac{\delta R_{A_{ij}}^0}{\delta A_{ij}}\end{aligned}\quad (1.27)$$

We can further simplify the equation above using the result we found in equation (1.26) and setting the uncertainty in all the other parameters to zero since we are currently only concerned with the effect of A on R .

$$\frac{\partial R}{\partial A_{ij}} \approx \frac{\delta R_{A_{ij}}^0}{\delta A_{ij}} = \frac{[(c^0)(A^0 + \delta A)^{-1}(b^0) - R^0]}{\delta A_{ij}} \quad (1.28)$$

Similarly we can show for the parameters b and c :

$$\frac{\partial R}{\partial b_i} \approx \frac{\delta R_{b_i}^0}{\delta b_i} = \frac{[(c^0)(A^0)^{-1}(b^0 + \delta b) - R^0]}{\delta b_i} \quad (1.29)$$

$$\frac{\partial R}{\partial c_i} \approx \frac{\delta R_{c_i}^0}{\delta c_i} = \frac{[(c^0 + \delta c)(A^0)^{-1}(b^0) - R^0]}{\delta c_i} \quad (1.30)$$

We now have a set of explicit relations for each of the sensitivities but there remains a rather serious problem: Inverting the matrices A^0 and $(A^0 + \delta A)$. Since systems of equations in computer codes are typically solved by iteration, we usually do not have the matrix $(A^0)^{-1}$ immediately available and certainly not the matrix $(A^0 + \delta A)^{-1}$, which would need to be recalculated anytime δA is changed. Matrix inversion is a computationally expensive operation and becomes even more time consuming as the size of the matrix increases. Clearly it would be of great benefit to find some way of avoiding matrix inversion for each new perturbation δA , and this can be done using the Adjoint Sensitivity Analysis Procedure (ASAP).

In order to proceed, we will need to define a useful generalization of the derivative known as the Gâteaux derivative [8]. The Gâteaux derivative can be defined as follows [9]:

Let f be a function on an open subset U of a Banach space X into the Banach space Y . The function f is Gâteaux differentiable at $x \in U$ if there is a bounded and linear operator $T : X \rightarrow Y$ such that

$$\lim_{t \rightarrow 0} \frac{f(x + th) - f(x)}{t} = T_x(h) \quad (1.31)$$

for every $h \in X$. The operator T is called the Gâteaux derivative of f at x .

Applying this definition to equation (1.23) and solving for δx yields:

$$\left\{ \frac{d}{d\varepsilon} [(A^0 + \varepsilon \delta A)(x^0 + \varepsilon \delta x) - (b^0 + \varepsilon \delta b)] \right\}_{\varepsilon=0} = 0 \quad (1.32)$$

$$\{A^0(\delta x) + (\delta A)x^0 + 2\varepsilon(\delta A)(\delta x) - \delta b\}_{\varepsilon=0} = 0$$

$$A^0(\delta x) + (\delta A)x^0 = \delta b \quad (1.33)$$

$$\delta x = (A^0)^{-1}[\delta b - (\delta A)x^0] \quad (1.34)$$

Applying the definition of the Gâteaux differential to equation (1.24) gives:

$$\left\{ \frac{d}{d\varepsilon} [(R^0 + \varepsilon \delta R) - (c^0 + \varepsilon \delta c)(x^0 + \varepsilon \delta x)] \right\}_{\varepsilon=0} = 0 \quad (1.35)$$

$$\{\delta R - c^0(\delta x) - (\delta c)x^0 - 2\varepsilon(\delta c)(\delta x)\}_{\varepsilon=0} = 0$$

$$\delta R = c^0(\delta x) + (\delta c)x^0 \quad (1.36)$$

Substituting the previously found value for δx :

$$\delta R = c^0(A^0)^{-1}[\delta b - (\delta A)x^0] + (\delta c)x^0 \quad (1.37)$$

We have managed to get rid of the $(A + \delta A)^{-1}$ term from equation (1.26) which significantly reduces the computational effort required to solve for δR when A is large. Obtaining the sensitivities using equation (1.37) is known as the Forward Sensitivity Analysis Procedure (FSAP) [8]. Although the FSAP is more efficient than equation (1.26), there is still room for improvement. As A becomes large, the product $(A^0)^{-1}[\delta b - (\delta A)x^0]$ will typically take longer to compute and will need to be recalculated anytime the uncertainty in any entry in b or A changes. To address this problem, we will start with equation (1.33) and re-arrange it into a more convenient form:

$$A^0(\delta x) = \delta b - (\delta A)x^0 \quad (1.38)$$

We will then introduce a new vector φ of the same dimensions as x and take the inner product of φ with both sides.

$$\langle \varphi, A^0(\delta x) \rangle = \langle \varphi, \delta b - (\delta A)x^0 \rangle \quad (1.39)$$

The next stage takes advantage of a useful property of hermitian adjoints²:

$$\langle Ax, y \rangle = \langle x, A^\dagger y \rangle \quad (1.40)$$

Where A^\dagger is the hermitian adjoint of A . If all of the entries in A are real numbers, then the hermitian adjoint A^\dagger is simply the transpose A^+ of the matrix A . Applying this knowledge to equation (1.39) gives:

$$\langle \varphi, A^0(\delta x) \rangle = \langle (A^0)^+ \varphi, \delta x \rangle = \langle \delta x, (A^0)^+ \varphi \rangle \quad (1.41)$$

Note that we can reverse the order of the inner product if both entries are real. Up to this point, the vector φ has been left undefined. We are now ready to choose a definition that will become beneficial later on.

$$(A^0)^+ \varphi = c^0 \quad (1.42)$$

Using this definition along with equations (1.39) and (1.41) gives:

$$\langle \varphi, \delta b - (\delta A)x^0 \rangle = \langle \delta x, (A^0)^+ \varphi \rangle = \langle \delta x, c^0 \rangle = c^0(\delta x) \quad (1.43)$$

Lastly, we invoke equation (1.36) to get the final result:

$$\delta R = c^0(\delta x) + (\delta c)x^0 = \langle \varphi, \delta b - (\delta A)x^0 \rangle + (\delta c)x^0 \quad (1.44)$$

Note that the result is similar to that found in equation (1.37). The second term $(\delta c)x^0$ is identical but the first term has been replaced with the inner product between the adjoint function $\varphi = ((A^0)^+)^{-1} c^0$ and the term $\delta b - (\delta A)x^0$. A side by side comparison of the FSAP result (equation (1.45)) and the ASAP result (equation (1.46)) is shown below.

$$\delta R = c^0(A^0)^{-1}[\delta b - (\delta A)x^0] + (\delta c)x^0 \quad (1.45)$$

$$= \langle (A^0)^+{}^{-1} c^0, \delta b - (\delta A)x^0 \rangle + (\delta c)x^0 \quad (1.46)$$

When comparing these two terms, at first glance it does not appear that we have saved much work. Essentially we have just changed the order of multiplication so

² The hermitian adjoint is also sometimes referred to as the “hermitian conjugate” or simply the “adjoint.”

that instead of c^0 being multiplied by $(A^0)^{-1}$ and then by $\delta b - (\delta A)x^0$, we are multiplying³ $((A^0)^+)^{-1}$ by c^0 and then taking the inner product with $\delta b - (\delta A)x^0$. Both yield the same results and when the matrix A is populated with numbers only, there is no advantage to using the ASAP. However consider what would happen when A is populated with operators as would be the case when A contains a set of differential equations. In this case, we cannot solve equation (1.45) by simply inverting A^0 . We must re-arrange equation (1.33) as shown below in equation (1.47) and iteratively solve for δx term by term. Moreover, this set of equations must be solved again every time the uncertainty in δb or δA changes. As A becomes larger and larger this becomes very impractical.

$$A^0(\delta x) = \delta b - (\delta A)x^0 \quad (1.47)$$

In the ASAP, $((A^0)^+)^{-1}$ is multiplied by c^0 instead of $\delta b - (\delta A)x^0$. In the case where A is populated with operators, we cannot simply invert $(A^0)^+$ and so we are forced to iteratively solve the adjoint equation:

$$(A^0)^+ \varphi = c^0 \quad (1.48)$$

Note that this equation has no dependence on δb or δA and thus does not need to be solved again if these parameters change. The adjoint equation also does not depend on the nominal solution x^0 .

When the adjoint method is used to find the sensitivity of input parameters with respect to the multiplication constant⁴ k , it is called Classical Perturbation Theory (CPT). The sensitivity of other reactor physics parameters is calculated via a response function R such as the one in Equation (1.21) and is referred to as Generalized Perturbation Theory (GPT) [10].

In conclusion, adjoint sensitivity method (ASAP) is a much more efficient alternative to the FSAP and OAT methods since it requires only a fraction of the amount of computation when the system contains many parameters. The drawback is that it is more difficult to implement than the OAT method since it requires the calculation of adjoints for the relevant equations used in the code through which the uncertainty is to be propagated. If these functions are to be retrofitted into already existing codes, the task becomes more difficult since an understanding of the source code is required in addition to the adjoint functions.

³ The term $((A^0)^+)^{-1}$ is actually multiplied by the transpose of what we previously defined as c^0 (a column vector) to permit proper matrix multiplication.

⁴ For a description of the multiplication constant, please see section 2.7.2 which describes neutron transport theory.

1.4 Covariance Matrices

Although they differ in their approaches to calculating the output uncertainty, the sensitivity and Monte Carlo methods do have one important feature in common: *The resulting calculated uncertainties both depend directly on the choice of the input parameter covariance matrix.* The random numbers generated in the Monte Carlo method are generated according to the given covariance between input parameters. Changing this matrix will change how the input parameters will vary which will inevitably affect how the output parameters will vary. Likewise, both sensitivity based methods use the sandwich rule [equation (1.16)] to calculate the output uncertainty, which depends directly on the sensitivities of the input parameters and their covariance.

Despite the important role that the input parameter covariance matrix plays in determining the output uncertainty, there can be much variation between covariance matrices from different evaluators. Moreover, there is little consensus on exactly how to deal with problems such as dilution dependency of the covariances, temperature dependency, and the applicability of covariance matrices between different evaluations. Furthermore, in some cases the covariances come in raw/continuous energy format within evaluated nuclear data libraries and in other cases they have already been processed into multi-energy group form. The goal of this work was to study the effects of each of these factors and apply what was learned to the OECD Nuclear Energy Agency (NEA) benchmark on Uncertainty in Analysis in Modelling (UAM).

1.5 Reactor Physics Calculation Chain

There are several stages required to perform a simulation of a full reactor core (see Figure 1.3). Nuclear properties are first evaluated by experiment in order to find the probability that a reaction will occur when a nucleus comes into contact with particles of various energies. Of most interest to reactor physicists are the probabilities of interaction between neutrons of various energies and nuclei commonly present in nuclear reactors such as U235. The probability of interaction is represented by what is known as a cross section. The cross section has units of area and conceptually represents the area around a target nucleus seen by an incident particle which, when crossed by that incident particle, will cause a reaction to occur. Cross sections depend on the energy of the incident particle and so they are recorded over a range of energies. In the case of nuclear reactors, the range of neutron energies can easily vary from less than 10^{-2} eV to over 10^7 eV, which is 9 orders of magnitude. A combination of experimental data, nuclear modelling, and fitting is used to develop continuous energy nuclear data over this

range. The results are stored in an evaluated nuclear data library as a set of data points as well as the recommended interpolation schemes for these points. For isotopes with strong resonance features, the data libraries also include tabulated integral values which can be used to reconstruct the interaction behaviour near these resonance peaks.

Once reconstructed, evaluated nuclear data libraries are then processed into a format that can be read by simulation programs. Simulation programs can be divided into deterministic and Monte Carlo (stochastic) based on the solution methodology and assumptions employed. In the case of deterministic codes, the information must be put into multi-energy group format. Since the evaluated nuclear data libraries are in continuous energy format, they must be processed into discrete energy groups or bins. This process, known as spectral homogenization, is carried out such that it attempts to conserve the reaction rates and common neutronic behaviour (including tabulated resonance integrals as a function of dilution) within a discrete energy group when compared to its continuous energy counterpart. Common group structures include 69 and 172 groups and this is the structure of WIMS-D4 format multigroup libraries.

Once a multigroup library has been established, the user will provide the simulation program with information about the fuel geometry, isotopic dilution, composition, temperature, density etc. and the program will retrieve the nuclear data that it requires to perform the calculation. In the case of deterministic codes such as DRAGON [11], the calculation involves solving the neutron transport equation over a subset of the reactor domain since solving this equation for a full core is computationally expensive and is thus not usually done. Since reactors typically contain a repeating pattern of fuel elements, the smallest regularly repeating feature is often chosen as the lattice cell and is used in the simulation. The neutron transport equation is then solved using the problem-specific geometry, dilution factors, etc. as well as the appropriate multigroup data. The output of deterministic codes commonly includes the infinite lattice multiplication factor k_{∞} (k -infinite) and a set of cross sections which may be further homogenized into fewer energy groups as well as homogenized spatially over the area of the lattice cell. These subsequent homogenized properties can be passed onto a full core simulation code such as DONJON [12] to finally model the full reactor. These homogenized properties are essentially a weighted average of all the nuclear properties within the cell and allow for the full core to be modelled as a mosaic of homogenized cells. This reduces the amount of computation required and allows for the full core calculation to be performed using the diffusion equation instead of the more complicated neutron transport equation.

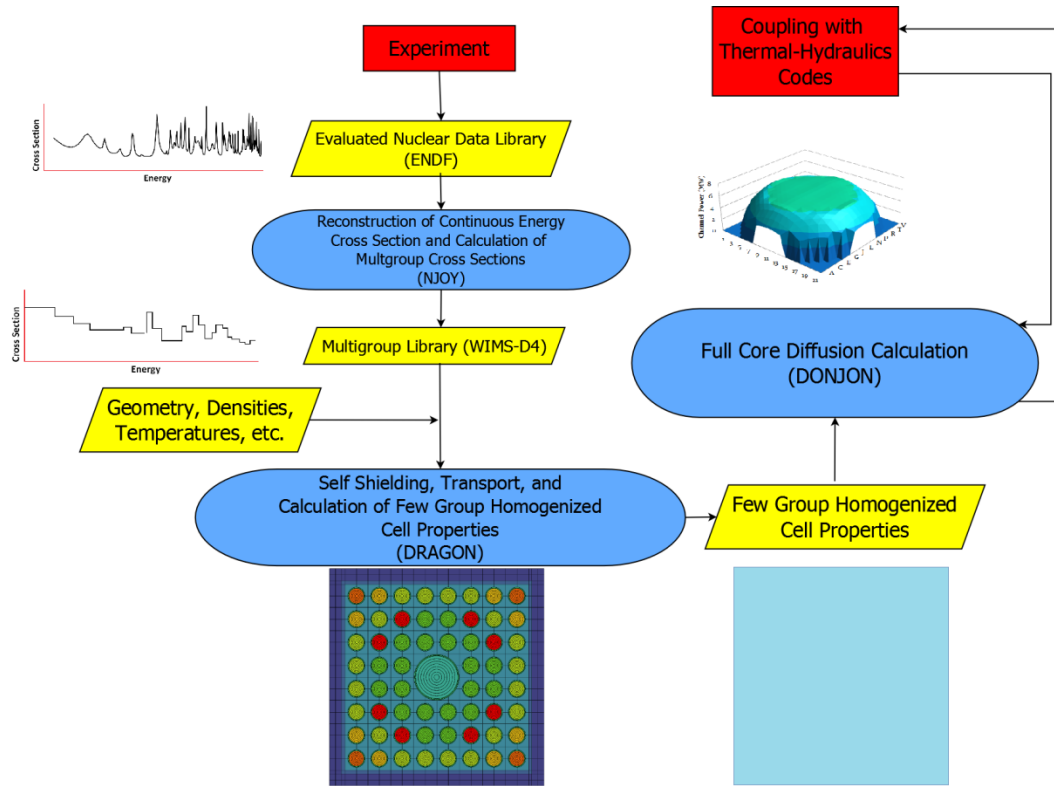


Figure 1.3 – Reactor Physics Calculation Chain

1.6 Project Scope

Previous work has looked at uncertainty starting from the multigroup library stage and propagating the errors through to the homogenized few group cell properties [3]. This work aimed to improve on this methodology by starting from a set of perturbed evaluated nuclear data libraries at a more primitive stage in the calculations and using them to calculate multigroup covariances at differing temperatures and dilutions. Where significant differences were seen, the effects on the homogenized few group cell properties were investigated as well in order to evaluate the validity of some of the assumptions made in previous works with regards to covariance matrices as outlined in Section 1.4. Of particular interest is the treatment of resonance integrals which must be carefully studied since they have a dilution dependency due to spectral resonance self-shielding.

Chapter 2

Tools and Methodology

The completion of this work required the use of several existing computer codes and the development of a new program named COCOAPUFFS that is able to create and format covariance matrices at varying dilutions. The purpose of this section is to thus to briefly explain how the codes employed in this project work as well as establish the need for the development of COCOAPUFFS by reviewing the current capabilities of other codes used for uncertainty analysis of nuclear reactors.

2.1 Methodology Overview

In order to generate multigroup covariance matrices at varying dilutions, a set of perturbed evaluated nuclear data libraries, known as TENDL libraries, in ENDF format were obtained from the Nuclear Research and Consultancy Group (NRG) website⁵. These libraries were created by randomly perturbing parameters used in the reconstruction of continuous energy cross sections [13]. Changing these parameters affects the position, width, and size of resonance peaks as well as the other nuclear interaction data stored in the file. This is known as the Total Monte Carlo approach and differs from current Monte Carlo methods which perturb multigroup cross sections accounting solely for the uncertainty due to vertical displacement of the continuous energy cross section which will always estimate a decrease in the uncertainty with dilution [14]. However uncertainty in the positions of resonances and their widths can cause the uncertainty with dilution to increase as is shown later in this work.

The perturbed TENDL libraries were processed into 69 groups in WIMS-D4 format using NJOY. The covariance between these cross sections at all energies was then calculated using a script written in the programming language Python that was developed for this work known as COCOAPUFFS (Covariance Calculation by Analysis of Perturbed Fundamental Files). Covariances calculated with COCOAPUFFS were validated against a spreadsheet program. Since NJOY can calculate multigroup cross sections at multiple dilutions, it was possible to calculate covariances between cross sections of finite dilution, something which is

⁵ www.talys.eu

only possible with the Total Monte Carlo approach. Plots were made of these multigroup covariances for visual comparison.

Only three reactions: Elastic scattering (MT=2), fission (MT=18), and radiative capture (MT=102) were available at multiple dilutions from the NJOY output so covariances as a function of energy within these reactions as well as between these reactions were calculated for finite dilutions. The other reactions were only available at infinite dilution. To investigate the effect of dilution on the covariance between the few group homogenized cross sections, a program named DINOSAUR [3] was used to sample from the IAEA library using the calculated covariances. First, the covariances for U235 and U238 at infinite dilution in the DINOSAUR covariance library⁶ were replaced with those calculated from the TENDL evaluations. DINOSAUR was then used to run a simulation of a pin cell from the TMI-1 PWR at hot full power as outlined in the Uncertainty Analysis in Modelling (UAM) benchmark created by the Nuclear Energy Agency (NEA) of the Organization for Economic Cooperation and Development (OECD) [15]. The infinite dilution covariances for elastic scattering, fission, and radiative capture (as well as the covariances between these reactions) were then substituted with covariances calculated as the closest available dilution to the true problem dilution. This corresponded to 1200 barns for U235 and 52 barns for U238. The covariance between the 2 group homogenized cross sections that emerged from DRAGON was then calculated from the output for both infinite and finite dilution cases as well as the uncertainty in k-infinite and the results are displayed in Chapter 4.

2.2 ENDF/B

The Evaluated Nuclear Data Files (ENDF/B) were initially developed as a method of storing experimental nuclear data in a computer-readable format mostly intended for use in thermal reactor research. There have been several evolutions of the ENDF/B libraries and they have expanded to include data for other applications such as radiation protection, medical radiotherapy, and radioactive waste disposal to name a few. The format has been largely successful and has been adapted by several other nuclear data organizations worldwide including the European JEFF files, the Russian BROND files, and the Japanese JENDL files. In order to distinguish between the format and the files themselves, the format has been named “ENDF-6 format”, while new evaluations of the files themselves are indicated with roman numerals (i.e. ENDF/B-VII). Each new

⁶ DINOSAUR uses the 44 group SCALE covariance library extrapolated to 69 groups with ANGELO2.

version of the library is subjected to strict scrutiny to ensure that it is properly tested and reviewed prior to release [16].

The creation of an evaluated nuclear data file starts with the collection of experimental data. An *evaluation* is then created by combining the experimental data with nuclear model predictions and fitting functions and the results are tabulated into an *evaluated nuclear data set*. The use of nuclear models is necessary to fill in the gaps where experimental results do not exist [17]. Since there are numerous ways of interpolating between a set of data points, the ENDF/B libraries also indicate the interpolation schemes required. This ensures that the data can be properly reconstructed and allows for the libraries to be more condensed. This is of particular value in the *resonance region* for heavier isotopes because these regions tend to contain numerous resonance peaks which would require many data points to accurately reproduce. Instead of having to store many data points for numerous peaks, a set of values that describe each peak are stored. The peaks can then be reconstructed using these values with one of the following reconstruction methods: Single-Level Breit-Wigner, Multi-Level Breit Wigner, Reich-Moore, Adler-Adler, Hybrid R-Function, or Generalized R-Matrix. At higher energies, the peaks become too closely spaced to resolve experimentally. This is known as the *unresolved range* and is dealt with in ENDF/B by using a set of average resonance parameters. These are stored in one of the following ways: Energy-Independent Parameters, Energy-Independent Parameters with Energy-Dependent Fission, or Energy-Dependent Parameters. These parameters can then be used to calculate the cross sections with the help of resonance theory [16].

ENDF/B nuclear data files are organized into materials, files, and sections. The material (MAT) number identifies the isotope to which the evaluation belongs. Evaluations come in separate files for each isotope and are labelled according to their sublibrary name, atomic number, atomic symbol, and mass number. For example the neutron sublibrary for U235 is n-092_U_235.endf. The sublibraries each have their own identification symbol.

Table 2.1 – ENDF/B Sublibraries

Sublibrary	Symbol
Photonuclear	g
Photo-atomic	photo
Radioactive decay	decay
Spontaneous fission yields	s/fpy
Atomic relaxation	ard
Neutron	n
Neutron fission yields	n/fpy
Thermal scattering	tsl
Standards	std
Electro-atomic	e
Proton	p
Deuteron	d
Triton	t
Helium-3	he3

Files are denoted with the label “MF” followed by a number. The table below summarizes the different file types [16]:

Table 2.2 – File Types in ENDF/B

MF	Contents
1	Description and miscellaneous data
2	Resonance parameter data
3	Cross sections as a function of energy
4	Angular distributions
5	Energy distributions
6	Energy-angle distributions
7	Thermal scattering data
8	Radioactivity data
9-10	Nuclide production data
12-15	Photon production data
30-36	Covariance data

Files are further subdivided into sections with the label “MT” followed by a number. A few of the commonly used MTs in this report are defined in the table below.

Table 2.3 – Common Reactions in ENDF/B

MT	Reaction
2	Elastic Scattering
4	Inelastic Scattering
16	(n,2n)
18	Fission
102	Radiative Capture (n, γ)
107	(n, α)
452	$\bar{\nu}$

ENDF/B libraries are a useful database of information but are typically not themselves usable for reactor physics simulations. The information contained in the ENDF/B libraries must thus be processed into a format readable by reactor physics codes. This is typically WIMS-D4 format for deterministic codes and ACE format for Monte Carlo codes and the formatting can be done using the code NJOY [18].

2.3 TENDL and TALYS

The Dutch Nuclear Research and Consultancy Group (NRG) in cooperation with the French Commissariat à l’Energie Atomique (CEA) at Bruyères-le-Châtel has created a tool for predicting nuclear reactions named TALYS. The goal of TALYS is to provide a user friendly program that is able to provide data over all possible nuclear reaction types. Moreover it aims to provide a more consistent approach to the production of evaluated nuclear data libraries so that the process is repeatable and transparent [19]. Data generated from TALYS has been used to create several “TALYS-based Evaluated Nuclear Data Libraries” (TENDLs) which are in ENDF-6 format, allowing them to be processed by NJOY. The NRG has also created a set of random nuclear data files in TENDL format which are generated by randomly perturbing some of the parameters used in the nuclear models according to their uncertainties when generating TENDL libraries [13] [20]. The resulting set of TENDL libraries represent some of the combinations that could exist within the known uncertainty ranges.

The random nuclear data libraries are available by isotope on the NRG website⁷. Since they are in ENDF-6 format, they can be processed by NJOY to produce multigroup cross sections in WIMS-D4 format for use in codes such as DRAGON or in ACE format for use in MCNP. The advantage of perturbing the evaluated nuclear data library is that the uncertainty in cross sections at non-

⁷ www.talys.eu

infinte dilutions can be seen since these calculations are performed when condensing cross sections into multigroup format.

2.4 NJOY

Cross sections in an evaluated nuclear data library such as ENDF/B-VII or TENDL are not directly usable in deterministic or Monte Carlo neutron transport codes. They require some processing and formatting and this is done using a nuclear data processing code such as NJOY [18]. NJOY is composed of several modules which perform specific functions according to what the user specifies in the input file. Input files are organized by module and module options are organized into lines called “cards” which are filled out by the user. The user must also specify what data is to be read by each module and what is to be output. All input and output is written to files called “tapes”, which can be in ASCII or binary format⁸. A brief overview of the modules used for the completion of this work is given in Table 2.4 [18].

Table 2.4 –Employed Modules of NJOY and their Function

Module	Purpose
RECONR	Reconstructs cross sections from ENDF into pointwise data.
BROADR	Performs Doppler broadening/thinning on pointwise cross sections.
THERMR	Creates cross sections and energy-to-energy matrices for free or bound scatterers in the thermal energy range.
GROUPE	Condenses pointwise cross sections into multigroup cross sections at multiple dilutions, generates group-to-group scattering matrices.
ERRORR	Creates multigroup covariance matrices from uncertainty data in the ENDF/B library.
COVR	Mainly used to convert the output of ERRORR for plotting.
MODER	Converts tapes between ASCII and binary format.
WIMSR	Generates multigroup libraries in WIMS-D4 format.
PLOTR	Plots cross sections and distributions.
PURR	Self-shields cross sections in the unresolved region using the probability table method.

The subsections that follow explain how these modules are typically used to convert an evaluation into a WIMS-D4 format multigroup library and accompanying set of multigroup covariance data.

⁸ The use of the terms “card” and “tape” are purely for nostalgic purposes.

2.4.1 MODER

MODER is typically called at the beginning of an NJOY run to convert an ASCII format nuclear data evaluation such as ENDF/B-VII into binary. Doing so will typically reduce the overall calculation time later in the NJOY run [18]. The user may also call MODER later in an NJOY run to convert a file into ASCII format to verify its contents, for example if the user wishes to plot the output of a specific module.

2.4.2 RECONR

RECONR is used to reconstruct cross sections using the data points and interpolation information contained in an ENDF-6 format nuclear data evaluation. It outputs cross section data vs. energy as a set of points called a pointwise-ENDF or PENDF tape. RECONR chooses an energy grid such that the cross section values between the given points can be interpolated to within a specified tolerance [18]. Cross section reconstruction is handled differently depending on the region of the cross section under consideration. An example cross section showing the different regions is given in Figure 2.1.

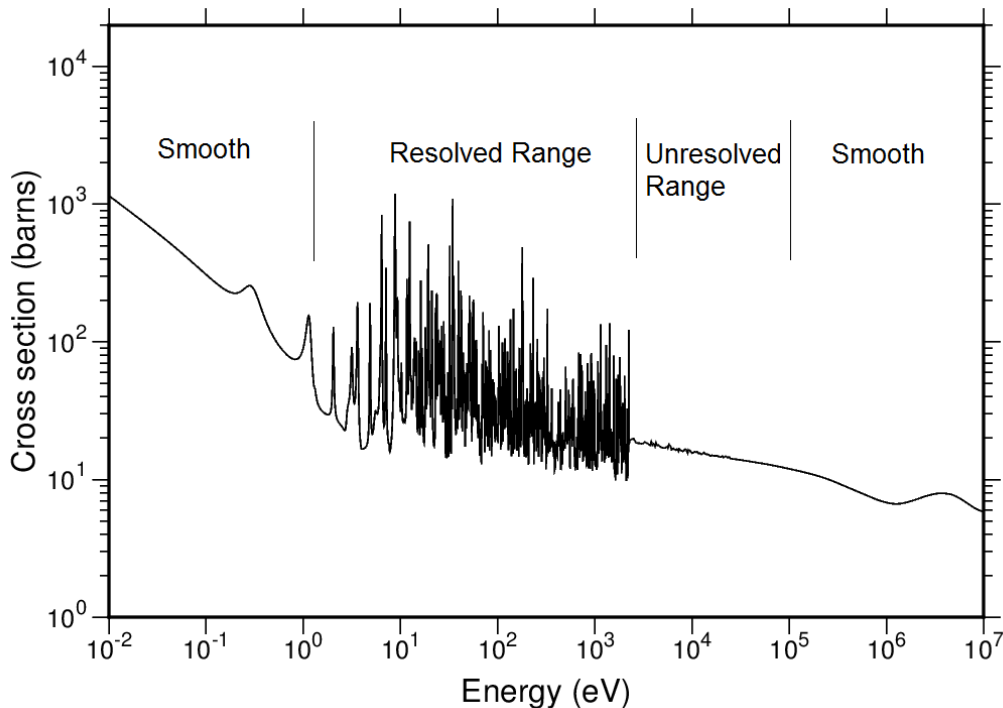


Figure 2.1 – U235 Fission Cross Section Showing the Various Cross Section Regions

In the smooth regions, reconstructing the cross section is done according to the recommended interpolation scheme given in the evaluated nuclear data library. There are 6 interpolation schemes used:

Table 2.5 – Interpolation Schemes Used in ENDF/B and NJOY

Interpolation Scheme	Description
INT = 1	Constant $y = c$
INT = 2	Linear $y = cx$
INT = 3	Linear-log $y = c \ln(x)$
INT = 4	Log-linear $\ln(y) = cx$
INT = 5	Log-log $\ln(y) = c \ln(x)$
INT = 6	y obeys a Gamow charged-particle penetrability law.

Regardless of which interpolation scheme is used, the results are always put onto a common grid by RECONR. The primary purpose of this is to ensure that cross sections which are by definition a sum of other cross sections will always obey this relationship, even when interpolated between points. For example, if we were to add one cross section which obeys a linear interpolation scheme to one that obeys a logarithmic interpolation scheme, the resulting sum will not be suitable for linear nor logarithmic interpolation between the points. RECONR thus chooses a new energy grid for all cross sections that can be approximated by linear interpolation to a desired accuracy. Cross sections that result from a sum of other cross sections are then calculated using the new grid and values that are linearly interpolated between these grid points for the summed variable will be equivalent to what would be calculated by summing the interpolated values of the variables which add up to this summed variable [16].

In areas where the cross section contains resolvable resonances, there are a number of reconstruction methods available: Single-Level Breit-Wigner, Multi-Level Breit-Wigner, Reich-Moore, Adler-Adler, Hybrid R-Function, and Generalized R-Matrix. Each has its own strengths and weaknesses and the choice of which method to use is given in the ENDF-6 format library read by NJOY. Most modern evaluations choose to store resonance information in the format used by the Reich-Moore method [16] [17].

At higher energies, the resonance peaks become so closely spaced that resolving them experimentally becomes impossible. Cross sections in this region are thus represented using average resonance parameters from which the cross sections can be calculated statistically from resonance theory. These resonance parameters can be either energy independent, energy independent with the exception of energy dependent fission parameters, and energy dependent parameters [16]. In the case of energy independent parameters, it is assumed that the energy dependence of factors such as the neutron wave number and penetrability dictate the shape of the cross section in the unresolved range [21].

Recall that cross sections constructed in the smooth regions are linearized and put onto a common grid to ensure that any summation relationships that exist between reactions hold true for data that is interpolated between the points. The same process is also applied to cross sections in the resolved and unresolved range after reconstruction. The end result is a set of continuous pointwise (PENDF) cross sections which contain a common grid with respect to energy. Furthermore, the linearization scheme ensures that cross sections which are calculated as a sum of other cross sections can be linearly interpolated to obtain data between the points, and that these interpolated points will still obey the summation relationship when its component cross sections are interpolated as well.

2.4.3 BROADR

When data is read from an evaluated nuclear data library and reconstructed using RENCONR, the resulting cross section represents a material at 0K [18]. The temperatures in a reactor normally range from around 293K to 1100K so in order for the data to be useful, temperature effects must be taken into account. When a neutron is passing through a material that is at a temperature superior to 0K, it will “see” the atoms in that material moving at a range of velocities relative to itself depending on the the speed and direction of the atoms in the material and the speed and direction of the neutron. As the temperature of the material increases, the range of velocities seen by the neutron also increases. Picture a neutron that is moving with a velocity that is close to, but slightly slower than, the velocity required to cause absorption by a resonance peak in the material which it is moving through. Furthermore we will assume that the atoms in that material are motionless in the laboratory frame of reference (ie. the material has a temperature of 0K). In this case, no absorption will take place since a collision of sufficient energy will not occur. However now consider the case where the material is at a temperature greater than 0K. Now the atoms in that material will be moving and the neutron will see a distribution of relative velocities between itself and the surrounding atoms as they move in different directions. In this second case, there is a chance that one of the atoms nearby will be moving towards the incident neutron with the right velocity to cause their relative velocity to fall within the range of the resonance peak and cause an absorption event. Despite the fact that the neutron had the same energy as in the first case, the resonance peak has been effectively broadened from the perspective of the neutron to permit absorptions to take place at neutron velocities slightly higher and lower than the original 0K peak. This is called Doppler broadening and is accounted for by the BROADR module in NJOY. Note that this module is used to Doppler broaden the resolved region only, the unresolved region undergoes a different procedure for Doppler broadening (see section 2.4.4).

To take the temperature dependence of the cross section into account, NJOY defines an effective cross section which is equal to what the cross section would need to be for a material at 0K (stationary nuclei) in order to give the same reaction rate as is observed in the material at temperature T.

$$\rho v \bar{\sigma}(v, T) = \int \rho |v - v'| \sigma(|v - v'|) P(v', T) dv' \quad (2.1)$$

Where ρ is the material density, v is the incident neutron velocity, v' is the velocity of the target nuclei, σ is the cross section for stationary nuclei (0K material), and $P(v', T)$ is the distribution of target nuclei velocities relative to the laboratory frame of reference. Typically this is the Maxwell-Boltzmann distribution:

$$P(v', T) dv' = \frac{(\alpha)^{3/2}}{\pi^{3/2}} e^{-\alpha(v')^2} dv' \quad (2.2)$$

$$\alpha = M/2kT$$

Where M is the target mass, k is Boltzmann's constant, T is temperature of the target nuclei, and v' is the velocity of the target nuclei in the material. The broadening effect with temperature can be seen in the figure below.

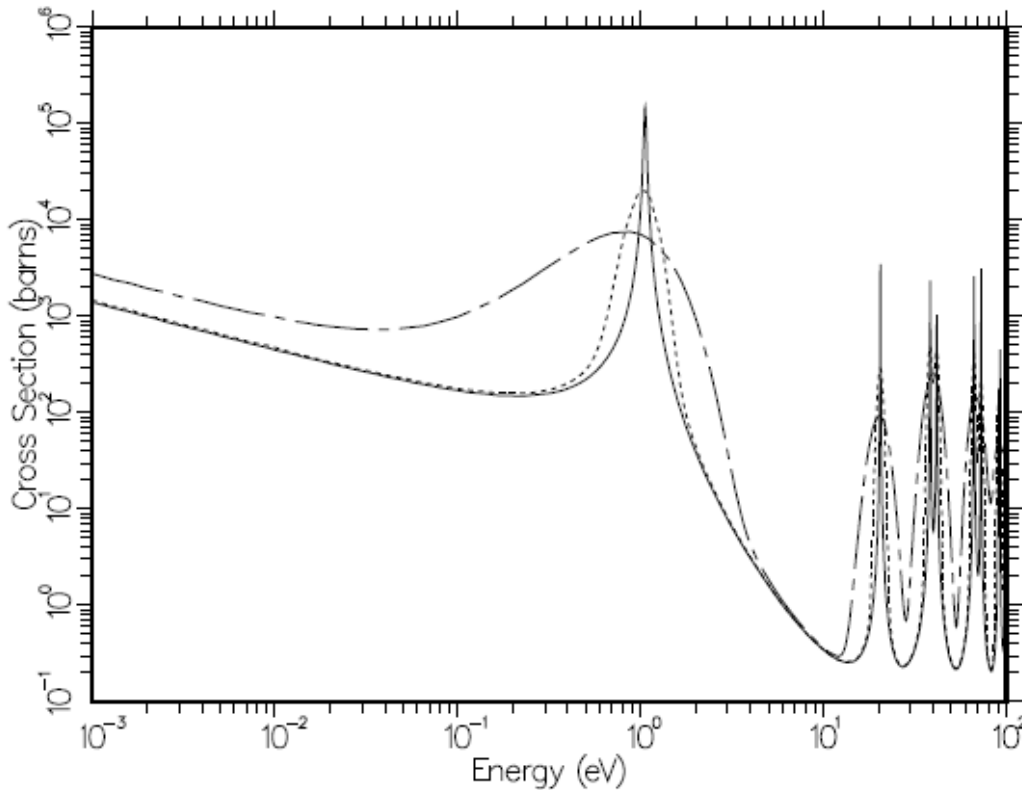


Figure 2.2 – ^{240}Pu (n, γ) Cross Section at 0K (solid line), 30 000K (dotted line) and 300 000K (dashed-dotted line) [18]

2.4.4 PURR

The PURR module of NJOY is designed to Doppler broaden and self-shield cross sections in the unresolved region. This task can also be performed by the UNRESR module but the results given by PURR are preferred to those from UNRESR in most modern versions of NJOY. Since we do not know true location or size of any of the resonances in the unresolved region, a statistical approach must be taken. In ENDF-6 format nuclear data evaluations, the average spacing of resonances as well as the distribution of the spacings (known as the Wigner distribution) are given as well as the average resonance partial widths and the distribution for these widths (which follow a chi-square distribution). These values are specified for multiple spin sequences which are all statistically independent. With this information at hand, it is possible to generate a set of resonances by random sampling. A centre for the first resonance is chosen using a uniform distribution and its partial width is chosen by sampling from the distribution of partial widths. The centre of the second resonance is next chosen using the distribution of the resonance spacings and its partial width is chosen by sampling. The process is continued until the unresolved energy range has been filled. The process is repeated over all spin sequences. The set of cross sections

over the unresolved range for all spin sequences is referred to as a “ladder.” In order to get an accurate representation of the average properties of the unresolved region, it is necessary to use many ladders so the process is repeated as many times as the user specifies [21]. The final result is a probability table which can be converted into cross sections using the Single Level Breit Wigner approximation and Doppler Broadened using the ψ - χ method, which is an approximation to the Doppler broadening equation [22]. They can also be self-shielded using the Bondarenko method, which is described in the GROUPR section of this report (section 2.4.6).

2.4.5 THERMR

The THERMR module is used to create pointwise scattering cross sections for neutrons at thermal energies. The module is able to calculate the cross sections for coherent scattering (which occurs in crystalline materials and is always elastic) and incoherent scattering (which occurs in non-crystalline materials and can be both elastic and inelastic). The computed scattering cross sections are added to the PENDF tape and passed onto the next module [18].

2.4.6 GROUPR

Once the evaluated nuclear data has been reconstructed and Doppler broadened and scattering data has been calculated, the PENDF file is ready to undergo spectral self-shielding calculations and conversion into multigroup format⁹. The tape that emerges is called a GENDF file (groupwise-ENDF). Group to group scattering matrices are also computed and attached to the GENDF tape. The spectral self-shielding calculation can be performed using the Bondarenko narrow-resonance weighting scheme, however NJOY also has its own flux calculator program which can be used to find an approximation to the flux for a given mixture of heavy absorbers in light moderators. This flux calculator is typically used at epithermal energies [18]. This module is of particular importance to the work in this report and so it shall be given extra attention.

Deterministic codes need their cross sections in multi-energy group format which means that some sort of averaging must occur over the energy range in each group. Furthermore, this averaging must be done such that the reaction rate is conserved. Since the reaction rate is the product of the cross section and the flux, it makes sense that the average cross section for a group is calculated by taking a flux-weighted average of the cross section over the energy range for that group. Immediately however there is a problem: In order to perform a flux

⁹ Cross sections in the unresolved region are an exception as they are self-shielded in either the UNRESR or PURR modules before GROUPR is called.

weighting, we require knowledge of the flux, but the whole reason for performing this calculation in the first place is to find the flux in a future problem. The solution is to use a pre-determined estimate of the flux shape. NJOY contains pre-calculated flux shapes for a variety of different types of reactors so accurate results can be achieved with this method, especially when applied to common reactor types such as light water thermal reactors. While pre-estimated flux shapes are good at approximating the overall flux, they cannot properly account for local effects due to resonances. When a strongly absorbing resonance occurs in the cross section, the flux will typically dip in the energy range over which the peak occurs. As a result, the peak is given a lower weight when computing the average cross section because the flux by which it is weighted is lower in the vicinity of the peak. If this is not accounted for, the group-averaged cross section will overpredict the reaction rate within that group.

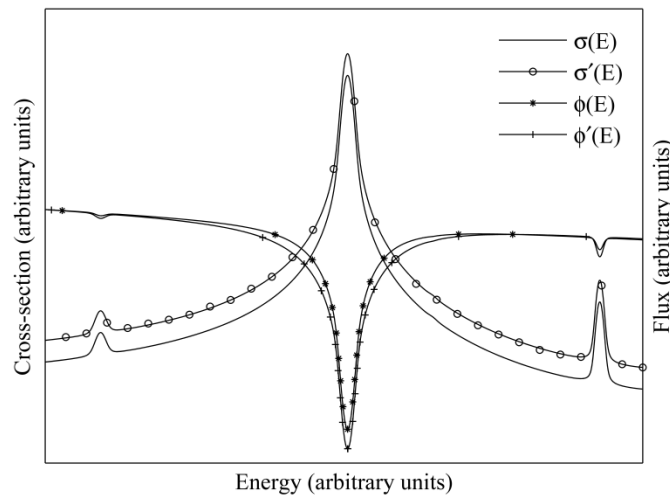


Figure 2.3 – Self-Shielding of the Flux in the Presence of a Resonance Peak [14]

Performing a spectral self-shielding calculation on the cross sections resolves the problem of locally predicting the flux shape but there is still one more problem: it is not known how much of an effect a peak will have on the flux. Imagine a large resonance peak for some non-fissionable material located in the fuel of a reactor. One would expect that peak to absorb many neutrons and cause a local dip in the flux but if the material containing this peak is only present in trace quantities, it may have no noticeable effect. The majority of absorption events will likely take place in the much more prevalent fuel atoms, despite the fact that their microscopic cross sections may not be as high. In other words, the cross section from our hypothetical material contributes very little to the overall macroscopic cross section of the fuel. In this case, we would say that the cross section is very dilute. The amount by which a cross section will affect the flux locally depends on the dilution of that material. Since we have no way of knowing

the dilution of a material ahead of time, spectral self-shielding is performed at multiple dilutions and stored in a library. Deterministic codes will calculate the dilution of a macroscopic cross section when performing a simulation and then interpolate the proper cross section from the values available in the library.

Cross sections may be self-shielded according to the Bondarenko method [18]. The local flux φ seen by material i is assumed to be a function of the estimated flux shape function $C(E)$ and the total macroscopic cross section $\Sigma_t(E, T)$ for the material containing isotope i .

$$\varphi^i(E) = \frac{C(E)}{\Sigma_t(E, T)} \quad (2.3)$$

Where E is energy and T is temperature. We can split the unknown total cross section for the material into two components: The contribution from isotope i and the contribution from all the other isotopes σ_0^i , which is called the background cross section.

$$\begin{aligned} \Sigma_t(E, T) &= \sum_j \rho^j(T) \sigma^j(E, T) \\ &= \rho^i(T) \sigma^i(E, T) + \sum_{j \neq i} \rho^j(T) \sigma^j(E, T) \\ &= \rho^i(T) \left[\sigma^i(E, T) + \frac{1}{\rho^i(T)} \sum_{j \neq i} \rho^j(T) \sigma^j(E, T) \right] \\ &= \rho^i(T) [\sigma^i(E, T) + \sigma_0^i] \end{aligned} \quad (2.4)$$

$$(2.5)$$

Where:

$$\sigma_0^i = \frac{1}{\rho^i(T)} \sum_{j \neq i} \rho^j(T) \sigma^j(E, T) \quad (2.6)$$

This is called the background cross section (also known as the dilution cross section) and is evaluated for each resonant energy group in each isotope. Note that the dilution cross section is often simply referred to as the “dilution” and is not be confused with the traditional definition of dilution as a concentration. “Dilution” when referring to self-shielding instead refers to the total cross section of all the other materials in a mixture as given in Equation (2.6). Cross sections that go into

multigroup libraries are typically evaluated at multiple dilutions¹⁰ so that when the true dilution is calculated for a particular problem, the cross section at that dilution can be interpolated from the stored values in the library. We continue the derivation by using our definition of the background cross section in equation (2.3).

$$\varphi^i(E) = \frac{C(E)}{\rho^i(T)[\sigma^i(E, T) + \sigma_0^i]} \quad (2.7)$$

This value for the flux can now be used to calculate the flux averaged cross section over the energy interval covering some group g .

$$\sigma_g^i(\sigma_0, T) = \frac{\int_{E_{min}}^{E_{max}} \frac{\sigma_t^i(E, T)}{\rho^i(T)[\sigma^i(E, T) + \sigma_0^i]} C(E) dE}{\int_{E_{min}}^{E_{max}} \frac{1}{\rho^i(T)[\sigma^i(E, T) + \sigma_0^i]} C(E) dE} \quad (2.8)$$

Where E_{min} and E_{max} represent the lower and upper limits of the group g . Note that we can bring the density outside of the integral and cancel it out since it does not depend on energy and appears in both the numerator and denominator.

$$\sigma_g^i(\sigma_0, T) = \frac{\int_{E_{min}}^{E_{max}} \frac{\sigma_t^i(E, T)}{\sigma^i(E, T) + \sigma_0^i} C(E) dE}{\int_{E_{min}}^{E_{max}} \frac{1}{\sigma^i(E, T) + \sigma_0^i} C(E) dE} \quad (2.9)$$

Since we do not know the dilution a priori, group averaged cross sections in the resonance range are calculated at several dilutions and the results are tabulated. When the library is used by a transport code such as DRAGON, the code will calculate the dilution and then interpolate the correct value for the cross section from the tabulated data. The evaluation of a multigroup cross section at high and low dilution is depicted in Figure 2.4 and Figure 2.5.

¹⁰ The exception to this would be cross sections with no resonance region.

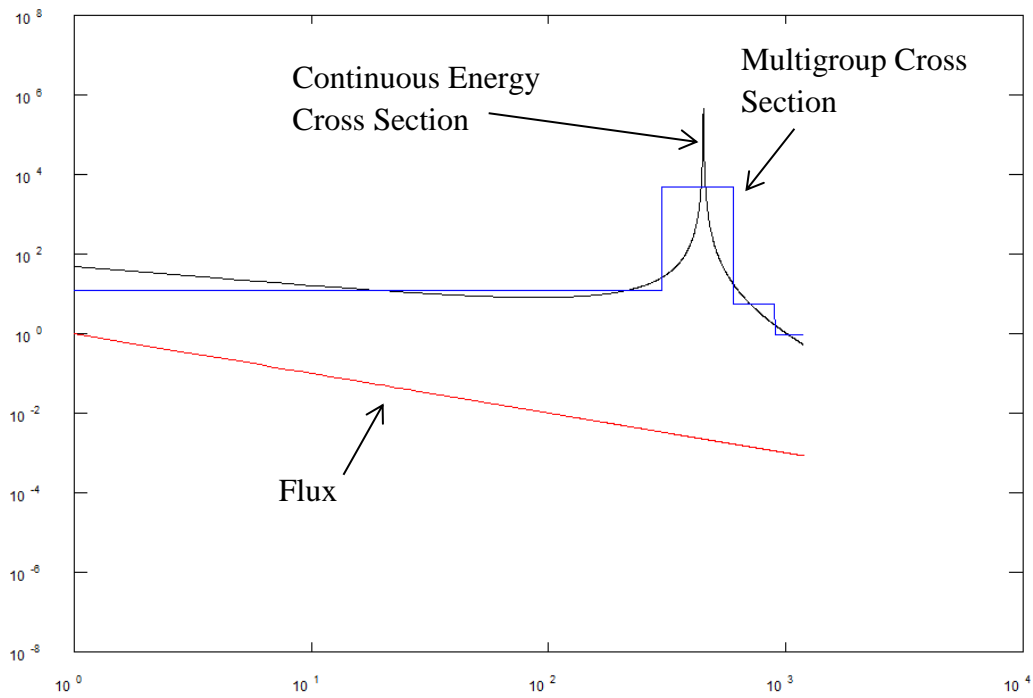


Figure 2.4 – Continuous Energy Cross Section and Corresponding Multigroup Cross Section (in 4 Groups) at Infinite Dilution

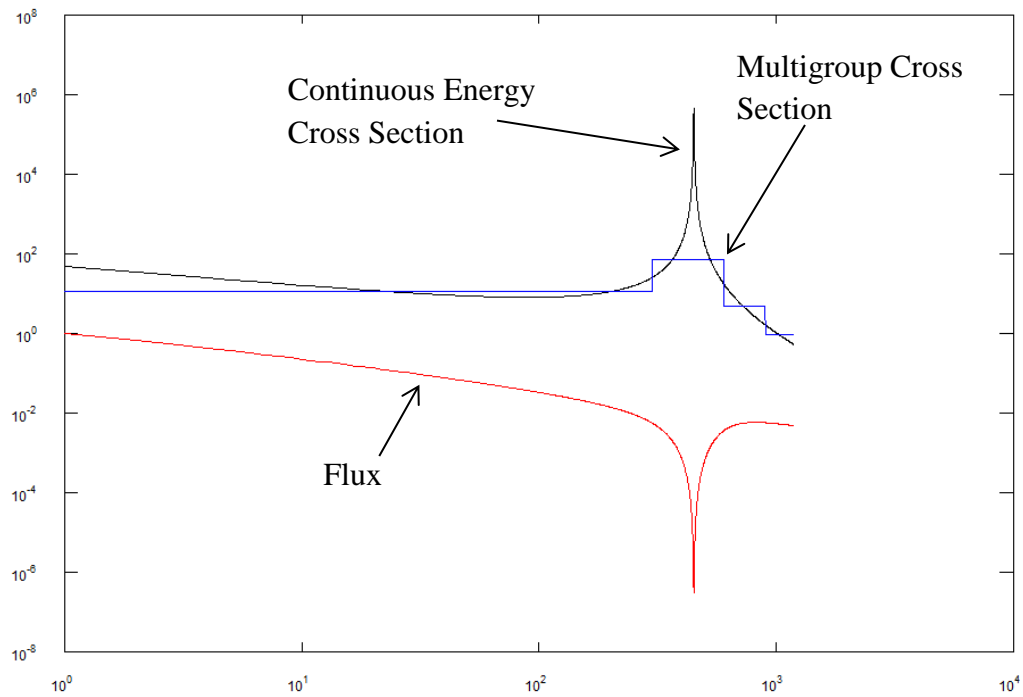


Figure 2.5 – Continuous Energy Cross Section and Corresponding Multigroup Cross Section (in 4 Groups) at a Dilution of 10 Barns

2.4.7 WIMSR

The WIMSR module of NJOY receives multigroup cross section data (in GENDF format) as well as scattering data and arranges it into WIMS-D4 format. Some cross sections and scattering data require modification before they can be used in the WIMS-D4 library. For example absorption reactions are all amalgamated into a single “absorption” cross section. In the resonance region, resonance integrals are stored in WIMS-D4 libraries instead of the cross sections calculated during self-shielding so WIMSR will perform the conversion. WIMSR can also perform transport correction on the P_0 scattering matrices if desired by the user. Lastly, the WIMSR module contains several pre-programmed decay chains which are used for the evaluation of burnup data. However the user has the option of adding fission yield data if they so choose [18].

2.4.8 ERRORR

Most modern evaluated nuclear data libraries contain covariance data that is provided by the evaluator. These covariances can be used for uncertainty analysis as well as to improve the data through further experimentation. In order for this information to be used to propagate uncertainty through a deterministic neutron transport code (such as DRAGON), it must be converted from its original energy-dependent format into multigroup format. Essentially, if we wish to find the uncertainty in results obtained using a 69 group library, the covariance information must also be in 69 group format. The ERRORR module was designed to perform this conversion, however in current versions of NJOY (ie. NJOY 99) ERRORR calculates covariance data for **infinitely dilute cross sections only** [18]. Since the spectral self-shielding calculation will, in general, change the covariance between cross sections in the resonance region, the covariances produced using ERRORR should not be applied to self-shielded cross sections. Instead, covariance matrices should be calculated at several values of dilution, as is done with the cross sections themselves.

2.4.9 COVR

COVR is used to process the output of ERRORR into a compressed format readable by sensitivity analysis programs. It can also be used to create high-quality covariance and correlation plots intended for publication.

2.4.10 PLOTR

PLOTR is a multipurpose plotting tool which can be used to view the output of the various modules of NJOY as well as produce plots intended for publication.

2.5 DINOSAUR

DINOSAUR (DRAGON Implementations of Numerical or Statistical Analysis of Uncertainties in Reactors) is an uncertainty propagation program created at McMaster University [3]. It is capable of using both the OAT sensitivity method as well as the Monte Carlo method to calculate the uncertainty in the results of DRAGON calculations. DINOSAUR uses the 44 group 44GROUPV6REC covariance library from the SCALE code package which was created at Oak Ridge National Laboratory. Since WIMS-D4 format libraries typically only come in 69 groups and 172 groups, this 44 group covariance library was interpolated using ANGELO2 [23] to 69 and 172 group formats. In this work, only the Monte Carlo option of DINOSAUR was used and the theory behind its operation is explained in section 1.2.

2.6 COCOAPUFFS

COCOAPUFFS (Covariance Calculation by Analysis of Perturbed Fundamental Files), is a program coded in the programming language Python that was developed as part of this work in order to create covariance libraries at several values of dilution for use in DINOSAUR. Once all of the perturbed TENDL format libraries have been processed by NJOY, COCOAPUFFS reads the NJOY output files and compiles lists of cross sections that are sorted according to dilution and reaction. A typical list will contain several hundred different perturbations of any given cross section. COCOAPUFFS then calculates the covariance between different energy groups within a reaction as well as between different energy groups in different reactions (this is sometimes called “cross covariance”) using equation (1.2). The results are then formatted so they can be read by the Monte Carlo package in DINOSAUR.

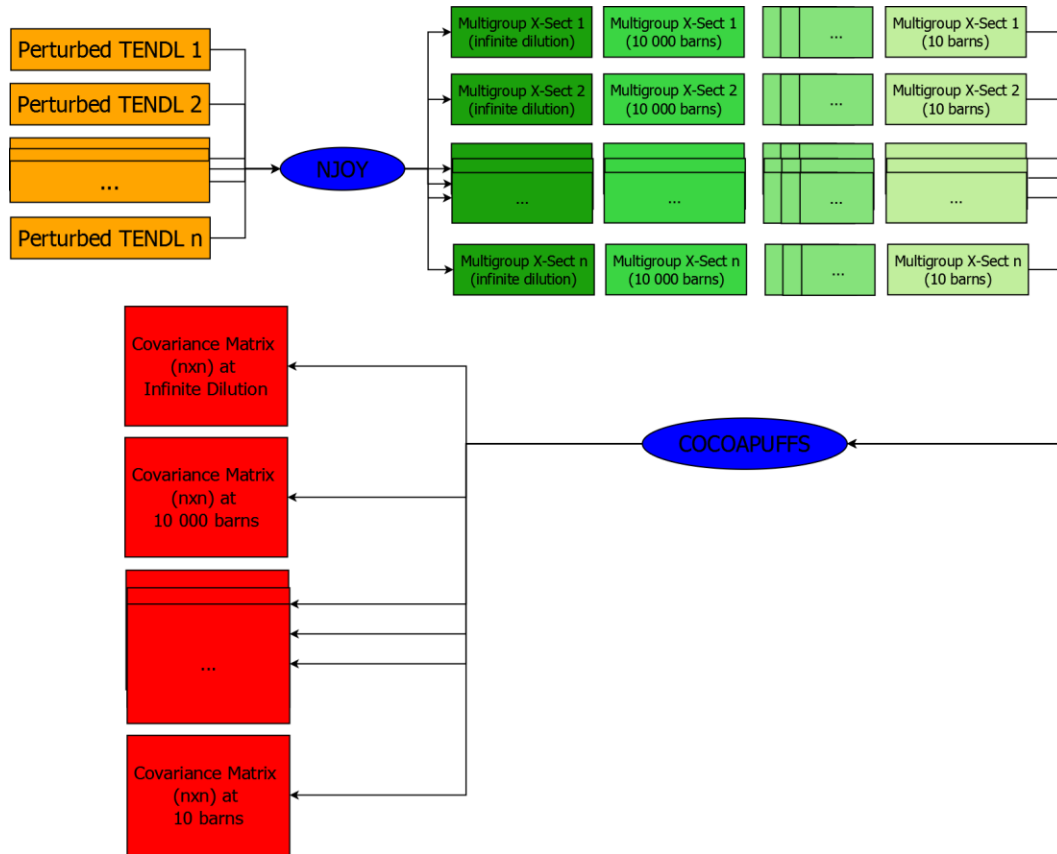


Figure 2.6 – Production of Multigroup Covariance Libraries at Multiple Value of Dilution Using NJOY and COCOAPUFFS

COCOAPUFFS was validated by comparing the covariance matrices (in 69 and 172 groups) produced by COCOAPUFFS to those calculated manually using a spreadsheet program. The results were found to correspond perfectly for covariance between energy groups within reactions as well between energy groups across reactions. Comparisons of the covariance calculated by COCOAPUFFS and by OpenOffice Calc¹¹ are shown in the figures that follow.

¹¹ OpenOffice Calc is a freeware spreadsheet program that is available on Linux.

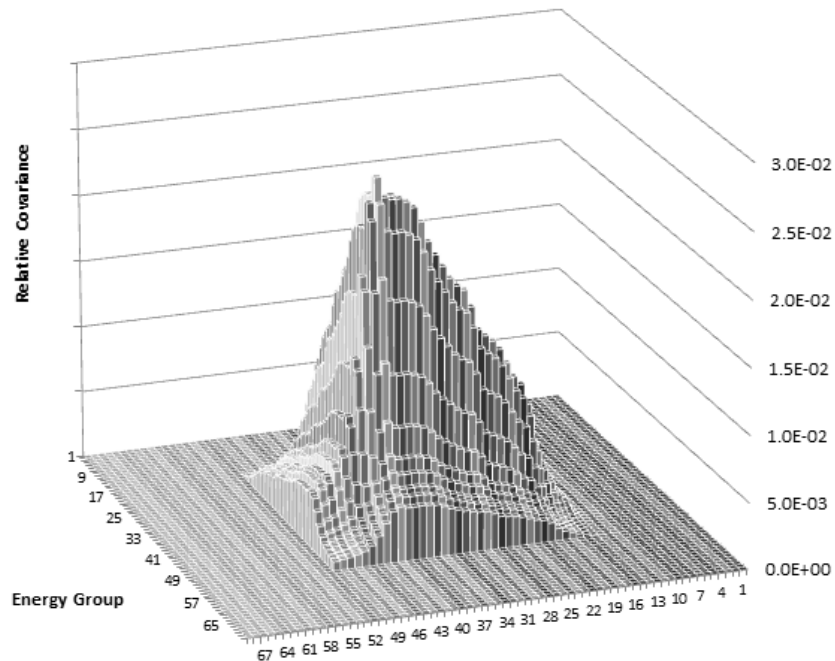


Figure 2.7 – U235 Inelastic Scattering Covariance as Calculated by COCOAPUFFS¹²

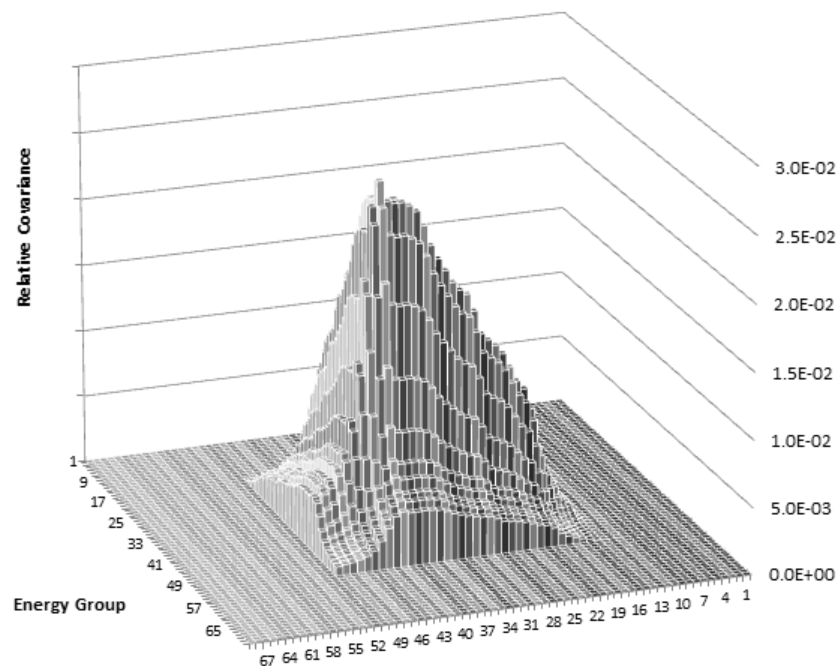


Figure 2.8 – U235 Inelastic Scattering Covariance as Calculated by OpenOffice Calc¹³

¹² Only the first 69 of 172 groups have been plotted in order to show more detail.

¹³ Only the first 69 of 172 groups have been plotted in order to show more detail.

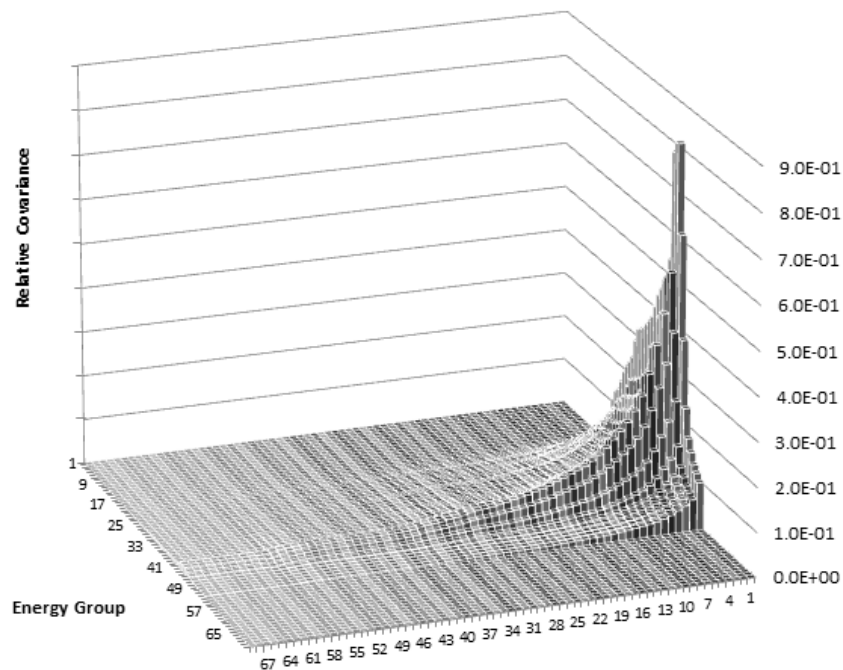


Figure 2.9 – U235 Cross-Covariance Between Fission and Elastic Scattering as Calculated by COCOAPUFFS¹⁴

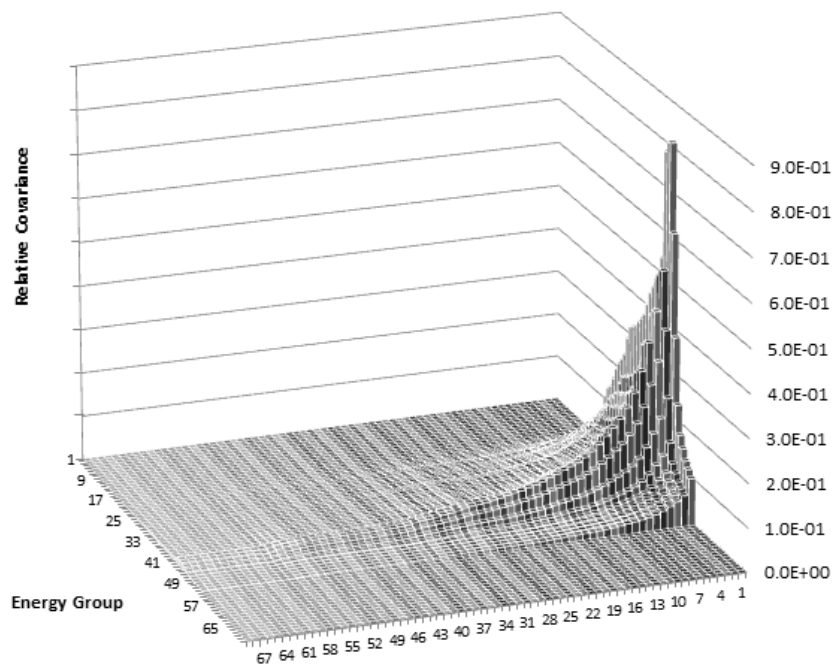


Figure 2.10 - U235 Cross-Covariance Between Fission and Elastic Scattering as Calculated by OpenOffice Calc¹⁵

¹⁴ Only the first 69 of 172 groups have been plotted in order to show more detail.

¹⁵ Only the first 69 of 172 groups have been plotted in order to show more detail.

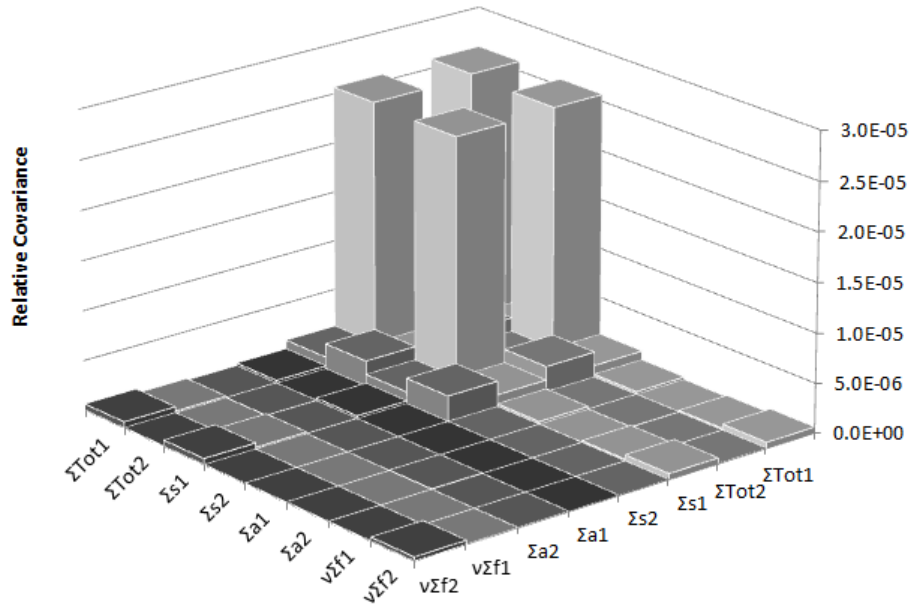


Figure 2.11 – 2 Group Homogenized Cross Section Covariance as Calculated by COCOAPUFFS

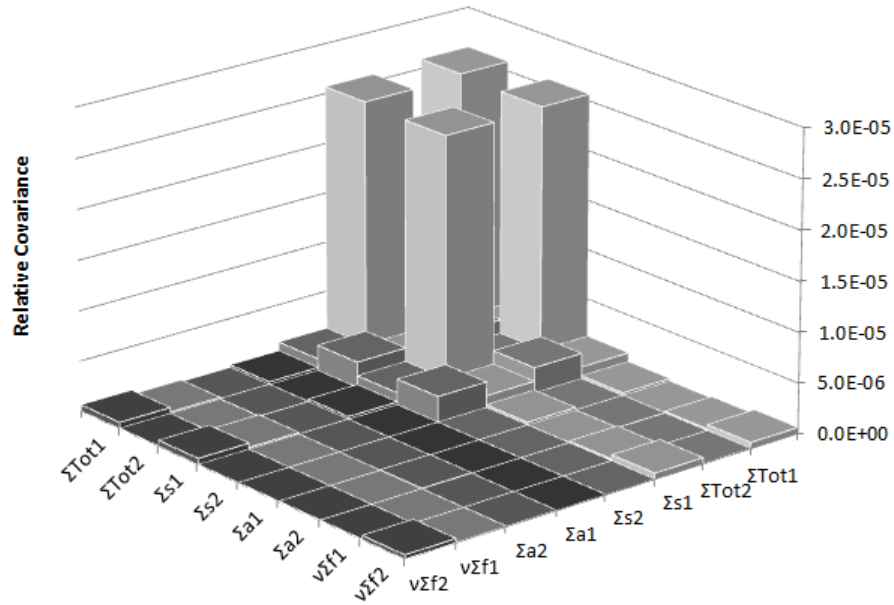


Figure 2.12 – 2 Group Homogenized Cross Section Covariance as Calculated by OpenOffice Calc

2.7 DRAGON

DRAGON is a program developed at the École Polytechnique de Montréal to solve the neutron transport equation for various fuel geometries. Typically this code is used to find the flux, the infinite lattice multiplication constant k -infinite, and the homogenized few group cross sections for a fuel lattice which can be passed onto a full core simulation program such as DONJON.

2.7.1 Progression of Calculations in DRAGON

The user starts a DRAGON simulation by specifying the geometry, temperature, density, and composition of the fuel lattice cell in an input file as well as all the data the user wants DRAGON to calculate. DRAGON, like NJOY, is composed of a collection of modules with specific functions which are called in the input file as they are needed. A common progression of modules for a fuel lattice calculation is shown below.

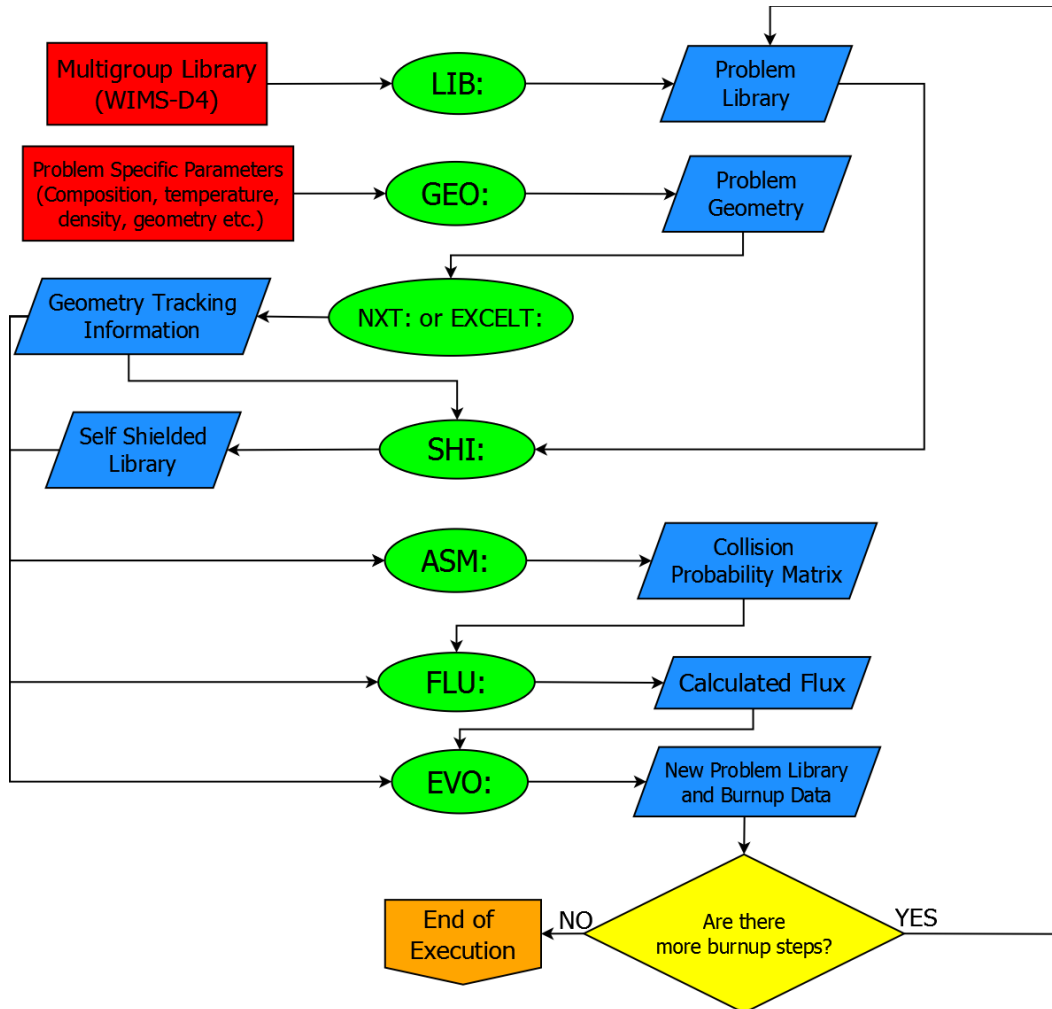


Figure 2.13 – Module Progression in a Typical DRAGON Lattice Cell Calculation

The function of each of these modules as well as their required inputs and outputs are detailed in Table 2.6. Note that the modules EDI: and CPO: are included in this table despite being omitted in Figure 2.13.

Table 2.6 – Commonly Used Modules for Lattice Physics Calculations in DRAGON

Module	Function
LIB:	Generates a microscopic and macroscopic cross section library containing the isotopes specified by the user as well as mixtures of isotopes defined for regions such as the fuel.
GEO:	Used to define the problem geometry.
EXCELТ:	Uses the output of GEO: to perform the cell collision probability tracking.
NXT:	Similar to EXCELТ: but able to handle more complicated geometries.
SHI:	Uses the library from LIB: and geometry tracking information from EXCELТ: or NXT: to calculate the background cross sections which are used to select the proper self-shielded cross sections from the library for interpolation.
ASM:	Uses tracking information from EXCELТ: or NXT: to create a collision probability matrix.
FLU:	Uses the collision probability matrix from ASM: to solve the neutron transport equation and calculate the flux.
EVO:	Calculates the changes in composition of the fuel over time as a result of neutron interaction and modifies the library accordingly.
EDI:	Used to calculate reaction rates, homogenized cross sections, and condense the cross sections into a different group structure for printing.
CPO:	Used to produce homogenized cross section tables that can be read by DONJON to perform a full core calculation.

In this work, burnup was not considered and so the EVO: module was not used. The EDI: module was used to condense the cross sections into the 2 group structure commonly used for full core diffusion calculations.

2.7.2 Neutron Transport

The primary function of DRAGON is to solve the neutron transport equation for a given fuel composition, geometry, temperature, and density. The neutron transport equation is also known as the Boltzmann transport equation and takes on the following form at steady state [24]:

$$\begin{aligned}
& \hat{\Omega} \cdot \nabla \phi(r, E, \hat{\Omega}) + \Sigma_T(r, E) \phi(r, E, \hat{\Omega}) \\
&= \int_{4\pi} d\hat{\Omega}' \int_0^\infty \Sigma_s(E' \rightarrow E, \hat{\Omega}' \rightarrow \hat{\Omega}) \phi(r, E', \hat{\Omega}) dE' \\
&+ \frac{\chi(E)}{4\pi} \int_{4\pi} d\hat{\Omega}' \int_0^\infty \bar{v}(r, E') \Sigma_f(r, E') \phi(r, E', \hat{\Omega}) dE'
\end{aligned} \tag{2.10}$$

Where $\hat{\Omega}$ is a unit vector pointing at a certain angle, φ is the neutron flux, r is a point in space, E is energy, Σ_T is the total reaction cross section, Σ_s is the scattering cross section, $E' \rightarrow E$ represents a neutron of energy E' having its energy reduced or increased to energy E , $\hat{\Omega}' \rightarrow \hat{\Omega}$ represents a neutron travelling at angle $\hat{\Omega}'$ being scattered such that it travels at angle $\hat{\Omega}$, χ is the distribution of neutron energies that result from fission, $\bar{\nu}$ is the average number of neutrons produced by a fission event, and Σ_f is the fission cross section. The significance of each term is detailed in the table below:

Table 2.7 – Contributions by Term to the Neutron Transport Equation

Term	Significance
$\hat{\Omega} \cdot \nabla \varphi(r, E, \hat{\Omega})$	Net leakage of neutrons of a particular energy out of the region and angle of interest.
$\Sigma_T(r, E) \varphi(r, E, \hat{\Omega})$	Removal of neutrons from the region and angle of interest due to absorption or scattering.
$\int_{4\pi} d\hat{\Omega}' \int_0^\infty \Sigma_s(E' \rightarrow E, \hat{\Omega}' \rightarrow \hat{\Omega}) \varphi(r, E', \hat{\Omega}') dE'$	Scattering of neutrons from various other angles and energies into the energy and angle of interest.
$\frac{\chi(E)}{4\pi} \int_{4\pi} d\hat{\Omega}' \int_0^\infty \bar{\nu}(r, E') \Sigma_f(r, E') \varphi(r, E', \hat{\Omega}') dE'$	Neutrons born into the region of interest from fission. Assumes isotropic prompt fission (delayed neutrons from fission are treated with a modification to this term).

In order for the system to remain at steady state, the production and loss of neutrons in the system must be in perfect balance. This condition is called “criticality” and is necessary for the time-independent neutron transport equation to be valid. When production exceeds loss, the system is said to be “supercritical” and when loss exceeds production the system is “subcritical”. Since having a system which is perfectly in balance is rare if not impossible, an eigenvalue k is added to the transport equation to permit minor variations from perfect criticality. If there is assumed to be no leakage of neutrons to the outside of the geometry under consideration, the k eigenvalue is called “ k -infinite” since this condition is representative of the geometry being surrounded by an infinite repeating lattice of itself. When leakage of neutrons to the outside is considered, k is called “ k -effective.” The k eigenvalue allows the equation to handle non-critical systems

provided that they do not deviate substantially from a criticality¹⁶. The modified neutron transport equation appears as follows:

$$\begin{aligned}
 & \hat{\Omega} \cdot \nabla \varphi(r, E, \hat{\Omega}) + \Sigma_T(r, E) \varphi(r, E, \hat{\Omega}) \\
 &= \int_{4\pi} d\hat{\Omega}' \int_0^\infty \Sigma_s(E' \rightarrow E, \hat{\Omega}' \rightarrow \hat{\Omega}) \varphi(r, E', \hat{\Omega}') dE' \\
 &+ \frac{\chi(E)}{4\pi k} \int_{4\pi} d\hat{\Omega}' \int_0^\infty \bar{v}(r, E') \Sigma_f(r, E') \varphi(r, E', \hat{\Omega}') dE'
 \end{aligned} \tag{2.11}$$

Maintaining a time-independent equation reduces the number of variables and allows the system to be solved by discretization. Time-dependance (changes in the fuel composition with time due to interaction with neutrons) can be handled using the Bateman equation [25].

Solving for the flux in the neutron transport equation can be done using several methods. In this work, two main methods were considered:

- Using a fixed buckling and choosing the infinite lattice multiplication factor (k-infinite) as the eigenvalue.
- Using a fixed effective multiplication factor (k-effective) and choosing the critical buckling as the eigenvalue.

Where the “buckling” describes the shape of the spatial distribution of the neutron flux. In simple geometries, the neutron flux typically peaks near the centre and drops to zero near the edges resembling the shape of a beam buckling under compression. The second method (known in DRAGON as “type B”) was chosen for this work as it is considered to give a more accurate representation of the flux [26] [27]. To ensure that the solution method did not significantly impact the calculated two group homogenized cross section covariance results, the calculations were repeated using the first method (known in DRAGON as “type K”). The results are given in Appendix F and the input files for each of these cases are given in Appendix G.

2.8 Existing Tools for Uncertainty Analysis

There exist several tools for assessing and propagating the uncertainty in lattice physics calculations. Table 2.8 below summarizes these tools and the covariance data they use to perform uncertainty analysis.

¹⁶ A useful consequence of this is the inability of deterministic neutron transport codes to be used to design highly supercritical systems such as explosives.

Table 2.8 – Tools Currently Available for Lattice Physics Uncertainty Analysis

Tool	Description
SCALE (TSUNAMI)	Only program able to account for the implicit effect that cross sections have on each other due to the background cross section used in self-shielding [3]. However TSUNAMI calculates the final uncertainties using the sandwich rule [see equation (1.15)] and the covariances used come from the SCALE covariance library.
SUSD3D	Designed to compute the uncertainty with the sandwich rule using either the output of NJOY or PUFF-2 and can also read the ZZ-VITAMIN-J/COVA library [28].
XSUSA	Performs a Monte Carlo sampling of self-shielded cross sections using the SCALE covariance library [29].
CASMO-5/DP	Proprietary CASMO-5 nuclear data library does not include covariances so the SCALE covariance library is used along with the sandwich rule [30].
DINOSAUR	Can use either the sandwich rule or Monte Carlo sampling of multigroup library cross sections for uncertainty analysis. In both cases the SCALE covariance library is used [3].

From the table above, it is clear that there are 4 main sources of covariance data: SCALE, NJOY, PUFF, and ZZ-VITAMIN-J/COVA. Of these, only SCALE and ZZ-VITAMIN-J/COVA are actual multigroup covariance libraries, NJOY and PUFF are codes that can be used to read the covariance data in evaluated nuclear data libraries such as ENDF/B-VII to produce multigroup covariance data. However NJOY only produces covariances for cross sections at infinite dilution [18] as described in section 2.4.8. The most recent version of PUFF (PUFF-4) does not claim to be able to produce multigroup covariance data at non-infinite dilutions either¹⁷ [31] [32]. The SCALE covariance library was produced using covariances from various evaluated nuclear data libraries that were processed by the PUFF-4 code so it does not include covariances for finite dilution cross sections [33]. Lastly, the ZZ-VITAMIN-J/COVA covariance library was developed by the NEA [34] using NJOY97.115 which is only capable of outputting multigroup covariance data at infinite dilution [18].

¹⁷ Although it is not explicitly stated in neither the PUFF-4 user manual [31] nor the paper presented at PHYSOR [32] that PUFF-4 cannot process covariance data at non-infinite dilutions, neither of these documents includes any indication that PUFF-4 can produce covariance data at non-infinite dilutions so it is assumed that it does not have this capability.

2.9 Problem Statement and Methodology

After reviewing the tools that currently exist for uncertainty analysis, it is clear that the effect of dilution on multigroup cross section covariance has been either overlooked or assumed to be negligible. In either case, an investigation of the effects of dilution on multigroup cross section covariance is required to demonstrate definitively what effect, if any, it will have on the uncertainty in the output of transport calculations and that is the goal of this work.

The typical procedure for Monte Carlo uncertainty propagation in DINOSAUR is detailed on the left side of Figure 2.14. A multigroup library is created by processing an evaluated nuclear data library using a code such as NJOY. This library is then perturbed according to the covariance data in the SCALE covariance library¹⁸. However recall from the previous section that these covariances are for cross sections at **infinite dilution**. Each perturbed library is then used to simulate a lattice cell in DRAGON and the distribution in the results is used to calculate the uncertainty.

¹⁸ Note the SCALE covariance library is interpolated to 69 or 172 groups using ANGELO2 to match the group structure in WIMS-D4.

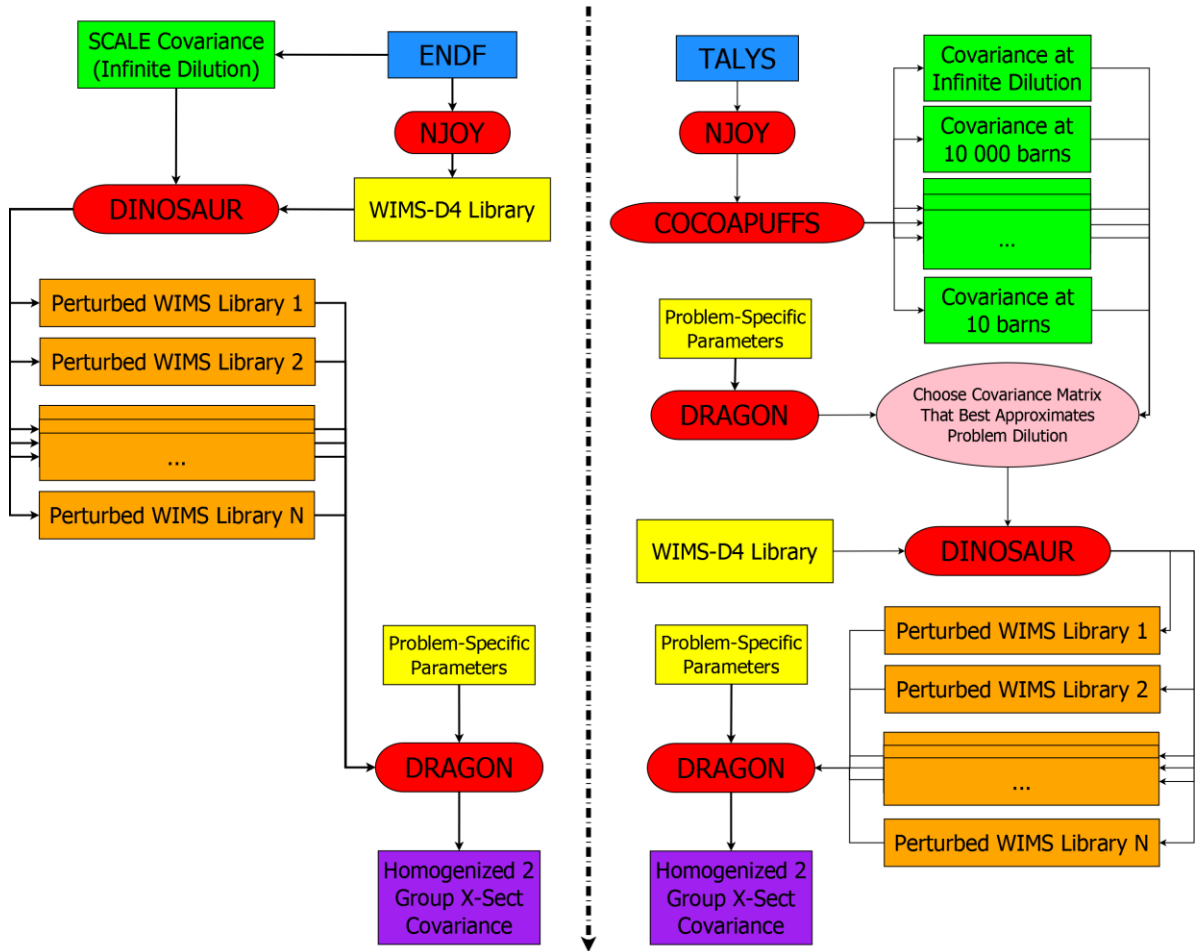


Figure 2.14 – Implementations of Monte Carlo Uncertainty Propagation Using DINOSAUR Alone (left) and the Modified Methodology Developed in This Work (right)

The procedure on the right side is the one that was implemented in this work to take into account the effect of using dilution-dependent covariances for statistical sampling. The perturbed TENDL format libraries calculated by the NRG using TALYS (see section 2.3) are used to generate many perturbed multigroup libraries with NJOY. Since the cross sections in these libraries are evaluated at multiple values of dilution, covariance matrices between these cross sections at varying levels of dilution can be produced and this is done using the COCOAPUFFS code developed during this work. The dilution is then calculated for a specific problem in DRAGON for each resonant energy group and the average is taken over these groups for each isotope. The covariance matrix which most closely corresponds to the average dilution value of the resonant groups in each isotope is then chosen. The procedure after this point is essentially identical to the normal procedure in DINOSAUR as detailed on the left in Figure 2.14. The selected finite dilution covariance matrix is used to perturb an existing multigroup

library. Each perturbed library is then used to simulate a lattice cell in DRAGON and the distribution in the results is used to calculate the uncertainty.

Only the isotopes U235 and U238 were processed at multiple values of dilution. This is because the DRAGON simulations were performed for fresh fuel only with no burnup and thus U235 and U238 are expected to be the dominating sources of uncertainty. Only the reactions MT=2 (elastic scattering), MT=18 (fission), and MT=102 (radiative capture) were evaluated at multiple values of dilution since these are typically the only isotopes processed at multiple values of dilution by NJOY for use in WIMS-D4 libraries. To ensure any differences seen in the results were only a result of the dilution of the covariance matrix, a SCALE/TENDL hybrid covariance library was prepared for this study which combines the SCALE covariances normally used in DINOSAUR and the covariances between the TENDL libraries calculated using COCOAPUFFS for U235 and U238. That is to say that the covariances for U235 and U238 in the SCALE covariance library were replaced by those calculated using COCOAPUFFS at infinite dilution. An uncertainty calculation was then done in DINOSAUR to establish the results for infinite dilution covariances only. The changes made to the SCALE covariance library are summarized in Figure 2.15.

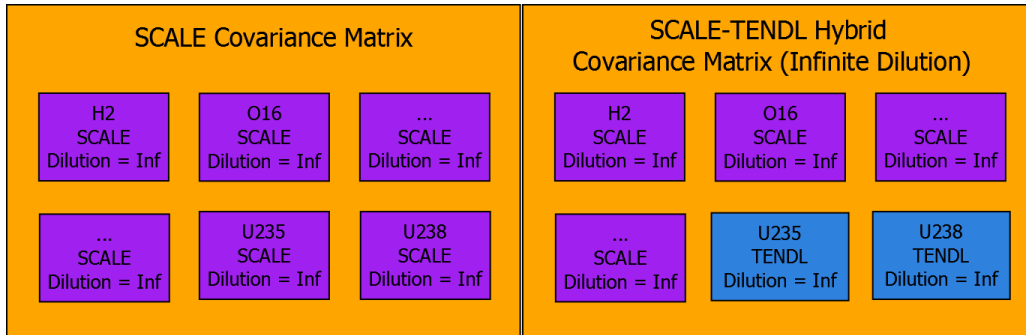


Figure 2.15 – Creation of a SCALE/TENDL Hybrid Covariance Library

Next the covariances calculated with COCOAPUFFS at the problem dilution for U235 and U238 reactions MT=2 (elastic scattering), MT=18 (fission), and MT=102 (radiative capture) were substituted into the SCALE/TENDL hybrid covariance library (see Figure 2.16). Thus the only difference between this matrix and the one used for the first calculation was that the covariances and cross covariances for MT=2 (elastic scattering), MT=18 (fission), and MT=102 (radiative capture) were calculated at the correct problem dilution instead of infinite dilution. This change is shown in Figure 2.17 and Figure 2.18 for U238 as an example. An uncertainty calculation was then performed in DINOSAUR to establish the results for finite dilution covariances and the results between the infinite and finite dilution results were compared. Note that simulations using the

SCALE covariances and the SCALE/TENDL hybrid covariances were also done and are included in the results.

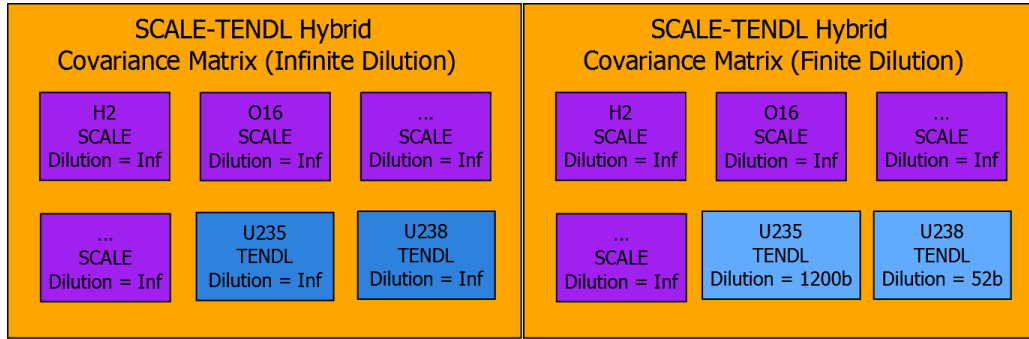


Figure 2.16 – Creation of a SCALE-TENDL Finite Dilution Covariance Library from the SCALE-TENDL Infinite Dilution Covariance Library

		Elastic Scattering	Inelastic Scattering	(n,2n)	Fission	Radiative Capture (n,gamma)	(n,alpha)	Fission Spectrum	Fission Neutron Yield (Nu)
		1 2 ... 68 69	1 2 ... 68 69	1 2 ... 68 69	1 2 ... 68 69	1 2 ... 68 69	1 2 ... 68 69	1 2 ... 68 69	1 2 ... 68 69
Elastic Scattering	1 2 ... 68 69	TENDL Dilution = Inf	TENDL Dilution = Inf	TENDL Dilution = Inf	TENDL Dilution = Inf	TENDL Dilution = Inf	TENDL Dilution = Inf	TENDL Dilution = Inf	TENDL Dilution = Inf
Inelastic Scattering	1 2 ... 68 69	TENDL Dilution = Inf	TENDL Dilution = Inf	TENDL Dilution = Inf	TENDL Dilution = Inf	TENDL Dilution = Inf	TENDL Dilution = Inf	TENDL Dilution = Inf	TENDL Dilution = Inf
(n,2n)	1 2 ... 68 69	TENDL Dilution = Inf	TENDL Dilution = Inf	TENDL Dilution = Inf	TENDL Dilution = Inf	TENDL Dilution = Inf	TENDL Dilution = Inf	TENDL Dilution = Inf	TENDL Dilution = Inf
Fission	1 2 ... 68 69	TENDL Dilution = Inf	TENDL Dilution = Inf	TENDL Dilution = Inf	TENDL Dilution = Inf	TENDL Dilution = Inf	TENDL Dilution = Inf	TENDL Dilution = Inf	TENDL Dilution = Inf
Radiative Capture (n,gamma)	1 2 ... 68 69	TENDL Dilution = Inf	TENDL Dilution = Inf	TENDL Dilution = Inf	TENDL Dilution = Inf	TENDL Dilution = Inf	TENDL Dilution = Inf	TENDL Dilution = Inf	TENDL Dilution = Inf
(n,alpha)	1 2 ... 68 69	TENDL Dilution = Inf	TENDL Dilution = Inf	TENDL Dilution = Inf	TENDL Dilution = Inf	TENDL Dilution = Inf	TENDL Dilution = Inf	TENDL Dilution = Inf	TENDL Dilution = Inf
Fission Spectrum	1 2 ... 68 69	TENDL Dilution = Inf	TENDL Dilution = Inf	TENDL Dilution = Inf	TENDL Dilution = Inf	TENDL Dilution = Inf	TENDL Dilution = Inf	TENDL Dilution = Inf	TENDL Dilution = Inf
Fission Neutron Yield (Nu)	1 2 ... 68 69	TENDL Dilution = Inf	TENDL Dilution = Inf	TENDL Dilution = Inf	TENDL Dilution = Inf	TENDL Dilution = Inf	TENDL Dilution = Inf	TENDL Dilution = Inf	TENDL Dilution = Inf

Figure 2.17 – Depiction of the U238 Covariance Matrix in the SCALE-TENDL Hybrid Covariance Library at Infinite Dilution

		Elastic Scattering	Inelastic Scattering	(n,2n)	Fission	Radiative Capture (n,gamma)	(n,alpha)	Fission Spectrum	Fission Neutron Yield (Nu)
		1 2 ... 68 69	1 2 ... 68 69	1 2 ... 68 69	1 2 ... 68 69	1 2 ... 68 69	1 2 ... 68 69	1 2 ... 68 69	1 2 ... 68 69
Elastic Scattering	1								
	2								
	...								
	68								
	69								
Inelastic Scattering	1								
	2								
	...								
	68								
	69								
(n,2n)	1								
	2								
	...								
	68								
	69								
Fission	1								
	2								
	...								
	68								
	69								
Radiative Capture (n,gamma)	1								
	2								
	...								
	68								
	69								
(n,alpha)	1								
	2								
	...								
	68								
	69								
Fission Spectrum	1								
	2								
	...								
	68								
	69								
Fission Neutron Yield (Nu)	1								
	2								
	...								
	68								
	69								

Figure 2.18 – Depiction of the U238 Covariance Matrix in the SCALE-TENDL Hybrid Covariance Library at The Problem Dilution

To summarize, the first results section (Chapter 3) contains multigroup covariance matrices from ENDF/B-VII, SCALE, and multigroup covariance matrices calculated using the perturbed TENDL libraries for comparison. The effects of parameters such as temperature and dilution on the multigroup covariance in TENDL are shown as well. The second results section (Chapter 4) shows the results of uncertainty propagation on the few group homogenized cross sections and k-infinite when using infinite and finite dilution multigroup covariances as well as when using SCALE only vs. the SCALE/TENDL hybrid covariance library created for this work.

Chapter 3

Analysis of Multigroup Covariance

After processing an evaluated nuclear data library with NJOY, the user will have at their disposal a multigroup library which can be used with a transport code such as DRAGON to calculate the homogenized few group cross sections which will be in turn used in a full core diffusion calculation. This chapter investigates the effects of different evaluations, temperature, and dilution on the multigroup library covariance (specifically in 69 groups).

3.1 Covariances from Different Evaluations

As shown in Chapter 1, the calculated uncertainty in the output will depend on the input parameter covariance matrix. Below is a comparison of the 69 group covariances between different groups for the U238 fission cross section according to TENDL (calculated using COCOAPUFFS), ENDF/B-VII (calculated using the ERRORR module of NJOY), and SCALE (interpolated from 44 groups by ANGELO2).

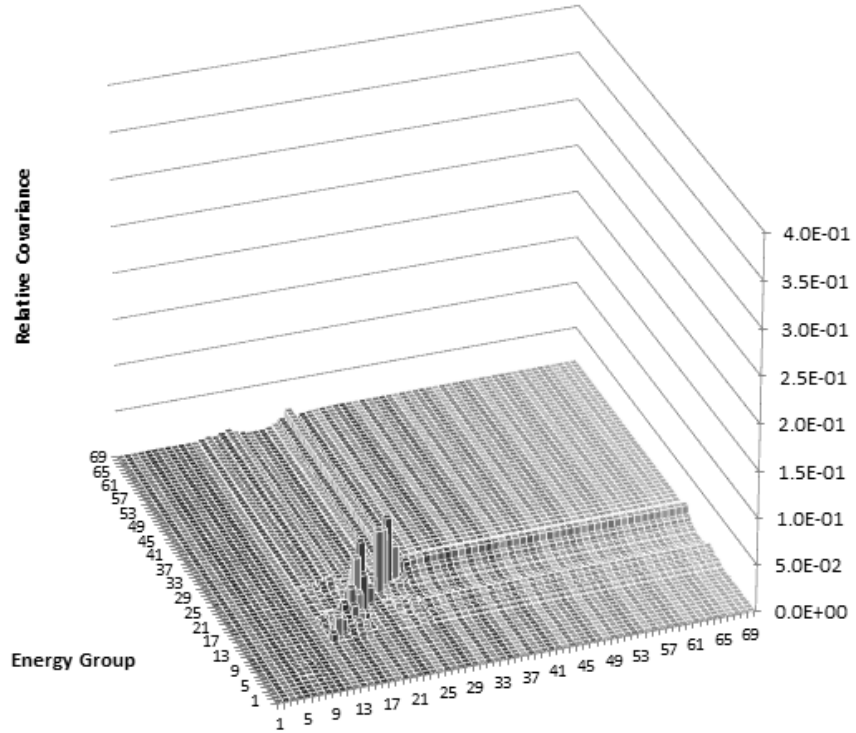


Figure 3.1 – Calculated TENDL Covariance in 69 Groups for U238 Reaction MT 18 (fission)

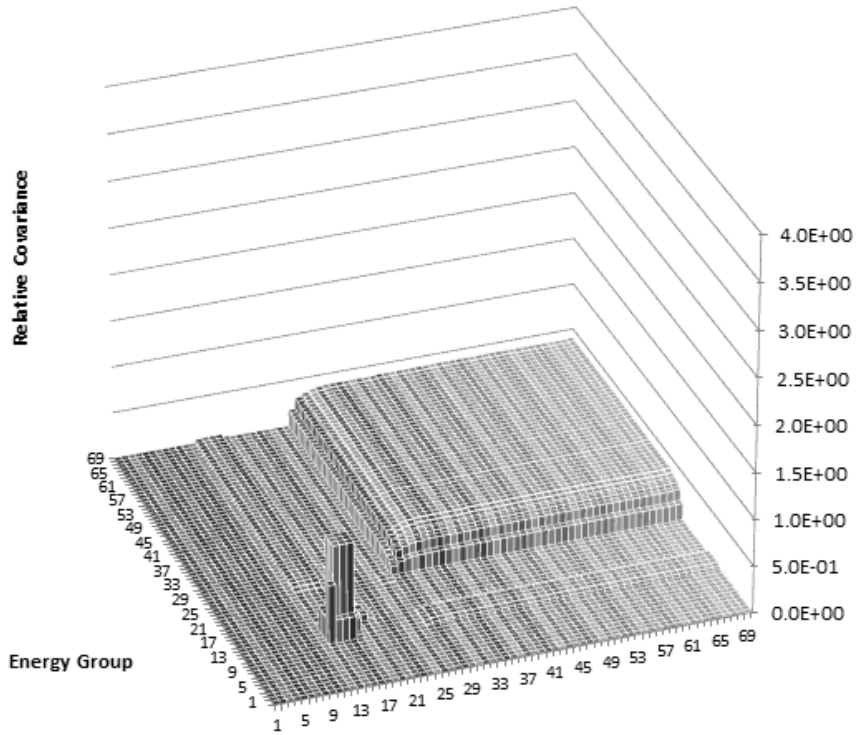


Figure 3.2 – 44 Group SCALE Covariance Interpolated to 69 Groups Using ANGELO2 for U238 Reaction MT 18 (fission) [3]

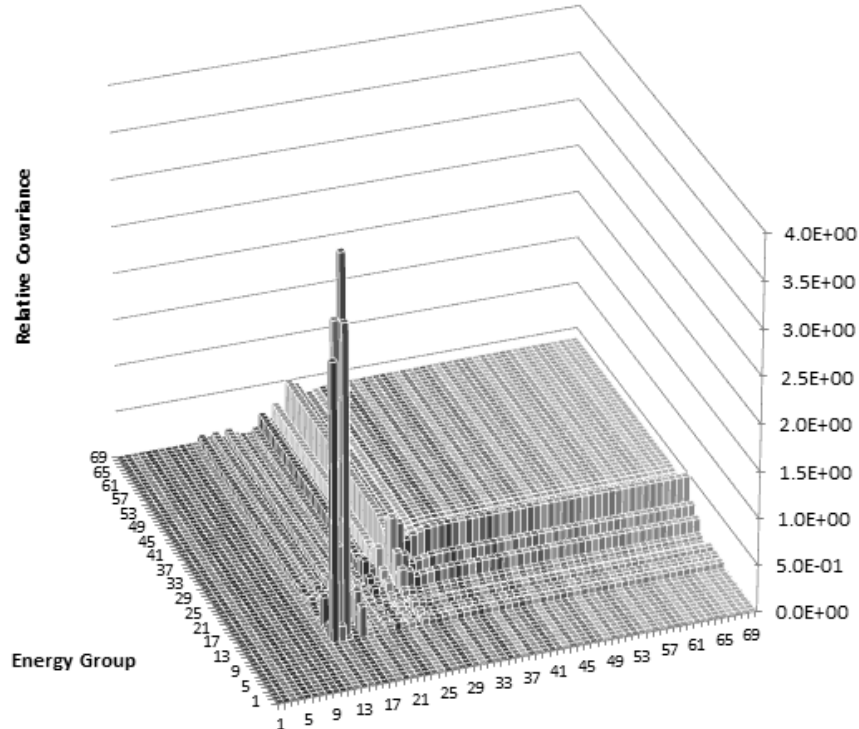


Figure 3.3 – Calculated ENDF Covariance Using ERRORR in NJOY in 69 Groups for U238 Reaction MT 18 (Fission)¹⁹

Since the SCALE covariance is based on the ENDF/B-VI evaluation, it is not surprising that it agrees fairly well with ENDF/B-VII. The TENDL covariances however come from a completely different evaluation and vary from those of SCALE/ENDF by one or even two orders of magnitude in some cases. In the plots above, the peak value in the ENDF covariance occurs between group 15 and group 15 and attains a value of $1.66\text{E}+1$. For comparison, the highest peak in the SCALE covariance (also occurring at the covariance between group 15 and group 15) reaches a height of $1.0\text{E}+0$. Finally, the TENDL covariance at group 15 and group 15 is only $6.96\text{E}-2$. This however is not the largest value, the peak value occurs between group 25 and group 25 and is $1.38\text{E}-2$. The rest of the plots for U238 are available in Appendix A. In general the TENDL covariances follow a similar shape as their counterparts in SCALE and ENDF but they often differ greatly in magnitude.

¹⁹ The largest peak actually attains a value of $1.66\text{E}+1$ and is truncated by the scale on this graph. However the scale was chosen to permit more detail to be seen and for better comparison with the other plots.

3.2 Temperature Effect

When an evaluated nuclear data library is processed by NJOY into a multigroup library, some isotopes (namely U235 and U238) will contain cross sections at multiple temperatures. To investigate any possible temperature effect on the covariance, COCOAPUFFS was used to calculate covariance matrices corresponding to different temperatures for U235 and U238. The covariance was found to change by less than 1% for most reactions but in some cases large changes were observed. Table 3.1 shows the largest relative change seen for each reaction type between the covariances at 293K and 1100K. Note that only the covariance within reaction types was considered (i.e. covariances between reactions were not considered).

Table 3.1 – Maximum Relative Change in Covariance Between 293K and 1100K

Reaction	MT Number	U235	U238
Fission	18	1.46E+2	2.5E-2
Radiative Capture	102	1.10E+1	3.3E+0
Elastic Scattering	2	3.80E-2	2.0E-1
(n, α)	107	3.80E-1	N/A
$\bar{\nu}$	452	3.98E-10	4.45E-6
Inelastic Scattering	4	0.00E+0	0.0E+0
(n,2n)	16	0.00E+0	0.0E+0
Fission Spectrum	N/A	0.00E+0	0.00E+0

In particular, MT 18 and MT 102 (fission and radiative capture respectively) for U235 stand out. Although they did experience some large changes with temperature, the majority of entries in these matrices changed by less than 1%. To eliminate the possibility that these changes were simply the result of numerical noise²⁰, plots were made that show the absolute change in covariance between 293K and 1100K for these two reactions.

²⁰ Subtraction with very small covariances can yield numbers on the order of the precision of the floats that represent them so they may appear to change dramatically relative to their original value.

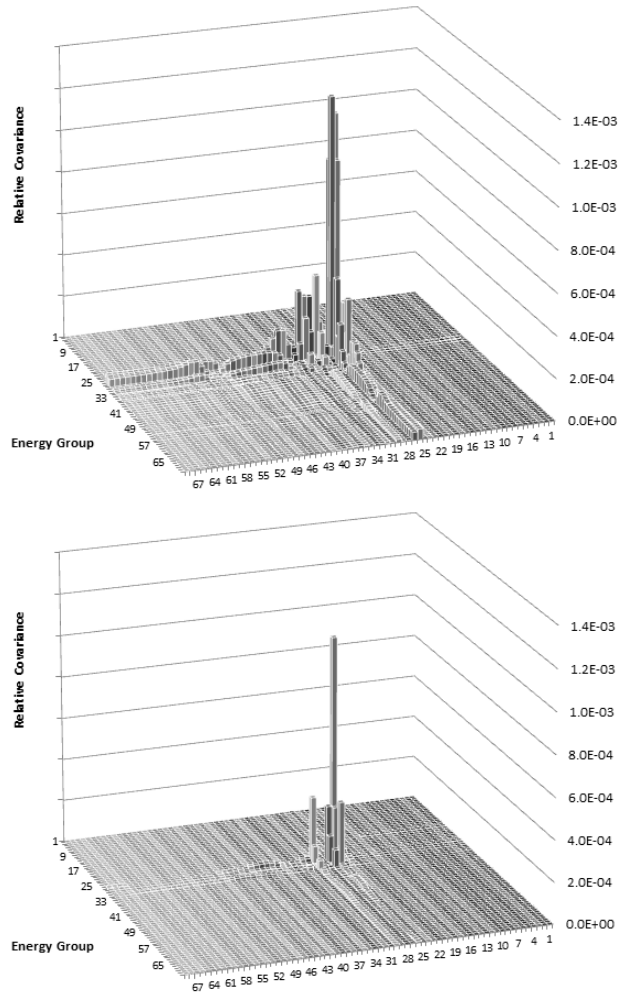


Figure 3.4 - Absolute Change in Relative Covariance for U235 Between 293K and 1100K for MT 18 (above) and MT 102 (below)

Looking at the covariance matrices for these two reactions, it is clear that the temperature dependence is generally confined to certain parts of the resonance region. Otherwise the temperature difference is negligible. It is thus concluded that while there are a few regions where the covariance depends on temperature, in the vast majority of cases the temperature dependence of the covariance is small.

3.3 Dilution Effect

When condensing a continuous energy cross section into a multigroup cross section, isotopes that are strong resonance absorbers require a spectral self-shielding correction to their cross sections in the resonance regions when these isotopes are present in significant quantities. This is because large peaks in the cross section at certain energies will cause the neutron flux to dip in the vicinity of

the peak and thus decrease the reaction rate near this energy. As a result, the multigroup cross sections for resonance absorbing isotopes are calculated in NJOY at several different levels of dilution. Once the proper dilution is found for a specific problem, the proper cross section can be interpolated from the dilutions present in the multigroup library. The value of a cross section at a non infinite dilution depends on the background cross section, which is the combined cross section of all the other isotopes present in the mix and the evaluated cross section at that energy. Since there will be uncertainty in the values of the cross sections that compose the background cross section, cross sections at non infinite dilutions may have a higher uncertainty than their infinite dilution counterparts. On the other hand, the self-shielding calculation reduces the reaction rate near resonance peaks which can also reduce the amount of uncertainty that this peak will contribute to the output. Thus there is a competing effect between more background cross section uncertainty and a smaller uncertainty contribution from some resonance peaks in the cross section.

To investigate the effect of dilution, COCOAPUFFS was used to generate a set of covariance matrices at various dilutions. Plots for each of the reaction types studies are included in Appendix C and Appendix D. It was noted that while all covariance matrices had some energy ranges that increased in uncertainty and some that decreased, the general trend for U235 was a decrease in uncertainty with dilution while for U238 the uncertainty typically increased. For both isotopes, the most significant change was seen in the scattering cross section (MT 2) and the difference is shown below. Note that for U238, the covariance increased in most of the resonance region while for U235 there is a slight decrease near the peak seen in the U235 MT 2 covariance (Figure 3.5 and Figure 3.6). The figures below have been plotted in terms of absolute change in covariance as opposed to relative change to prevent numerical noise on small numbers from obscuring the data. A table comparing the maximum relative change is also given.

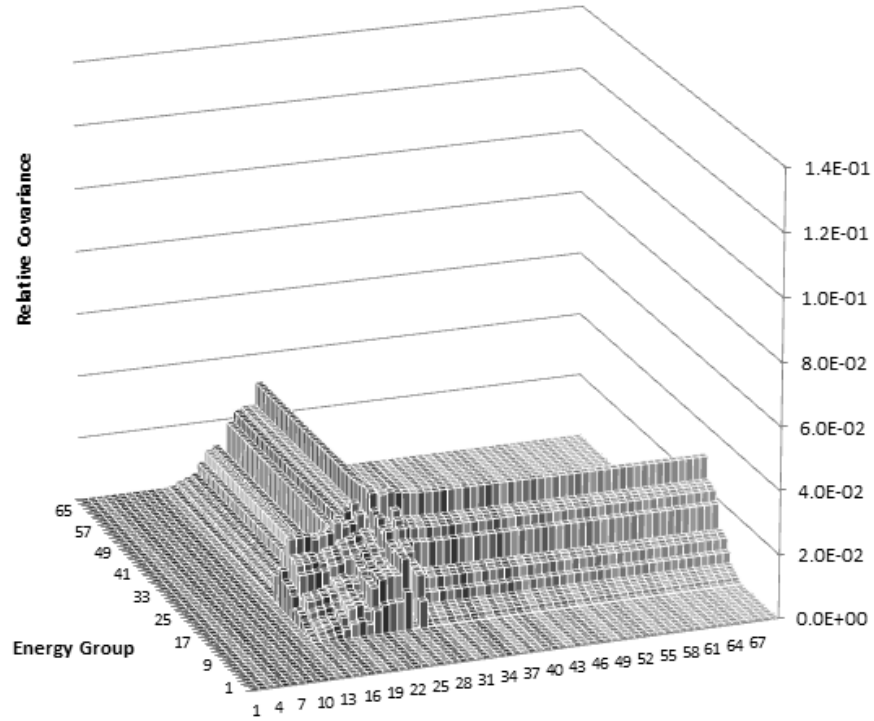


Figure 3.5 - Absolute Change in Relative Covariance for U238 MT 2 Between Infinite Dilution and 52 Barns (52b - ∞)

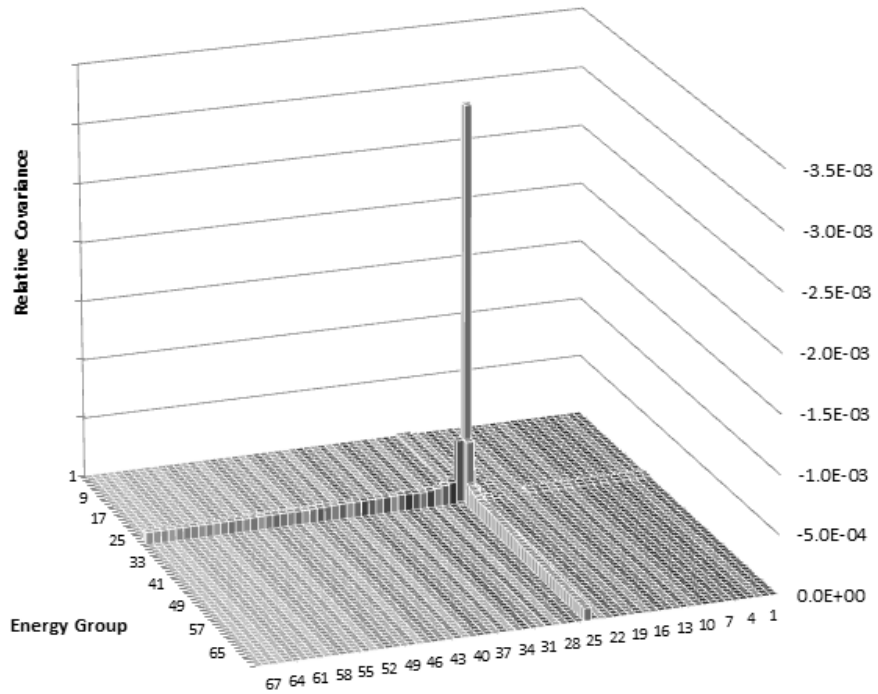


Figure 3.6 – Absolute Change in Relative Covariance for U235 MT 2 Between Infinite Dilution and 800 Barns (800b - ∞)

Table 3.2 - Maximum Relative Change With Dilution²¹

Reaction	U235	U238
2	3.5E+0	1.1E+2
18	3.2E+2	2.1E+2
102	5.8E+1	6.2E+3

It is clear that the dilution has a significant effect on the covariance. Changes of several hundred percent were not uncommon for many energy groups in the resonance region when comparing an infinite dilution covariance matrix to a non-infinite one. Moreover, the large changes seen are not highly localized as was seen in the case of temperature. They are widespread in the resonance region and thus it appears that using an infinite dilution covariance matrix is a poor approximation for the true finite dilution covariance values. The following section examines how these changes affect the calculated covariance between homogenized few group parameters when a cell homogenization calculation is performed in the code DRAGON.

²¹ For U235 the dilution used was 8.0E+2 barns and for U238 it was 5.2E+1 barns

Chapter 4

Analysis of Homogenized Few Group Covariance

Once the user has found the homogenized few group properties of each of the cells that compose a full reactor, they can be used as input to a full core diffusion code. In order to propagate error from nuclear data through to the full core calculation, the covariance in the homogenized few group properties are required²². This chapter looks at the effect of differing reference values, input covariance matrices, and dilutions on the resulting 2 group homogenized cross section covariance and k-infinity for the TMI PWR cell at hot full power (HFP) as outlined in the OECD NEA UAM benchmark [15]. The cell was modelled in DRAGON using 12 tracking angles (angular quadrature parameter of 12) and a polar quadrature order of 20.0. The full model input file can be found in Appendix G.

4.1 Input Covariance Matrix Effect

As discussed in the introduction, the input parameter covariance matrix has a direct effect on the calculated output uncertainties so if two very different matrices are used as input, one would expect a large change in the calculated uncertainty. However there are some effects which could reduce the impact such as flux averaging. In a transport code, the multigroup input cross sections are put through one spectral and one spatial averaging calculation to produce homogenized few group properties for the cell. Note that these calculations are different from the spectral flux averaging done in NJOY to condense a continuous energy cross section into multigroup format. Flux averaging can potentially reduce the error contribution by some of the large peaks in the cross section as mentioned in section 3.3. Shown below are the covariances between the 2 group homogenized cross sections calculated with DRAGON for the TMI PWR cell at HFP. A comparison is shown between the results obtained by the SCALE and TENDL 69 group covariances to various 69 group libraries in WIMS-D4 format

²² This is assuming the user doesn't have a set of perturbed few group properties at their disposal from the transport calculation.

available from the IAEA WLUP website²³. The 2 group covariance was calculated in each case by using the Monte Carlo perturbation module of DINOSAUR and the covariances from Chapter 3. The code was run for each library using first the SCALE covariances as input, then again for each library substituting the TENDL covariances for U235 and U238 in the SCALE covariance library. The TENDL covariances were calculated using COCOAPUFFS. The results are displayed in Figure 4.1 - Figure 4.4. The bars in the charts show the absolute value of the relative covariance.

²³ <http://www-nds.iaea.org/wimsd>

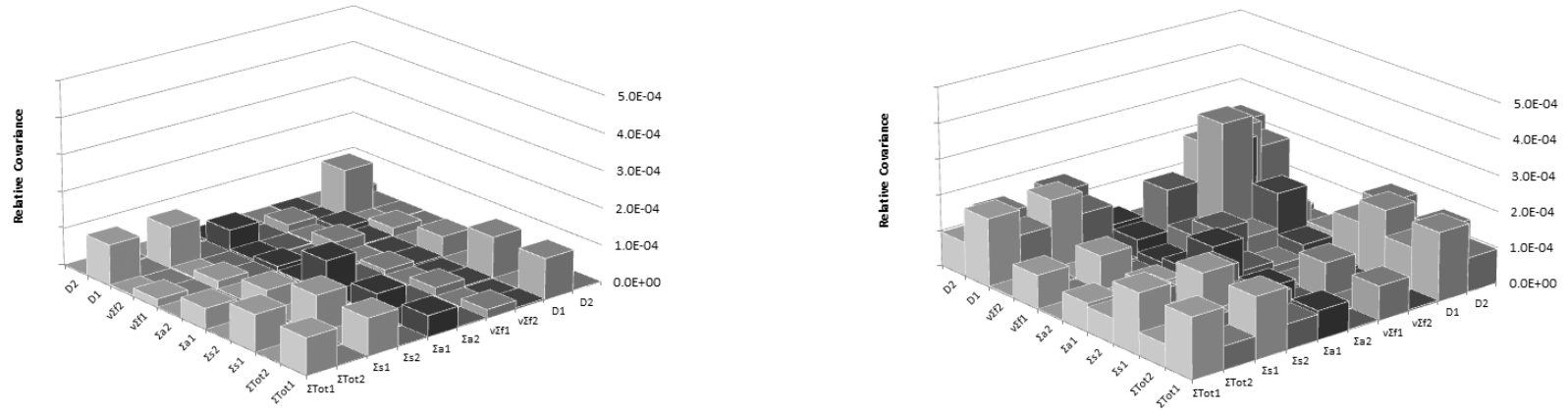


Figure 4.1 – Homogenous 2 Group Covariance from Perturbation of the 69 Group ENDF/B-VI Library Using Covariances from SCALE (left) and TENDL (right)

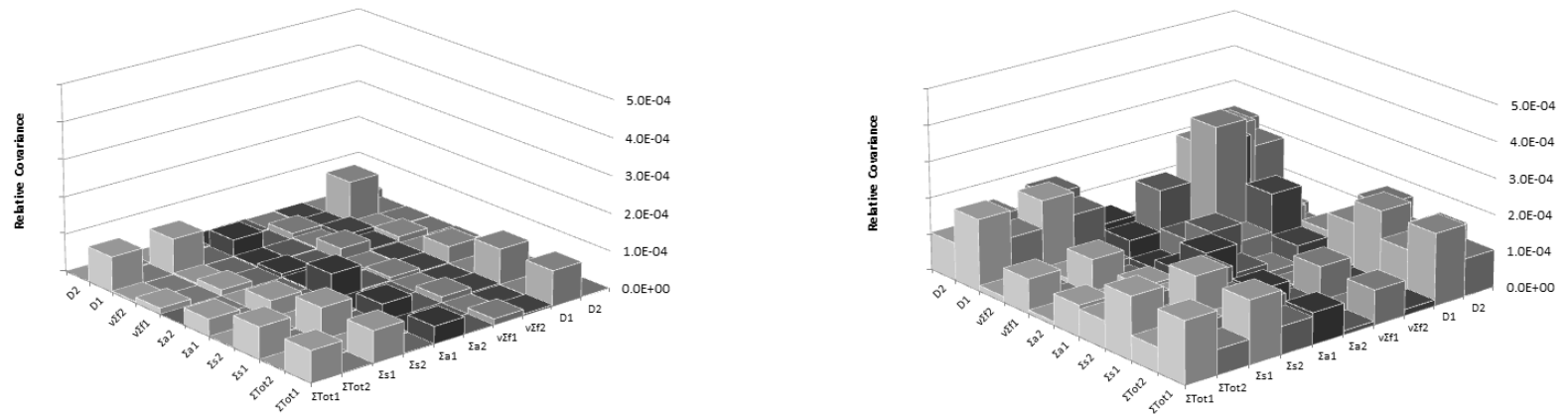


Figure 4.2 - Homogenous 2 Group Covariance from Perturbation of the 69 Group ENDF/B-VII Library Using Covariance from SCALE (left) and TENDL (right)

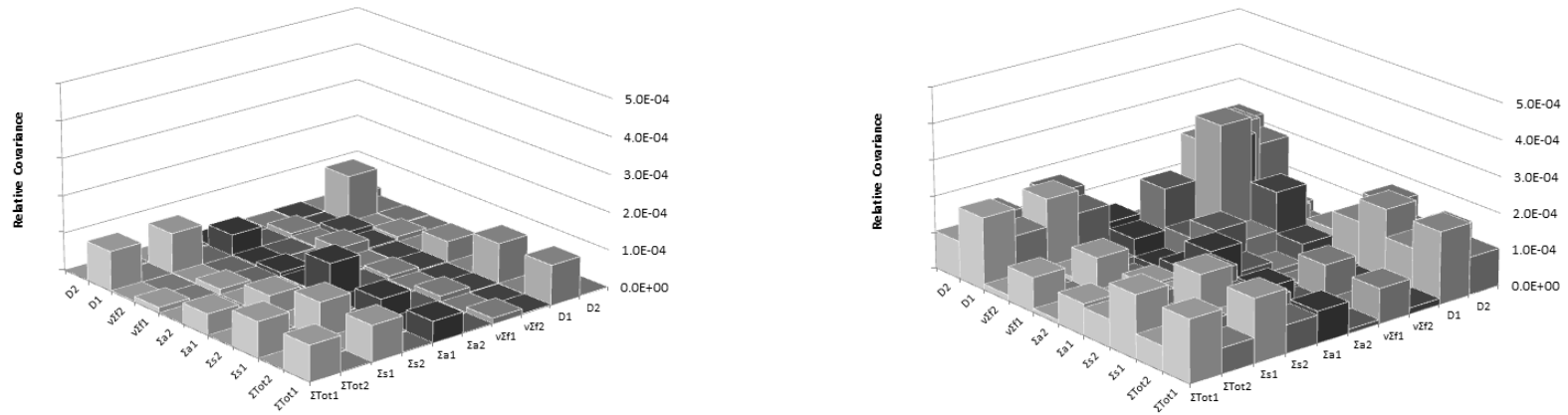


Figure 4.3 - Homogenous 2 Group Covariance from Perturbation of the 69 Group IAEA Library Using Covariance from SCALE (left) and TENDL (right)

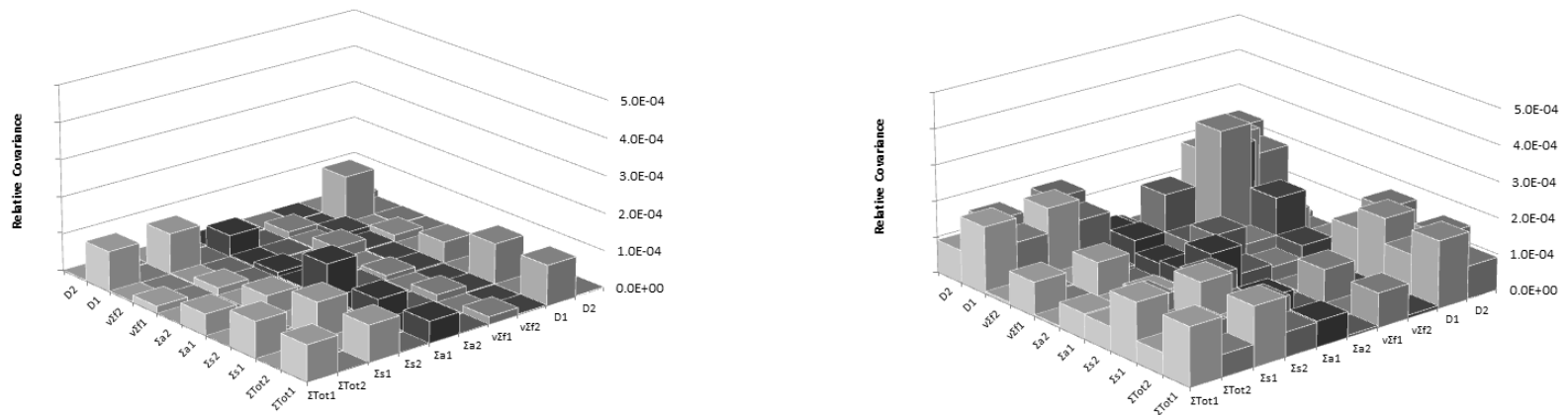


Figure 4.4 - Homogenous 2 Group Covariance from Perturbation of the 69 Group JEFF2.2 Library Using Covariances from SCALE (left) and TENDL (right)

There are two important results to be taken from these graphs and they are summarized as follows:

- A bias shift in the multigroup cross sections being perturbed has a negligible effect on the few group covariance.
- Changing the covariance matrix used to perform perturbations has a significant effect on the few group covariance.

It is thus concluded that while one can apply a set of covariances to a different library without significantly affecting the results, applying a different covariance matrix to any given library will have a significant effect. The severity of the difference will depend directly on how much the two covariance matrices differ. In the case of TENDL and SCALE, the differences are particularly striking since these covariance matrices differ considerably.

Although it is not required by full core diffusion codes, the k-infinity value calculated in transport codes is a useful indicator of how changes in the fuel affect the overall reactivity. As such, the uncertainty in k-infinite was also calculated using the SCALE and TENDL covariances. The results are shown in Figure 4.5. The uncertainty in the standard deviation in k-infinite was calculated using the standard deviation estimator formula (see equation (1.11)). The uncertainties in the plot represent a 95% confidence interval (two standard deviations). It is clear that TENDL predicts a statistically significantly higher uncertainty for k-infinite than the SCALE covariances. This is not surprising since, as can be seen in Figure 4.1 - Figure 4.4, TENDL consistently predicted a higher covariance between few group fission cross sections. Conversely, no significant difference is seen when applying perturbations to different multigroup libraries as shown in Figure 4.5.

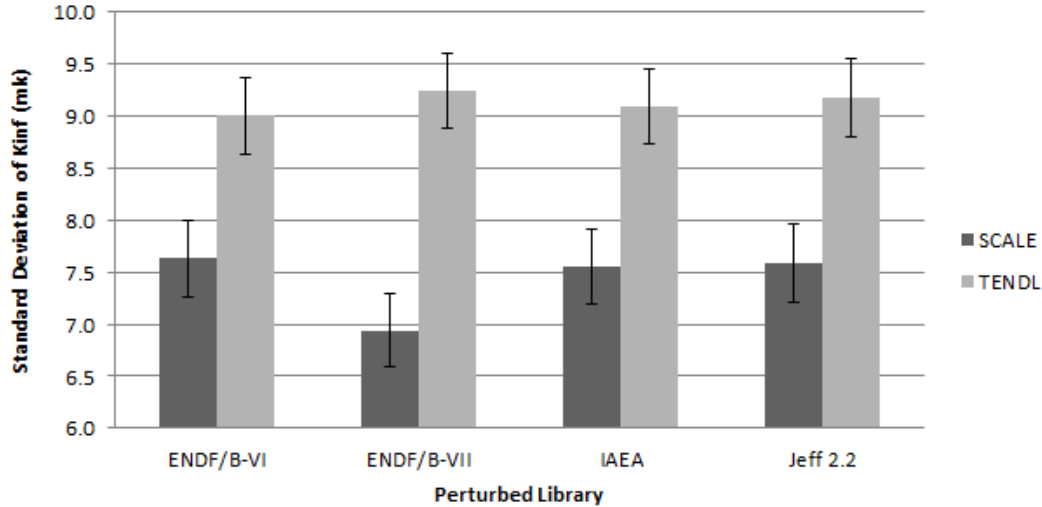


Figure 4.5 Standard Deviation of K-Inf Resulting from Perturbations of Various Libraries Using SCALE and TENDL Covariances

4.2 Dilution Effect

It was shown in section 3.3 that dilution can have a significant impact on the covariance between cross sections. Increases and decreases were seen in the input parameter covariance matrices when the dilution was changed and it was concluded that the infinite dilution covariance matrix was not an adequate substitute for cross sections at non-infinite dilutions. In this section, the results of Monte Carlo perturbations in DINOSAUR on the TMI PWR pin cell at HFP were analyzed using infinite dilution covariances and finite dilution covariances. The finite dilution values for U235 and U238 were calculated for reactions MT 2, MT 18, and MT 102 only since these were the only reactions available in the NJOY output at multiple dilutions. All other reactions were left at their infinite dilution values. Note that cross covariances²⁴ were also left at their infinite dilution values with the exception of cross covariances between MT 2, MT 18, and MT 102. The infinite dilution simulations were performed using the SCALE covariance library with the covariances of U235 and U238 replaced by the TENDL covariances calculated using COCOAPUFFS. Next, the dilutions of U235 and U238 in the TMI pin cell were found using DRAGON and the covariance matrices at the closest available dilution (for the reactions MT 2, MT 18, and MT 102) were selected for each isotope. These covariances and the cross covariances between these three reactions were then substituted for their infinite dilution counterparts in the covariance matrix used for the infinite dilution simulation. The reader is encouraged to review section 2.9 for a more detailed description. Table 4.1 below

²⁴ Cross covariance refer to covariances between covariances in different reactions. For example the covariance between group 23 in MT 2 and group 23 in MT 102 would be a cross covariance.

shows the calculated dilutions by group and the corresponding dilution of the selected covariance matrix.

Table 4.1 – Calculated Problem Dilutions and Chosen Covariance Dilution

Energy Group		Dilution (barns)	
Group	Energy Range (eV)	U235	U238
15	5.53E+3 - 9.12E+3	9.87E+2	4.79E+1
16	3.52E+3 - 5.53E+3	9.92E+2	4.82E+1
17	2.24E+3 - 3.52E+3	1.00E+3	4.86E+1
18	1.43E+3 - 2.24E+3	9.86E+2	4.81E+1
19	9.07E+2 - 1.43E+3	9.89E+2	4.81E+1
20	3.67E+2 - 9.07E+2	9.93E+2	4.85E+1
21	1.49E+2 - 3.67E+2	1.01E+3	4.92E+1
22	7.55E+1 - 1.49E+2	1.02E+3	4.93E+1
23	4.81E+1 - 7.55E+1	1.01E+3	5.04E+1
24	2.77E+1 - 4.81E+1	1.07E+3	5.08E+1
25	1.60E+1 - 2.77E+1	1.09E+3	5.14E+1
26	9.88E+0 - 1.60E+1	9.62E+2	5.12E+1
27	4.00E+0 - 9.88E+0	1.12E+3	5.08E+1
Average		1.02E+3	4.94 E+1
Closest Available Dilution		1.20E+3	5.20 E+1

The effect of dilution on the homogenized two group cross section uncertainty is displayed in Figure 4.6 - Figure 4.9. The bars show the absolute value of the relative covariance and some have been coloured to permit easier tracking between plots.

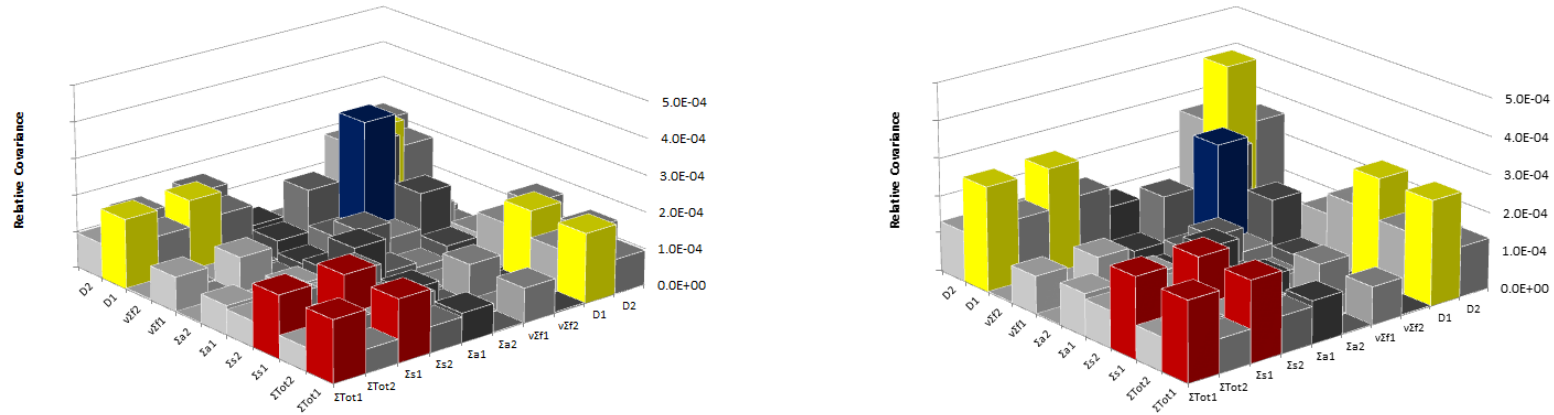


Figure 4.6 - Homogenous 2 Group Covariance from Perturbation of the 69 Group ENDF/B-VI Library Using Infinite (left) and Finite (right) Dilution Covariance

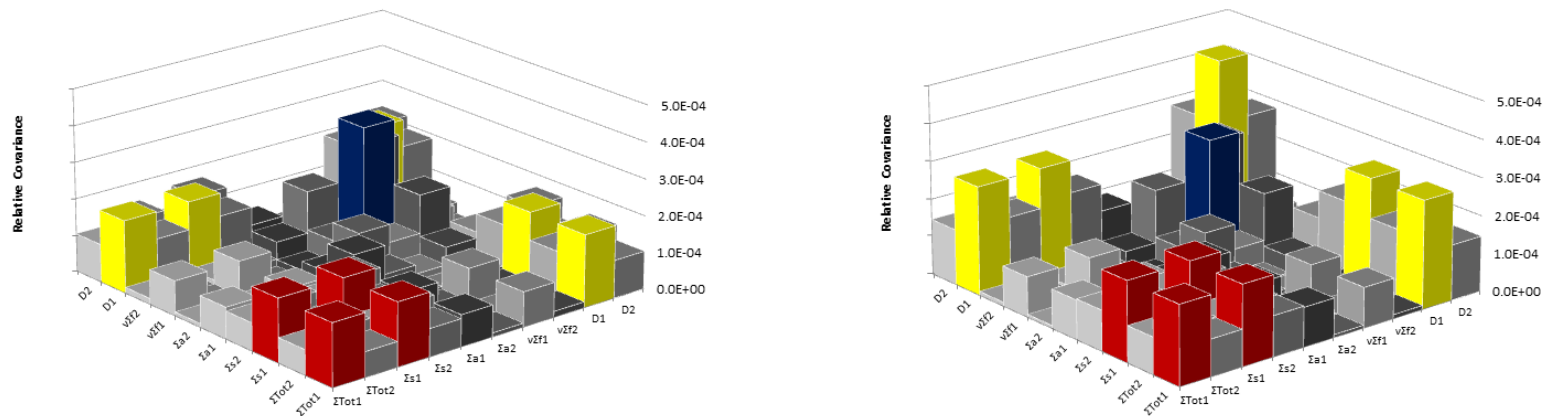


Figure 4.7 - Homogenous 2 Group Covariance from Perturbation of the 69 Group ENDF/B-VII Library Using Infinite (left) and Finite (right) Dilution Covariance

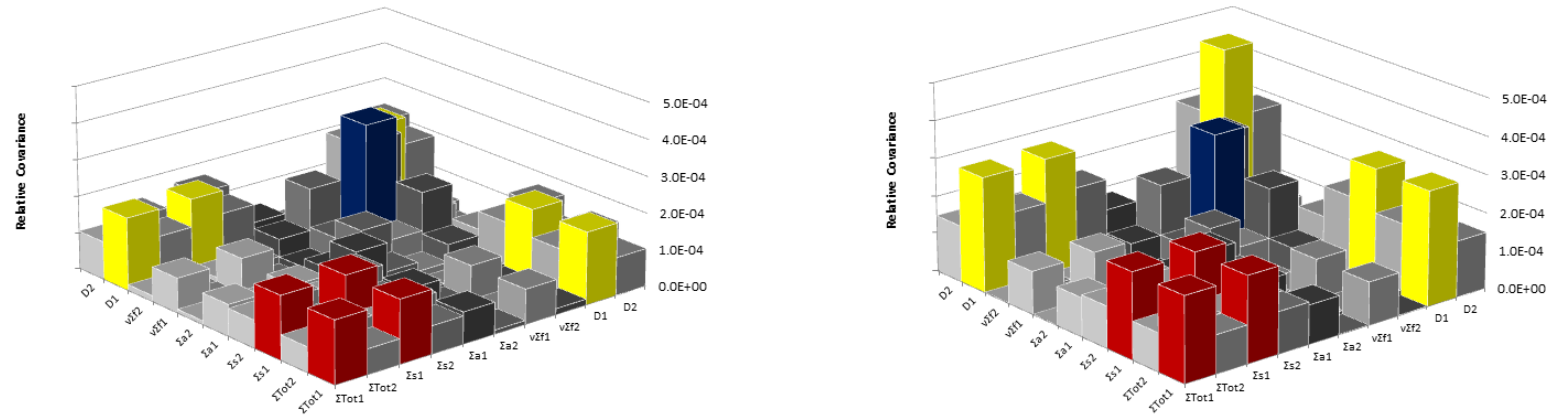


Figure 4.8 - Homogenous 2 Group Covariance from Perturbation of the 69 Group IAEA Library Using Infinite (left) and Finite (right) Dilution Covariance

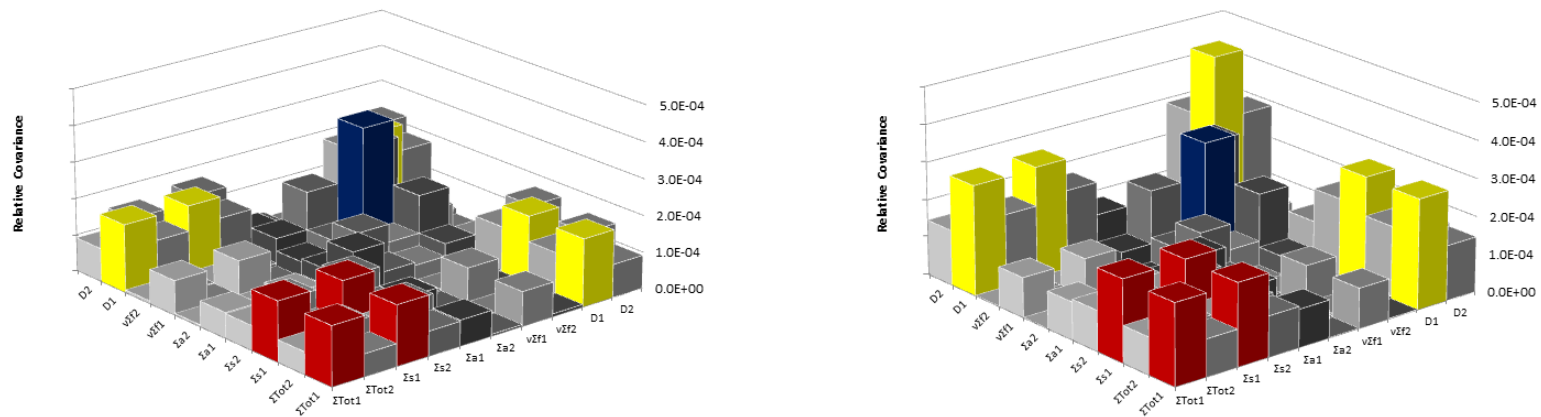


Figure 4.9 - Homogenous 2 Group Covariance from Perturbation of the 69 Group JEFF 2.2 Library Using Infinite (left) and Finite (right) Dilution Covariance

A common feature among these plots is a decrease in the variance²⁵ of $\nu\Sigma_f$ in the fast energy group (group 1) when moving to a finite dilution. This can be seen by following the blue bars in Figure 4.6 - Figure 4.9. An increase in the scattering cross section variance in the fast and thermal groups is also seen which causes an increase in the total cross section uncertainty as well (these bars are highlighted in red). Lastly, a prominent increase in the variance of the diffusion coefficient of the fast energy group can be seen. Since the diffusion coefficient effectively represents how far a neutron can move on average before undergoing a reaction, there is a negative covariance between the diffusion coefficient and the total cross section (which represents the probability of a neutron undergoing a reaction). Note that Figure 4.6 - Figure 4.9 are plotted as absolute values of the relative covariance to better show all of the data so all the bars appear positive. The same plots showing which data points are negative are given in Appendix E. The covariance between the diffusion coefficient and the total cross section increases in magnitude with decreasing dilution in the fast energy group as a result of the increase in the fast energy diffusion coefficient variance. The fast energy diffusion coefficient variance and its covariance with the fast energy total cross section as well as the fast energy scattering cross section are highlighted in yellow in Figure 4.6 - Figure 4.9. Note that the 69 group library chosen for perturbation had no major effect on the results, as was seen in the previous section. The results can be summarized as follows:

- Decrease in the $\nu\Sigma_f$ variance.
- Increase in the fast energy scattering variance which causes a corresponding increase in the covariance between fast energy scattering and the fast energy total cross section.
- Increase in the variance of the fast energy diffusion coefficient which causes an increase in the covariance between the fast energy diffusion coefficient and the fast energy total cross section.

The results here confirm what was claimed in section 3.3: The effect of dilution on the input parameter covariance matrix is indeed significant.

The increases seen in the uncertainty for some cross sections is an important result since it demonstrates that using multigroup covariances evaluated at infinite dilution only is **not a conservative approach**. Ignoring the effects of dilution can result in an underestimation of the uncertainty in the homogenized few group properties that emerge from transport calculations and consequently the uncertainty in any full core calculations performed using these cross sections.

²⁵ Recall that the variance is the covariance between a parameter and itself. The variances in Figure 4.6 - Figure 4.9 can be found along the diagonal.

The effects of using covariances at infinite and finite dilutions on the calculated uncertainty in k -infinite were investigated as well. Perturbations were carried out on several 69 group libraries using infinite and finite dilution covariances and the standard deviation in k -infinite was calculated. The results are plotted in Figure 4.10.

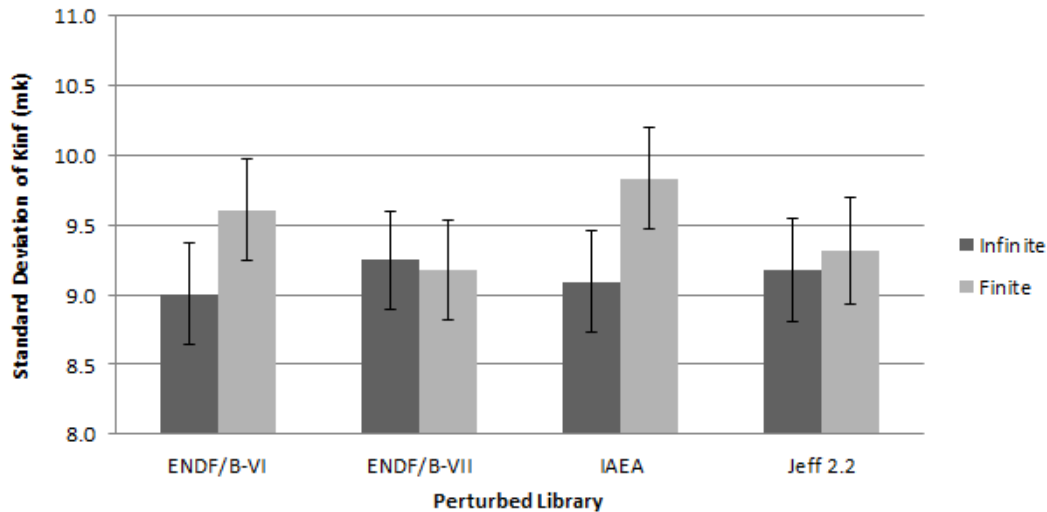


Figure 4.10 – Standard Deviation of K-Inf Resulting from Perturbations of Various Libraries Using Infinite and Finite Dilution Covariances

The uncertainty in the standard deviation in k -infinite was calculated using the standard deviation estimator formula and represents a 95% confidence interval. The results were not able to clearly show a statistically significant effect on the calculated uncertainty in k -infinite neither as a result of dilution nor as a result of the multigroup library chosen for perturbation, although the difference seen when perturbing the IAEA library using infinite and finite dilution covariances does approach statistical significance. However it should be noted that this is not a definitive proof that these effects do not have a statistically significant effect on the calculated uncertainty in k -infinite since it is possible that a study using more perturbations would be able to reduce the uncertainty enough to show such a trend. Furthermore, a study which takes into account the uncertainty in geometry, fuel composition, and burnup may be able to demonstrate a significant effect on the uncertainty in k -infinite when using finite vs. infinite dilution covariances. The uncertainty in k -infinite for the lattice cell is also not generally an indication of the uncertainty in k -effective for a full core calculation so future work which uses the homogenized few group covariance matrices calculated here to perform a Monte Carlo perturbation of a full core simulation are needed to definitively say whether covariance dilution needs to be

taken into account when performing uncertainty analysis on multigroup cross sections.

4.2.1 Effect of Dilution on the Fuel Only

Since only cross sections for U235 and U238 were perturbed, it is expected that performing a spatial homogenization of the fuel only would exaggerate the difference in the results between infinite and finite dilution covariances. The results of homogenizing only the fuel in 2 groups are presented in Figure 4.11 and Figure 4.12, which display the absolute value of the relative covariance. The differences appear small; however the reader is encouraged to compare the scale of the vertical axis on these plots to those in Figure 4.6 - Figure 4.9. The changes resulting from perturbations with infinite and finite dilution covariances when homogenizing only the fuel region are approximately two orders of magnitude larger than those seen when homogenizing the whole cell. This is to be expected since the cell as a whole contains materials whose cross sections do not require a self-shielding correction (hydrogen for example) and so neither their cross sections, nor their covariances are dilution dependent. As a result, the dilution dependancy of the homogenized 2 group cross sections for the whole cell is much lower than the dilution dependancy of just the fuel portion of the cell.

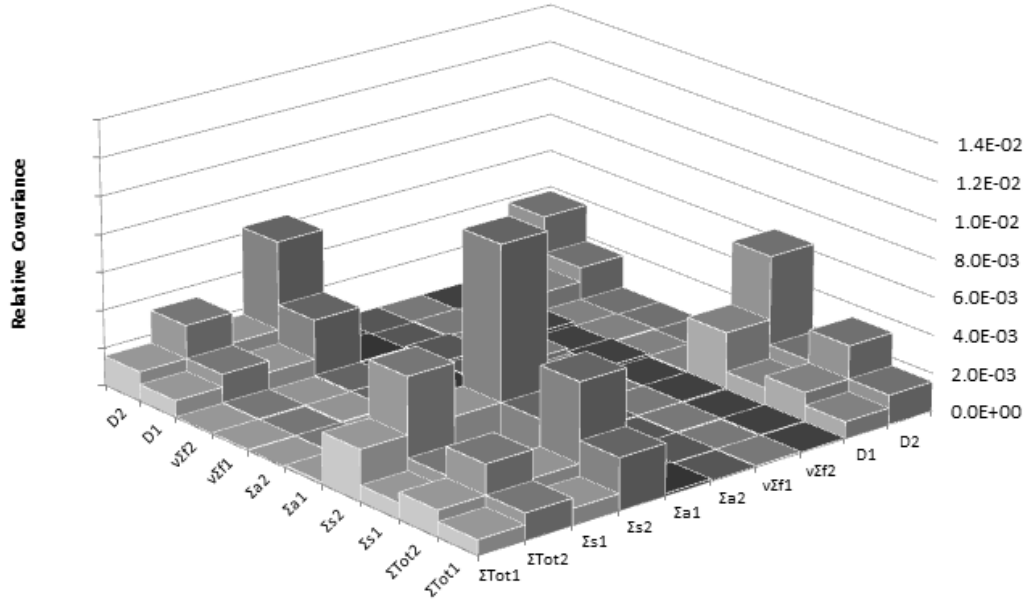


Figure 4.11 – 2 Group Homogenized Cross Section Covariance for Fuel Only Resulting from Perturbations with Infinite Dilution Covariances

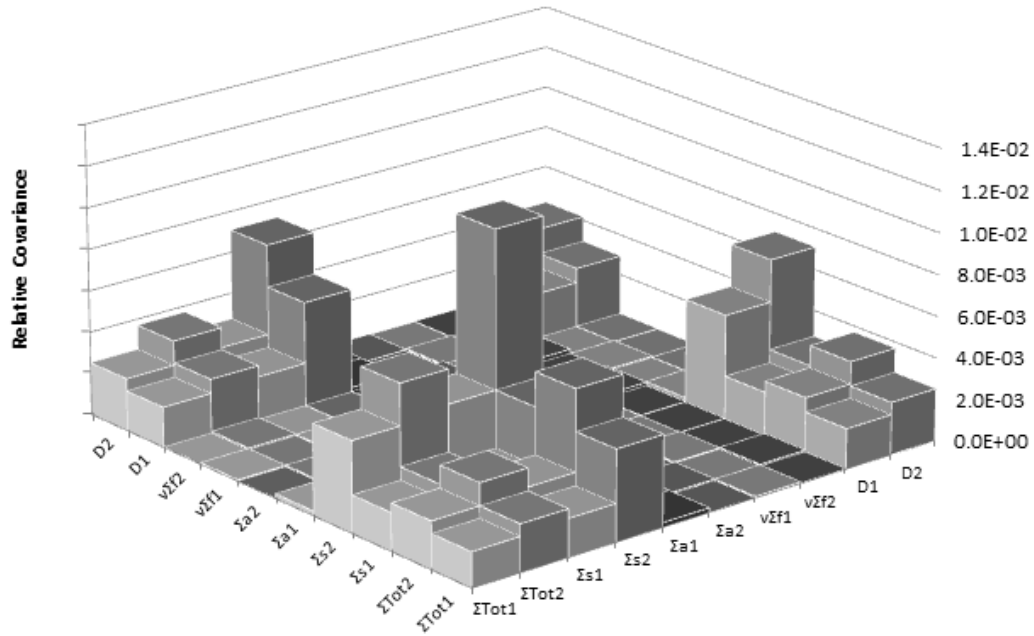


Figure 4.12 - 2 Group Homogenized Cross Section Covariance for Fuel Only Resulting from Perturbations with Finite Dilution Covariances

Chapter 5

Conclusions

Since the choice of input parameter covariance matrix can profoundly affect the calculated uncertainties in a lattice physics simulation, it is important to understand the effects of things like the choice of reference library, the source of the covariance data, the temperature, and the dilution. The goal of this work was thus to provide a clear demonstration of these effects for the multigroup covariances that correspond to the multigroup libraries used in lattice physics simulations as well as the few group homogenized cross section covariances that emerge from a lattice physics simulation to be passed onto a full core diffusion code.

5.1 Role of Reference Library

It was found that for fresh fuel, the choice of reference library had no significant effect on the uncertainty in the homogenized few group cross sections. Changing the reference library introduces a bias in the cross sections. However when they are perturbed, this bias has a very small effect on the results since it is the variation in the cross sections which causes uncertainty in the output rather than the cross section values themselves. Introducing a large enough bias could significantly affect the results especially if it induces a large change in the contribution of different cross sections to the final uncertainty. This effect may be seen in burnup calculations where the composition of the fuel changes with time. For example in thermal reactors, Pu239 will be produced in the fuel. How much Pu239 is produced will depend to some extent on the capture cross section of U238 so changing the value of this cross section will ultimately affect how much Pu239 will be present and thus how much uncertainty it will contribute to the cell properties.

5.2 Role of Temperature

The temperature of a material will determine how much its cross section will be Doppler broadened from the point of view of an incoming neutron. Doppler broadening will change the shape of resonance peaks, causing them to decrease in height and increase in width. Since the increase in width can cause a

resonance peak that exists in one energy group to stretch into the adjacent groups, it has the potential to change the covariance between multigroup cross sections.

The effect of temperature on multigroup cross section covariance was found to be mostly negligible with some large but localized changes near already existing peaks in the covariance.

5.3 Role of Covariance Source

Covariance information is ideally determined by the evaluator and included with an evaluated nuclear data library file. However different evaluators may produce different covariance matrices for the same isotope and so covariance data may differ between sources. In the case of TENDL and SCALE, the multigroup covariance data was found to differ by one or even two orders of magnitude. It should be noted that the TENDL covariances used for comparison are still relatively new and will likely be modified and improved with time.

When multigroup covariance matrices from different sources (SCALE vs. TENDL) were used to perform a Monte Carlo uncertainty propagation calculation on a PWR pin cell in DRAGON, they produced very different results for the few group homogenized cross section covariance.

5.4 Role of Dilution

Studying the effect of dilution on multigroup cross section covariance was the primary goal of this work. The level of dilution will determine how much spectral self-shielding occurs when condensing a continuous energy cross section into multigroup form. Lower levels of dilution cause resonance peaks to contribute less to the group averaged cross section since it will be weighed by a large depression in the flux. This process will also affect the covariance between multigroup cross sections in the resonance region and was shown in section 3.3 to be able to cause an increase or a decrease in multigroup covariance. Of particular concern are cases where the uncertainty increases when using finite dilution covariances since this demonstrates that assuming infinite dilution covariances can be applied to multigroup cross sections at finite dilution is **not a conservative approach**. Furthermore, changes were seen throughout the resonance region (not just locally as was seen with temperature) and it was thus concluded that the effect of dilution is not negligible at the multigroup level.

When multigroup covariance matrices at infinite and finite dilution were used to perform a Monte Carlo uncertainty propagation calculation on a PWR pin cell in DRAGON, the difference in the results for the homogenized few group covariance were significant. However the change was not nearly as significant as

that seen when using covariance data from different sources (SCALE vs. TENDL). The change in homogenized few group covariance with dilution was seen to be much more striking when only the fuel portion of the cell was homogenized. The differences seen were approximately two orders of magnitude larger than those seen when homogenizing the whole cell, however this is to be expected since the moderator and fuel cladding portions of the cell are not affected by self-shielding. Although the dilution of the multigroup covariance matrix was shown to have a significant effect on the homogenized few group properties, a statistically significant change in k -infinite could not be shown. It was concluded that although dilution was not shown here to significantly affect the uncertainty in reactivity for a single pin cell, the changes seen in the homogenized few group properties may induce significant changes in the uncertainty in k -effective in full core diffusion simulations and this should be investigated in future work.

5.5 Contributions to Knowledge Statement

This work, to the best knowledge of the author, represents the first attempt to test quantitatively the validity of applying multigroup covariances at a single temperature and infinite dilution to all multigroup cross sections²⁶ regardless of their actual temperature and dilution.

The few group homogenized cross section covariances calculated in this work could be used in future work to perform a Monte Carlo perturbation on a full core diffusion simulation using a code such as DONJON. The overall effect of dilution as well as the source of the covariance could then be assessed on the predicted uncertainty in parameters such as k -effective and bundle power to draw conclusions as to whether dilution needs to be taken into account when constructing covariance matrices and whether the large differences seen between covariances at the multigroup level between different sources significantly affect the outputs of full core simulations.

5.6 Future Work

The author proposes that the homogenized few group covariance matrices calculated in this work be used to perform uncertainty analysis for a full core simulation. This would be done using the results obtained with infinite dilution covariances only and then using those obtained by selecting the covariance matrix at the closest available dilution. By comparing the results at the full core scale,

²⁶ Here it is implied that the covariances and cross sections have the same energy group structure.

conclusions as to whether it is necessary to take into account the effect of dilution on multigroup cross section covariance could be made.

During this work, it was noted that in addition to the effect of dilution on multigroup covariance, little consideration has been given to how the choice of a flux estimate affects the resulting multigroup cross sections. Specifically, it would be interesting to create a library starting from an evaluated nuclear data library and use it to model a fuel geometry in a Monte Carlo code. The calculated flux spectrum from this simulation could then be used as the flux weighting function to create a multigroup library (using the same evaluated nuclear data library) and this multigroup library could be used in a deterministic code to model the same fuel geometry. The results would then be compared to those obtained by the Monte Carlo code as well as those obtained using a traditional flux weighting function (such as one of the pre-determined ones available in NJOY).

5.7 Publications

1. C. E. McEwan, M. R. Ball, and D. R. Novog, "Uncertainty in Reactor Lattice Physics Calculations – The Effect of Dilution on the Covariance of Multigroup Cross Sections," in *Proceedings of the 34th Annual Conference of the Canadian Nuclear Society*, Toronto, Canada, 2013.
2. M. R. Ball, C. E. McEwan, D. R. Novog and J. C. Luxat, "The Dilution Dependency of Multi-Group Uncertainties," *Science and Technology of Nuclear Installations*, [submitted for publication], 2013.

Bibliography

- [1] J. Taylor, "An Introduction to Error Analysis," University Science Books, Sausalito, USA, 1997.
- [2] D. G. Cacuci, "A Comparative Review of Sensitivity and Uncertainty Analysis of Large-Scale Systems-II: Statistical Methods," *Nuclear Science and Engineering*, no. 147, pp. 204-217, 2004.
- [3] M. Ball, *Uncertainty in Lattice Reactor Physics Calculations*, Hamilton, Canada: McMaster University (Ph.D. Dissertation), 2011.
- [4] H. J. Park, H. J. Shim and C. H. Kim, "Uncertainty Propagation Analysis for PWR Burnup Pin-Cell Benchmark by Monte Carlo Code McCARD," *Science and Technology of Nuclear Installations*, Article 616253, 2012.
- [5] S. S. Wilks, "Order Statistics," *Bulletin of the American Mathematical Society*, vol. 54, pp. 6-50, 1948.
- [6] S. Wilks, "Determination of Sample Sizes for Setting Tolerance Limits," *The Annals of Mathematical Statistics*, vol. 12, no. 1, pp. 91-96, 1941.
- [7] Z.B. Alfassi, "Uncertainty analysis based on sensitivity analysis," in *Statistical Treatment of Analytical Data*, Oxford, Blackwell Sciences, 2004.
- [8] D. Cacuci, *Sensitivity and Uncertainty Analysis Theory (Volume I)*, Boca Raton, Florida: CRC Press LLC, 2003.
- [9] D. Behmardi and E. D. Nayeri, "Introduction of Fréchet and Gâteaux Derivative," *Applied Mathematical Sciences*, vol. 2, no. 20, pp. 975-980, 2008.
- [10] M. Pusa, "Perturbation-Theory-Based Sensitivity and Uncertainty Analysis with CASMO-4," *Science and Technology of Nuclear Installations*, vol. 2012, Article ID 157029, 11 pages, 2012. doi:10.1155/2012/157029..
- [11] G. Marleau, A. Hébert and R. Roy, "A User Guide for DRAGON 3.06,"

École Polytechnique de Montréal, Montréal, Canada, 2012.

- [12] E. Varin, A. Hébert, R. Roy and J. Koclas, "A User Guide for DONJON Version 2.01 - Date 00/05/15," École Polytechnique de Montréal - Institut de Génie Nucléaire, Montréal, Canada, 2000.
- [13] D. Rochman et al., "Exact Nuclear Data Uncertainty Propagation for Fusion Neutronics Calculations," *Fusion Energy and Design*, vol. 85, no. 5, pp. 669-682, 2010.
- [14] M. R. Ball, C. E. McEwan, D. R. Novog and J. C. Luxat, "The Dilution Dependency of Multi-Group Uncertainties," *Science and Technology of Nuclear Installations*, [submitted for publication], 2013.
- [15] K. Ivanov, M. Avramova, I. Kodeli and E. Sartori, *Benchmark for Uncertainty Analysis in Modelling (UAM) For Design, Operation, and Safety Analysis of LWRs*, OECD Nuclear Energy Agency, 2007.
- [16] R. MacFarlane, "An Introduction to the ENDF Formats," Los Alamos National Laboratory, Los Alamos, USA, 2000.
- [17] M. Herman and A. Trkov, "ENDF-6 Formats Manual," Brookhaven National Laboratory, Upton, NY, 2010.
- [18] R. MacFarlane and D. Muir, "The NJOY Nuclear Data Processing System Version 91," Los Alamos National Laboratory, Los Alamos, USA, 1994.
- [19] A. Koning, S. Hilaire and S. Goreily, "TALYS-1.4 A nuclear reaction program - User Manual," Nuclear Research and Consultancy Group, Petten, The Netherlands, 2011.
- [20] A. Koning and D. Rochman, "Modern Nuclear Data Evaluation: Straight from Nuclear Physics to Applications," *Journal of the Korean Physical Society*, vol. 59, no. 2, pp. 773-778, 2011.
- [21] R. MacFarlane and A. Kahler, "Methods for Processing ENDF/B-VII with NJOY," Los Alamos National Laboratory, Los Alamos, USA, 2010.
- [22] G. Yesilyurt, *Advanced Monte Carlo Methods for Analysis of Very High Temperature Reactors: On the Fly Doppler Broadening and Deterministic/Monte Carlo Methods*, Michigan, USA: University of Michigan (Ph.D. Dissertation), 2009.

- [23] I. Kodeli, "Manual for ANGELO2 and LAMBDA Codes," NEA-1798 Package, 2008.
- [24] J. Duderstadt and L. Hamilton, Nuclear Reactor Analysis, Michigan, USA: John Wiley & Sons, 1976.
- [25] G. Marleau, A. Hébert and R. Roy, "A User Guide for DRAGON 3.06," École Polytechnique de Montréal, Montréal, Canada, 2012.
- [26] M. Nicolas and A. Hébert, "Adaptation of the B1 Leakage Model to Monte Carlo Criticality Calculations," in *Proceedings of the International Conference on Mathematics and Computational Methods Applied to Nuclear Science and Engineering*, Rio de Janeiro, Brazil, 2011.
- [27] A. Hébert, *Neutron Leakage (Course Notes for ENE6101:Week 11)*, Montréal, Canada: École Polytechnique de Montréal.
- [28] I. Kodeli, "SUSD3D, A Multi-Dimensional, Discrete Ordinates Based Cross Section Sensitivity and Uncertainty Code," in *Proceedings of the 23rd Symposium on Fusion Technology*, Issy-les-Moulineaux, France, 2005.
- [29] W. Zwermann, L. Gallner, M. Klein, B. Krzykacz-Hausmann, I. Pasichnyk, A. Pautz and K. Velkov, "Status of XSUSA for Sampling Based Nuclear Data Uncertainty and Sensitivity Analysis," in *WONDER-2012 - 3rd International Workshop on Nuclear Data Evaluation for Reactor Applications*, Aix-en-Provence, France, 2012.
- [30] W. Wieselquist, A. Vasiliev and H. Ferroukhi, "Towards and Uncertainty Quantification Methodology with CASMO-5," in *International Conference on Mathematics and Computational Methods Applied to Nuclear Science and Engineering*, Rio de Janeiro, Brazil, 2011.
- [31] D. Wiarda and M. Dunn, "PUFF-IV: A Code for Processing ENDF Uncertainty Data into Multigroup Covariance Matrices," Oak Ridge National Laboratory, Oak Ridge, USA, 2006.
- [32] D. Wiarda, M. Dunn, N. Greene, N. Larson and L. Leal, "New Capabilities for Processing Covariance Data in Resonance Region," in *PHYSOR-2006 ANS Topical Meeting on Reactor Physics*, Vancouver, Canada, 2006.
- [33] M. Williams, D. Wiarda, G. Arbanas and B. Broadhead, "SCALE Nuclear Data Covariance Library," Oak Ridge National Laboratory, Oak Ridge, USA,

2011.

- [34] I. Kodeli and E. Sartori, "ZZ-VITAMIN-J/COVA - Covariance Matrix Data from Sensitivity Analyses," NEA-Data Bank, NEA 1264/03-/05, 1991-2003.

Appendix A – U238 Covariance Data in 69 Groups

*All plots in this section are given as absolute values of the relative covariance.

MT 2 – Elastic Scattering

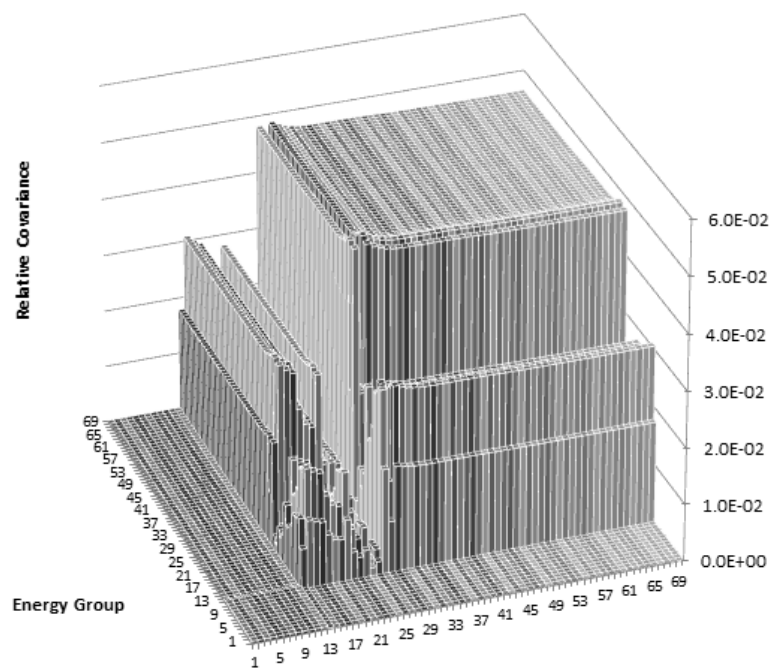


Figure A.1 – 69 Group Covariance for Reaction MT 2 in TENDL

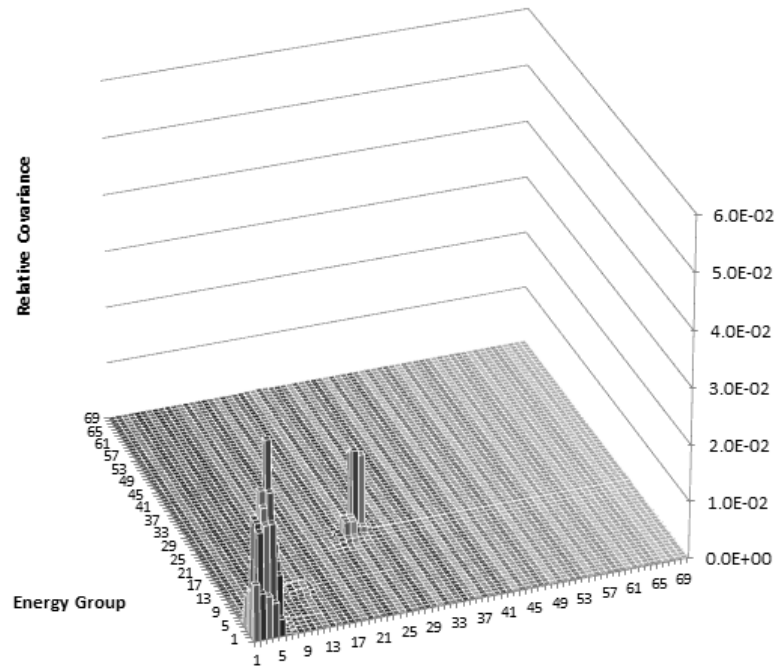


Figure A.2 – 69 Group Covariance for Reaction MT 2 in SCALE

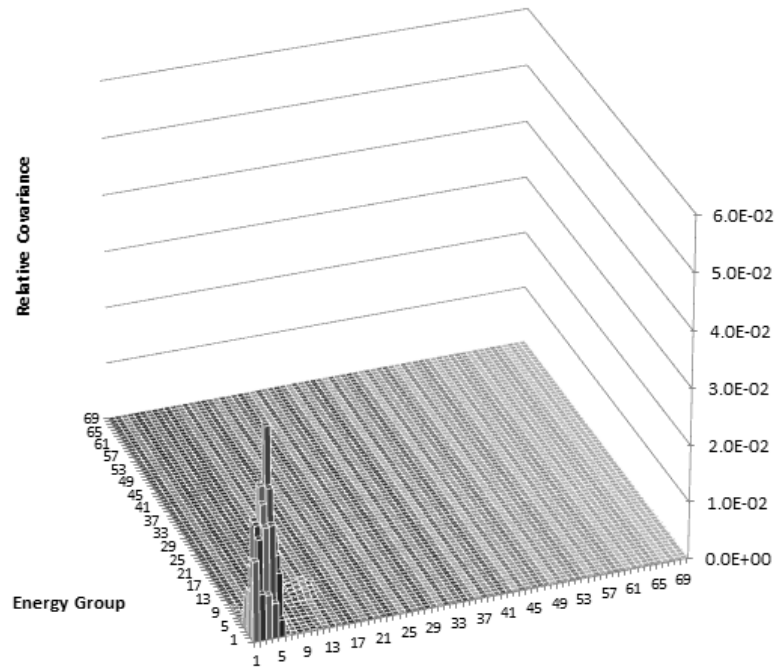


Figure A.3 – 69 Group Covariance for Reaction MT 2 in ENDF/B-VII

MT 4 – Inelastic Scattering²⁷

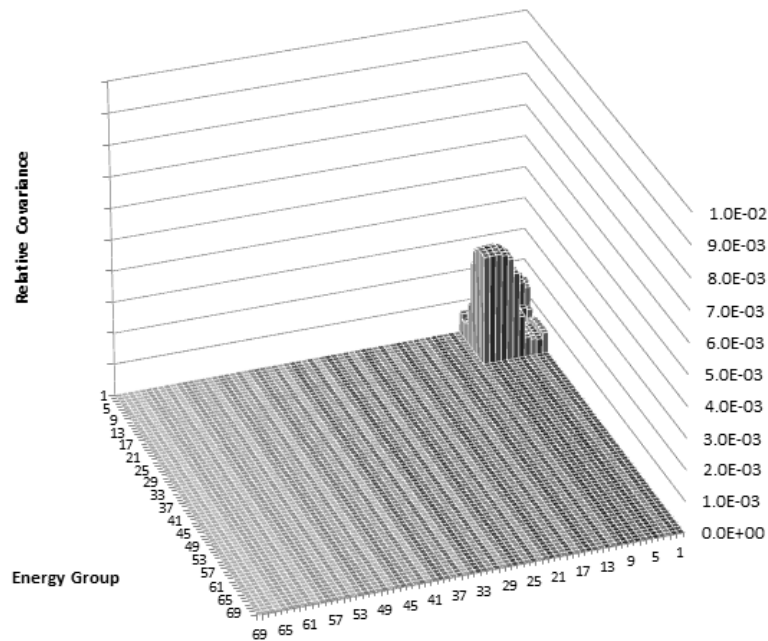


Figure A.4 – 69 Group Covariance for Reaction MT 4 in TENDL

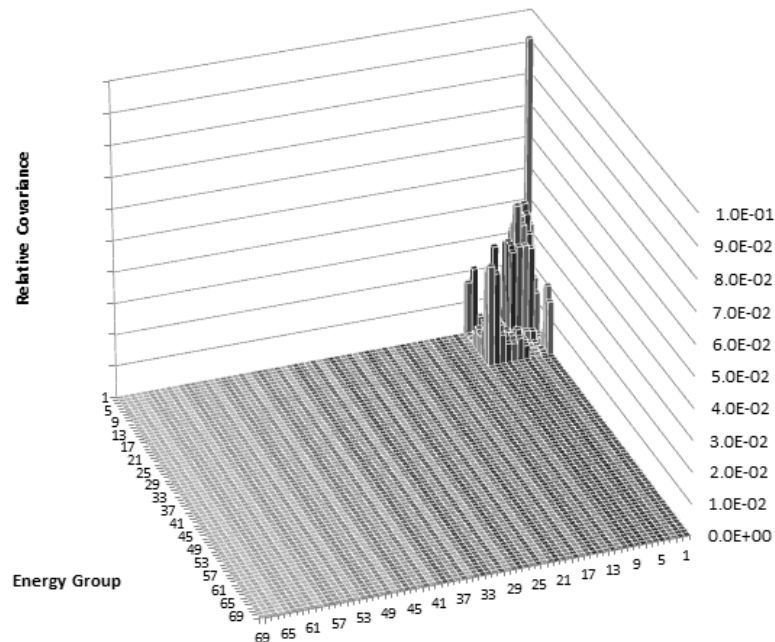


Figure A.5 – 69 Group Covariance for Reaction MT 4 in ENDF/B-VII

²⁷ SCALE covariance not available, note that axes are not on the same scale.

MT 16 – (n,2n)

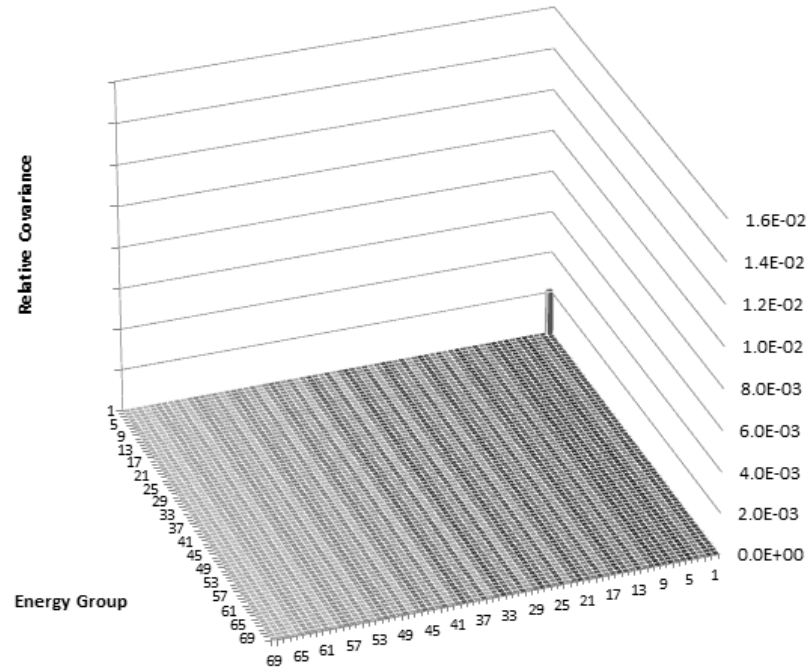


Figure A.6 – 69 Group Covariance for Reaction MT 16 in TENDL

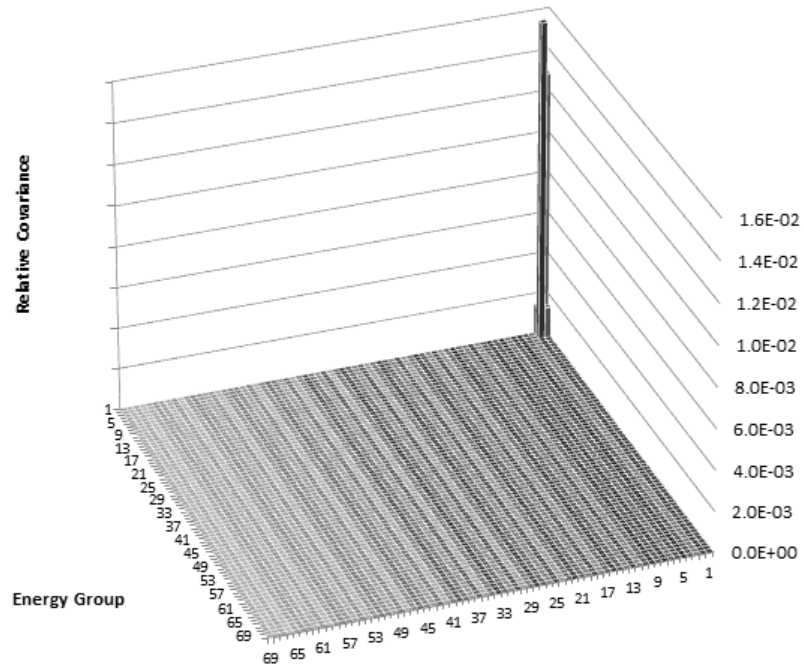


Figure A.7 – 69 Covariance for Reaction MT 16 in SCALE

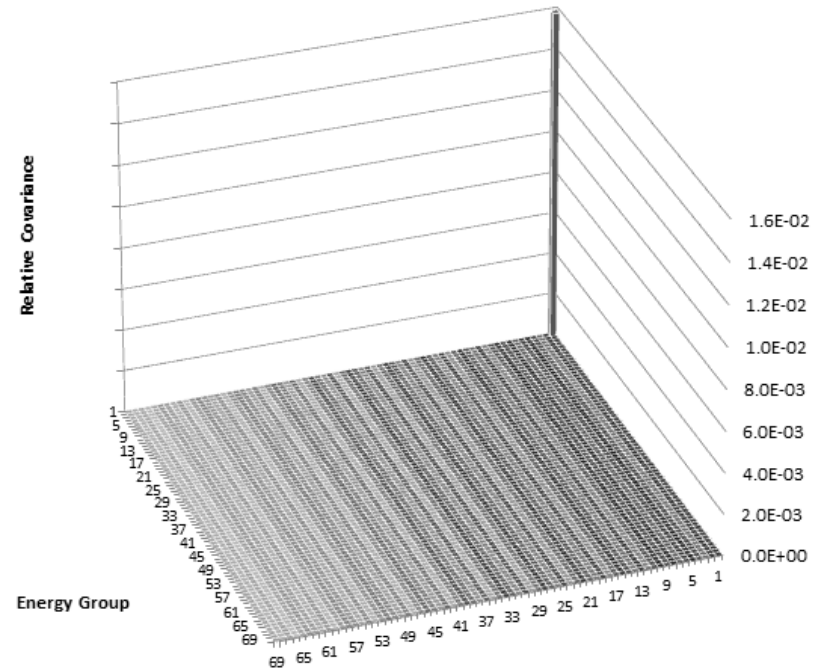


Figure A.8 – 69 Group Covariance for Reaction MT 16 in ENDF/B-VII

MT 18 - Fission²⁸

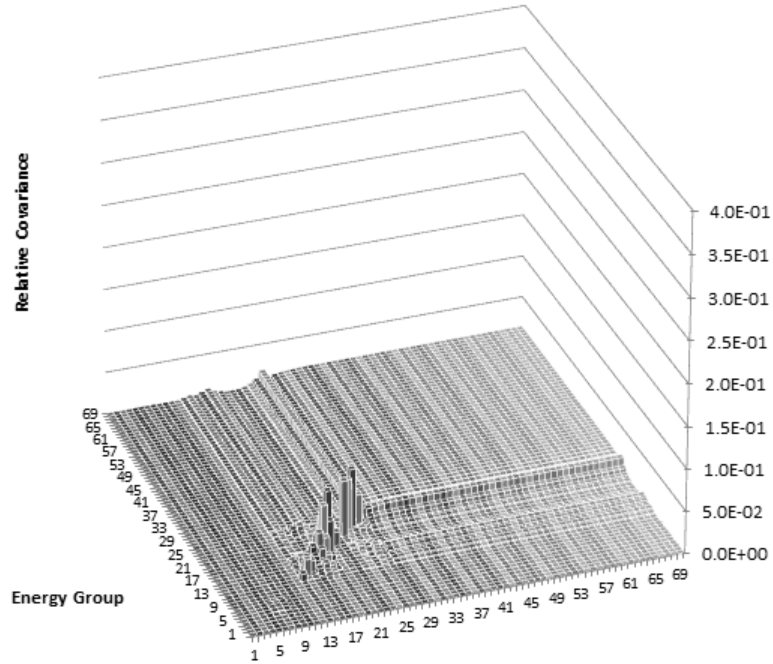


Figure A.9 – 69 Group Covariance for Reaction MT 18 in TENDL

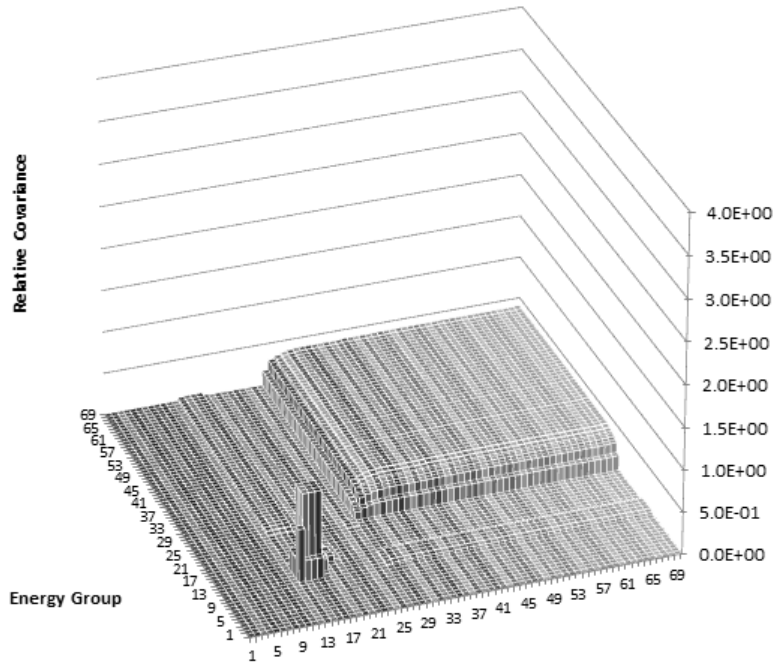


Figure A.10 – 69 Group Covariance for Reaction MT 18 in SCALE

²⁸ Axes for TENDL covariances are not on the same scale as the other two.

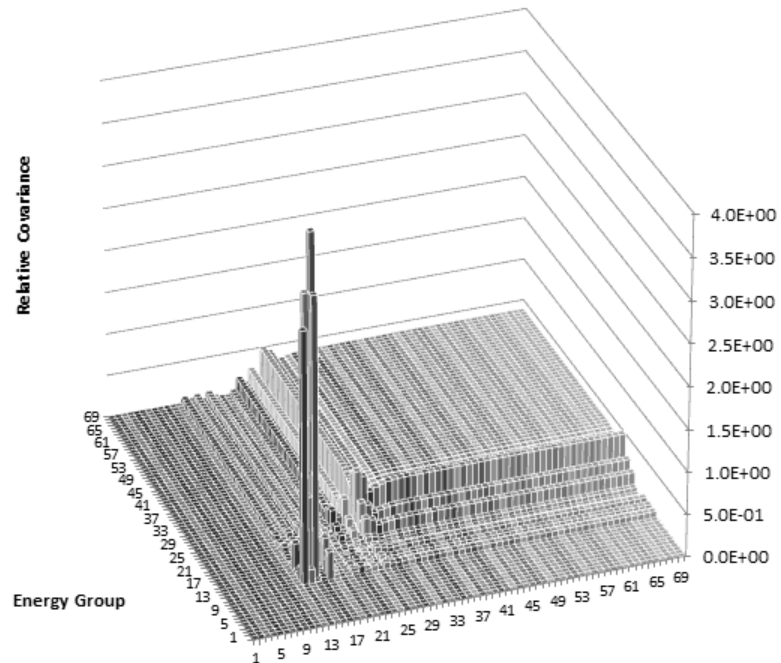


Figure A.11 – 69 Group Covariance for Reaction MT 18 in ENDF/B-VII*

*Note that the large peak representing the covariance between group 15 and group 15 goes off-scale with a magnitude of $1.66\text{E}+1$. The maximum of $4.0\text{E}+0$ was chosen to allow the reader to see detail in the covariance between the other groups.

MT 102 – Radiative Capture

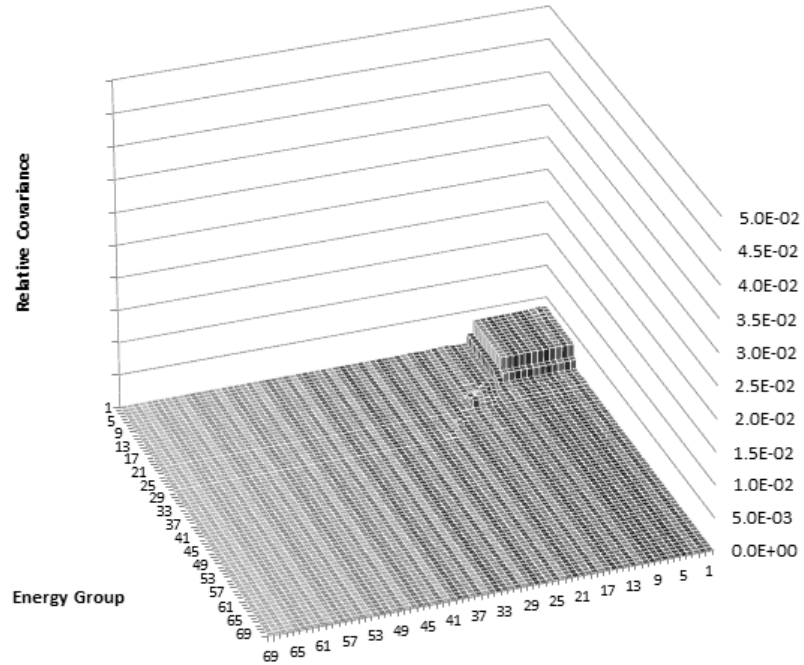


Figure A.12 – 69 Group Covariance for Reaction MT 102 in TENDL

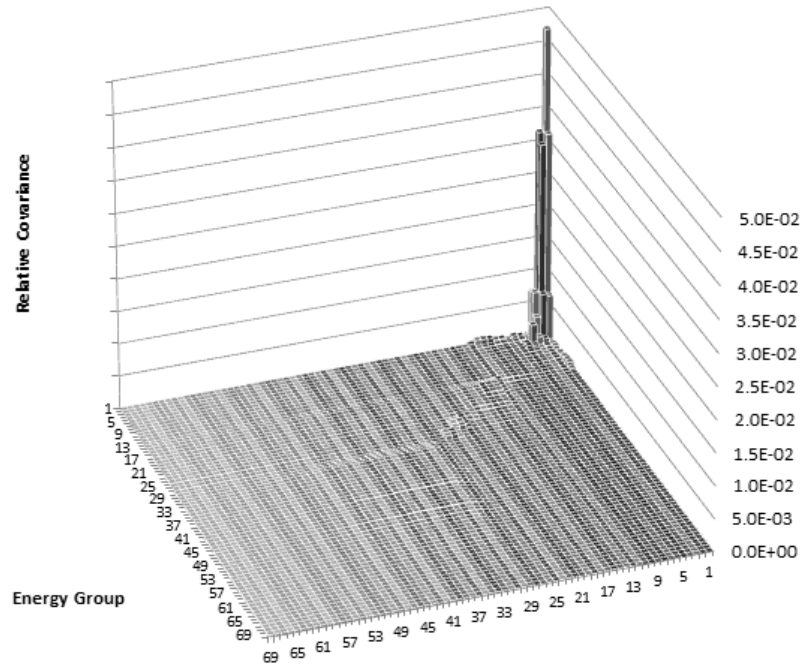


Figure A.13 – 69 Group Covariance for Reaction MT 102 in SCALE

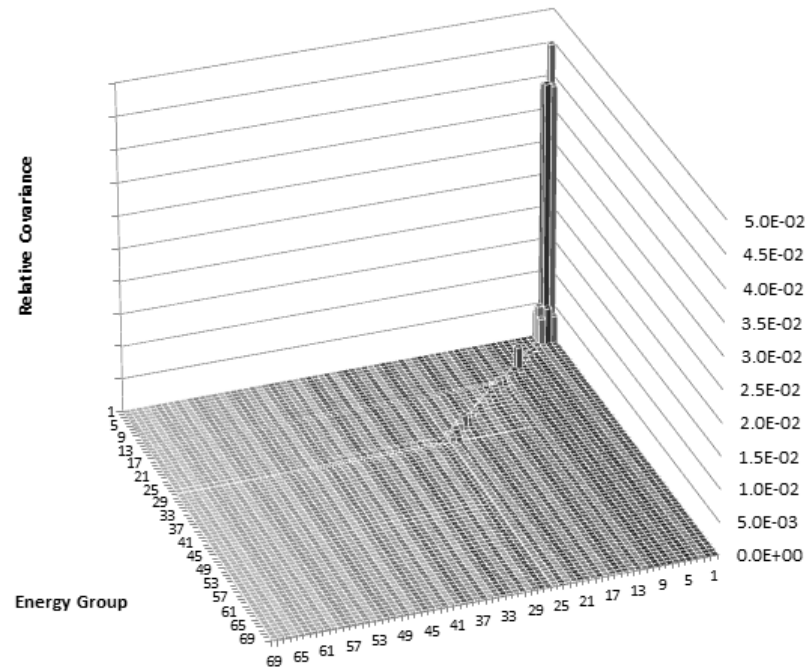


Figure A.14 – 69 Group Covariance for Reaction MT 102 in ENDF/B-VII

MT 452 – Fission Neutron Yield $(\bar{\nu})^{29}$

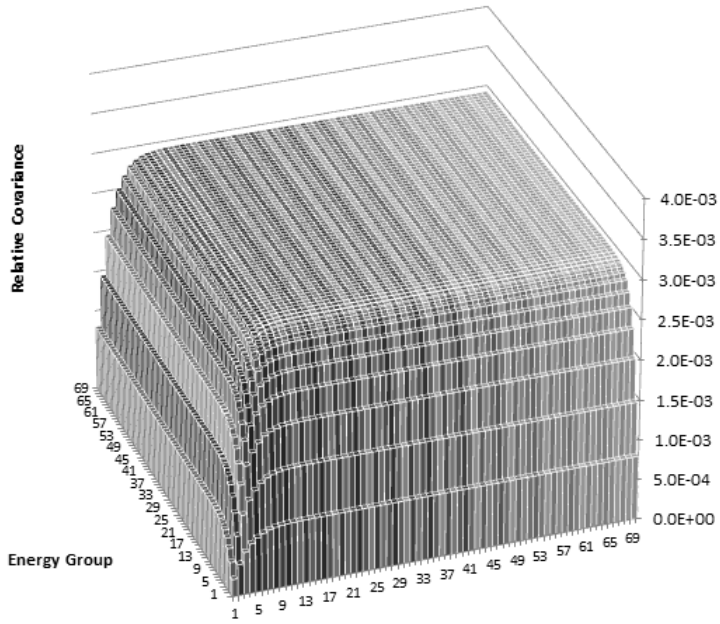


Figure A.15 - 69 Group Covariance for Reaction MT 452 in TENDL

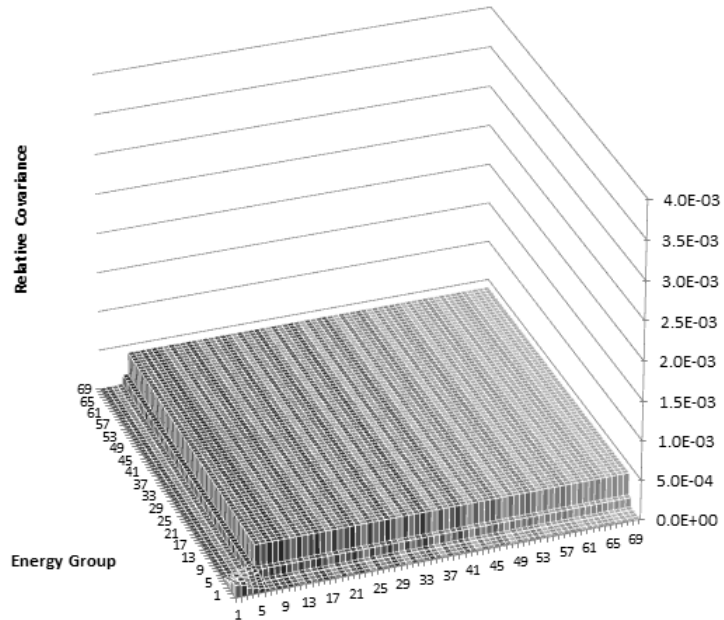


Figure A.16 – 69 Group Covariance for Reaction MT 452 in SCALE

²⁹ ENDF covariance not available.

Fission Spectrum (χ)³⁰

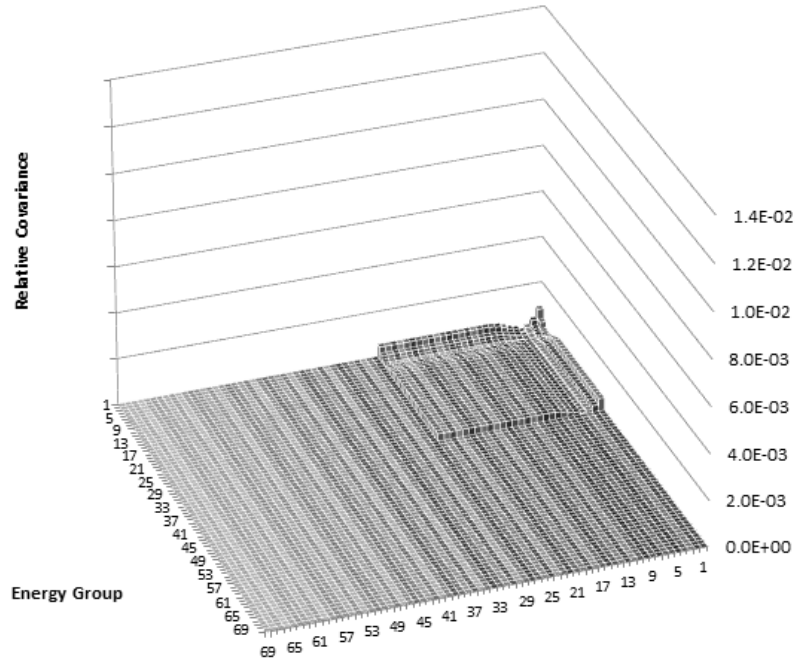


Figure A.17 – 69 Group Covariance for Fission Spectrum in TENDL

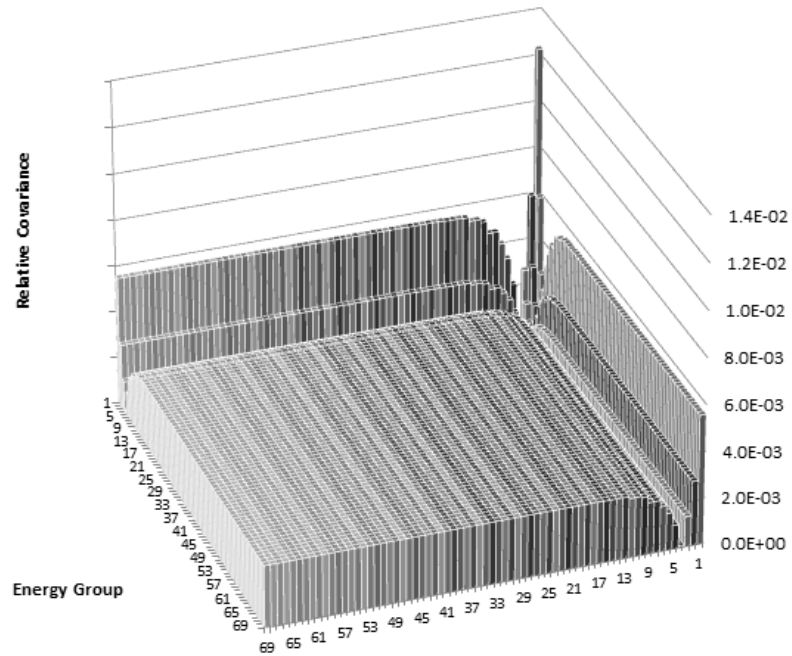


Figure A.18 – 69 Group Covariance for Fission Spectrum in SCALE

³⁰ ENDF covariance not available.

Appendix B – U235 Covariance Data in 69 Groups

*All plots in this section are given as absolute values of the relative covariance.

MT 2

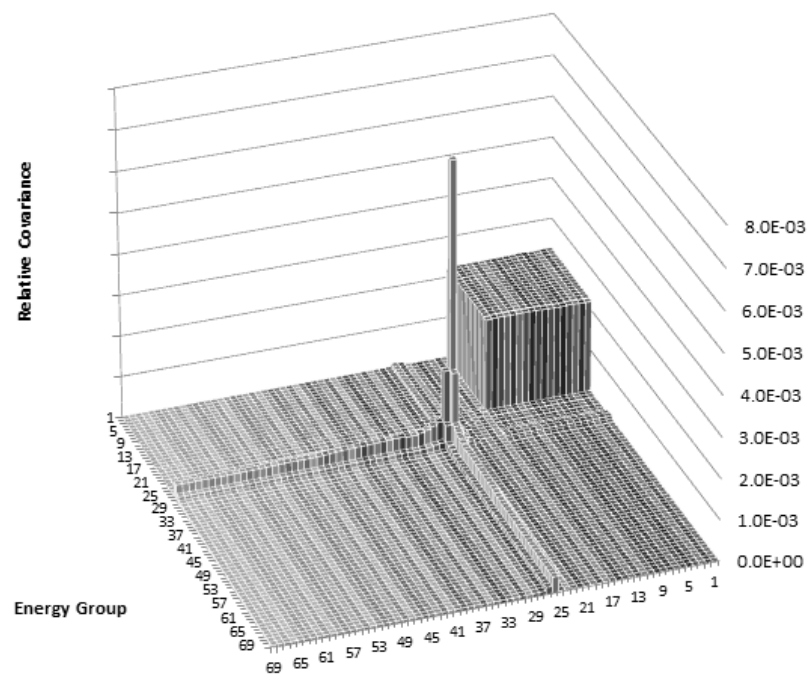


Figure B.1 – 69 Group Covariance for Reaction MT 2 in TENDL

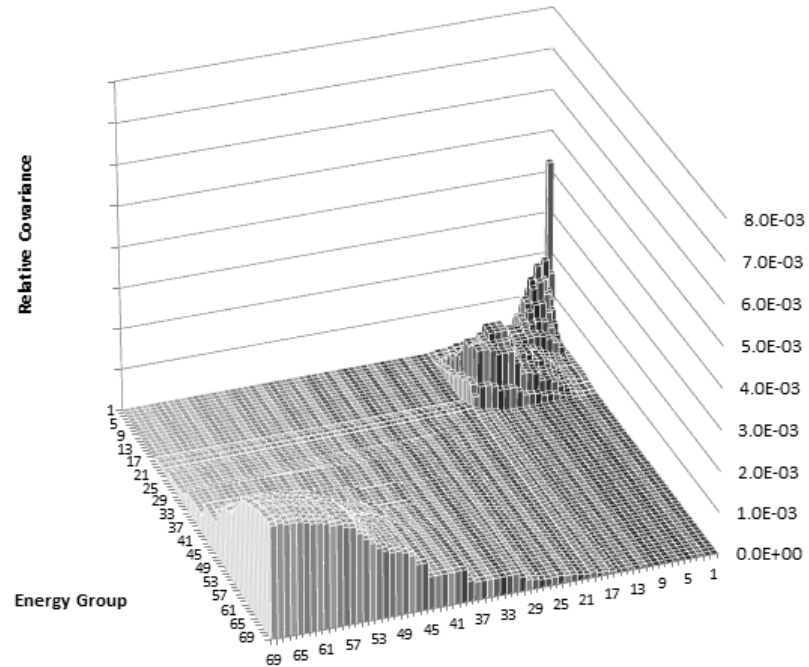


Figure B.2 – 69 Group Covariance for Reaction MT 2 in SCALE

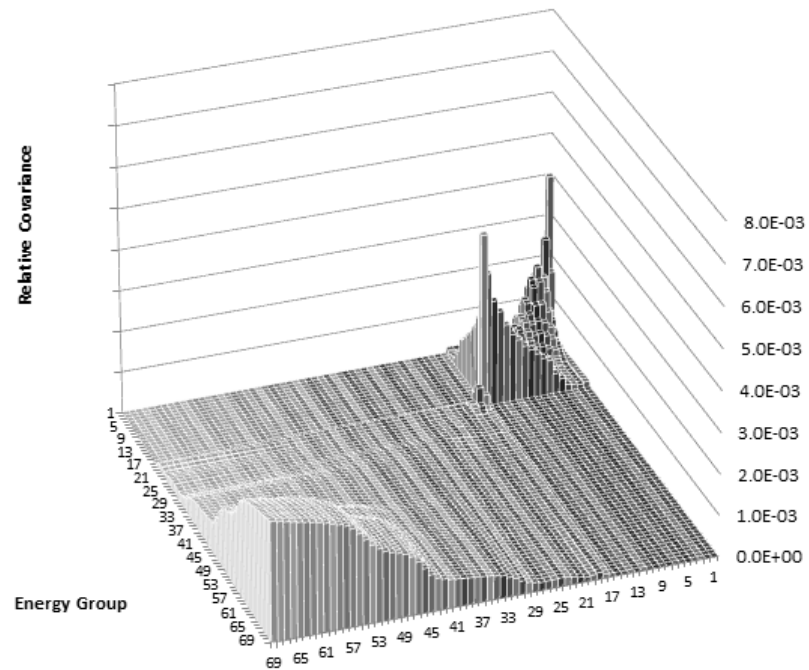


Figure B.3 – 69 Group Covariance for Reaction MT 2 in ENDF/B-VII

MT 4

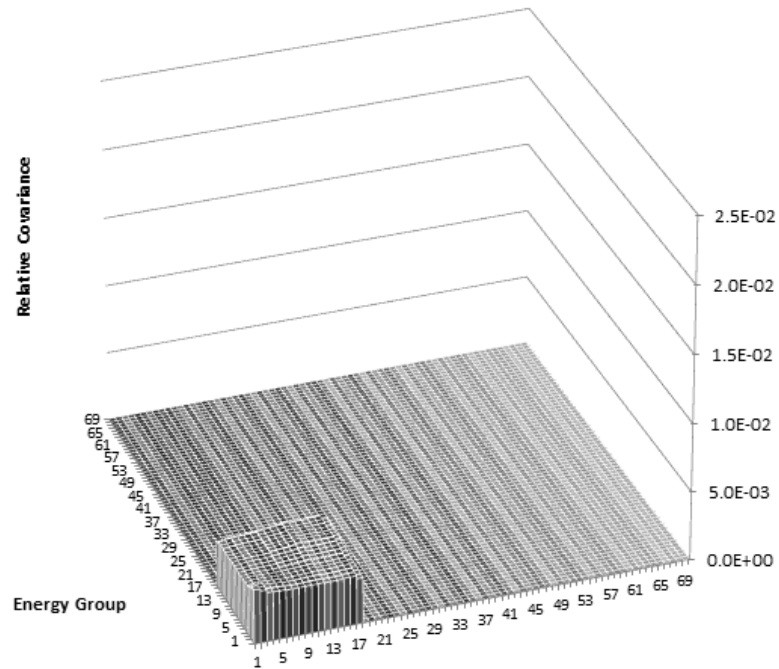


Figure B.4 – 69 Group Covariance for Reaction MT 4 in TENDL

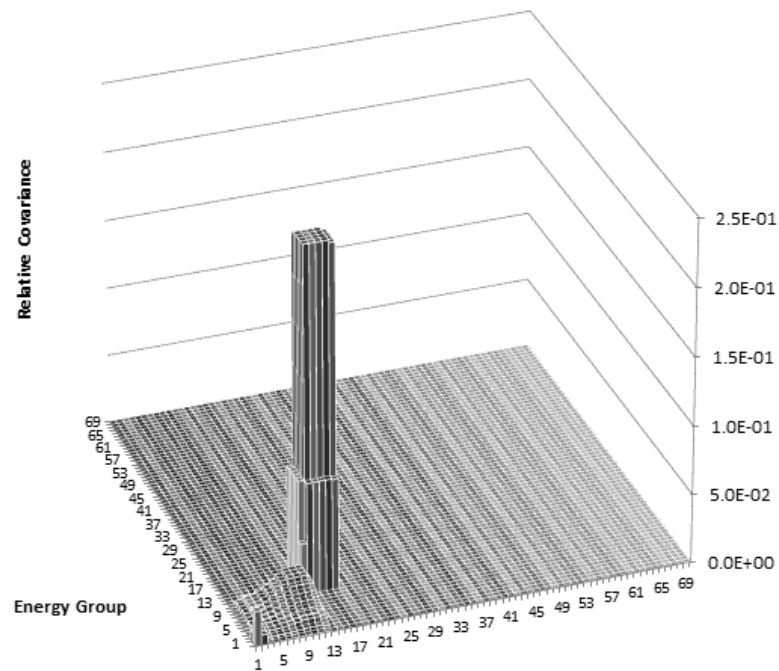


Figure B.5 – 69 Group Covariance for Reaction MT 4 in ENDF/B-VII

MT 16

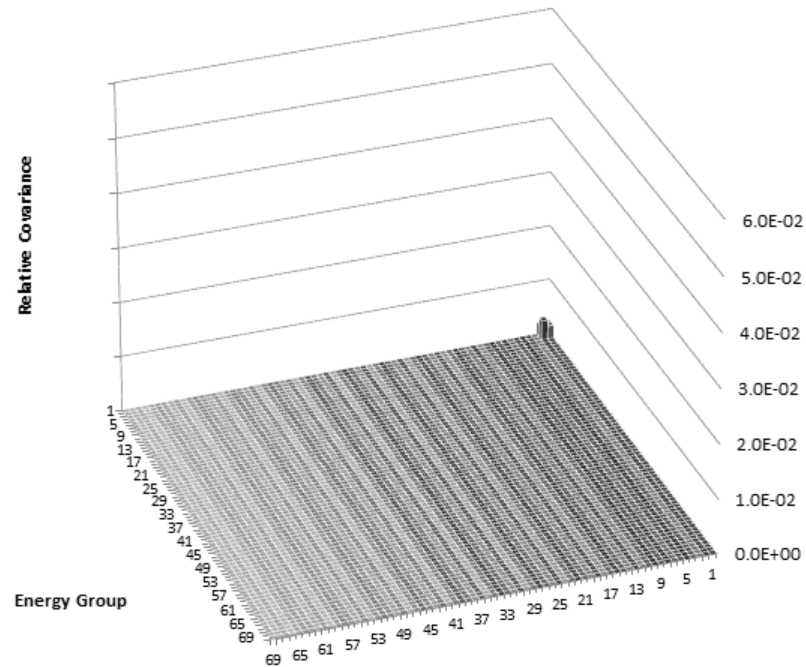


Figure B.6 – 69 Group Covariance for Reaction MT 16 in TENDL

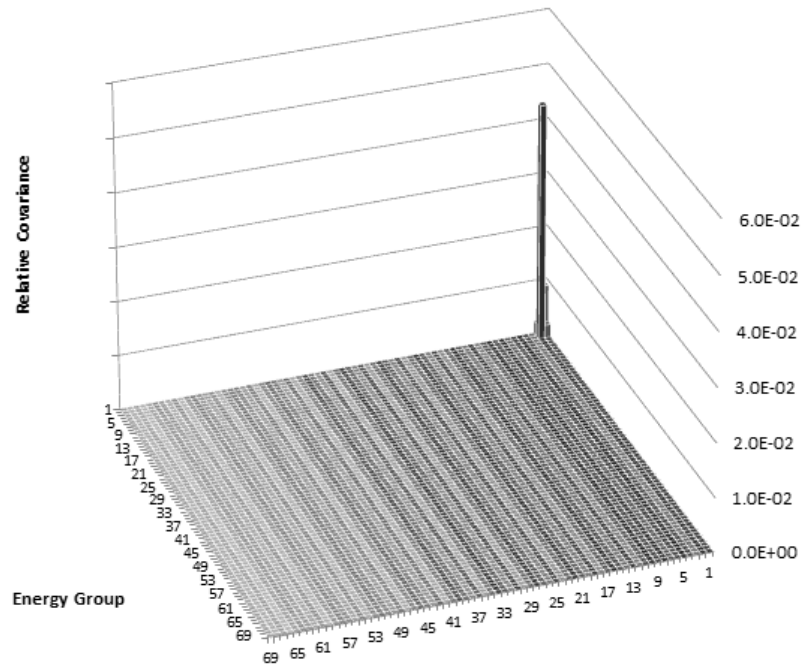


Figure B.7 – 69 Group Covariance for Reaction MT 16 in SCALE

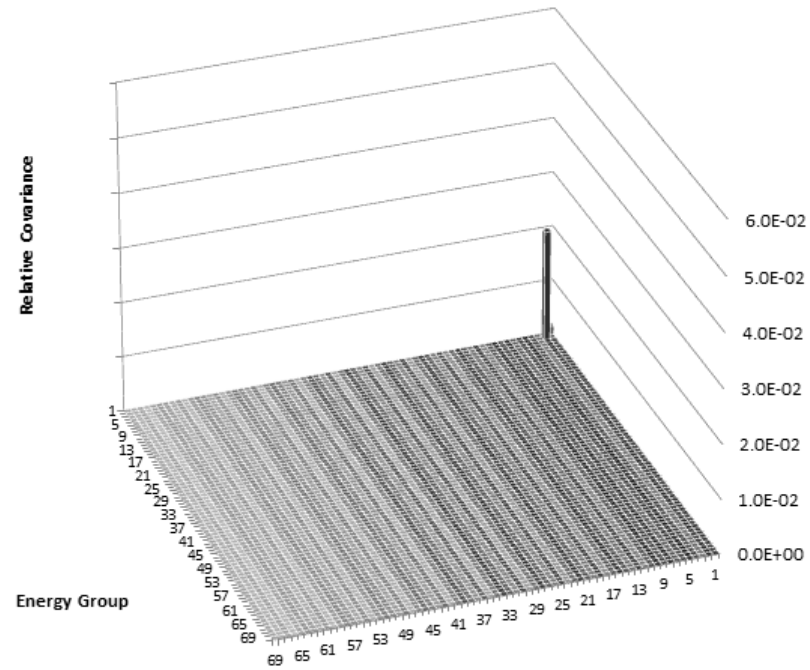


Figure B.8 – 69 Group Covariance for Reaction MT 16 in ENDF/B-VII

MT 18³¹

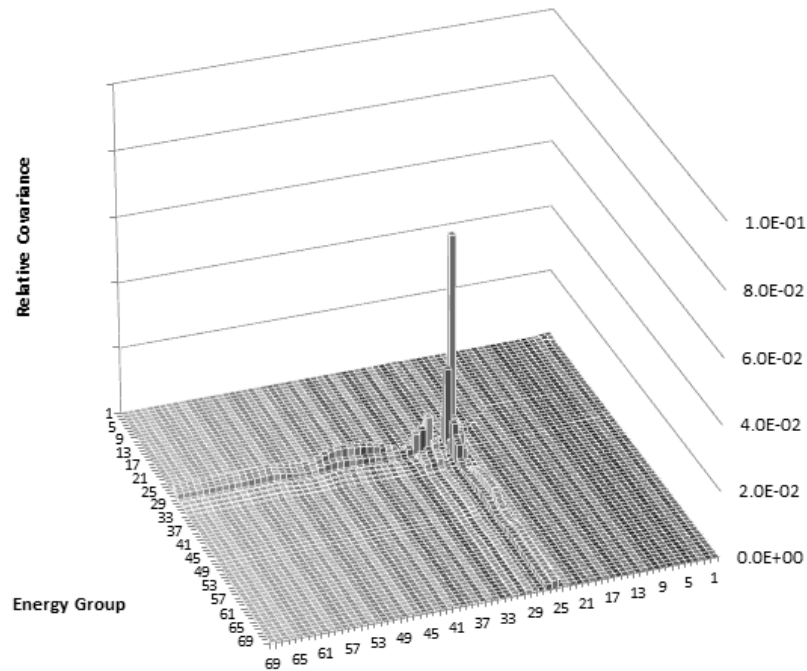


Figure B.9 – 69 Group Covariance for Reaction MT 18 in TENDL

³¹ Axes in all three plots are on different scales.

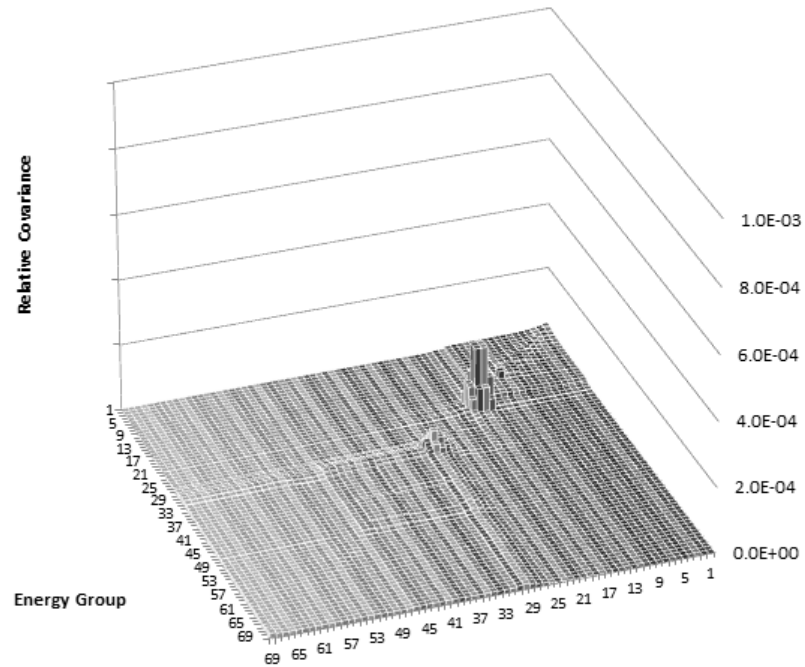


Figure B.10 – 69 Group Covariance for Reaction MT 18 in SCALE

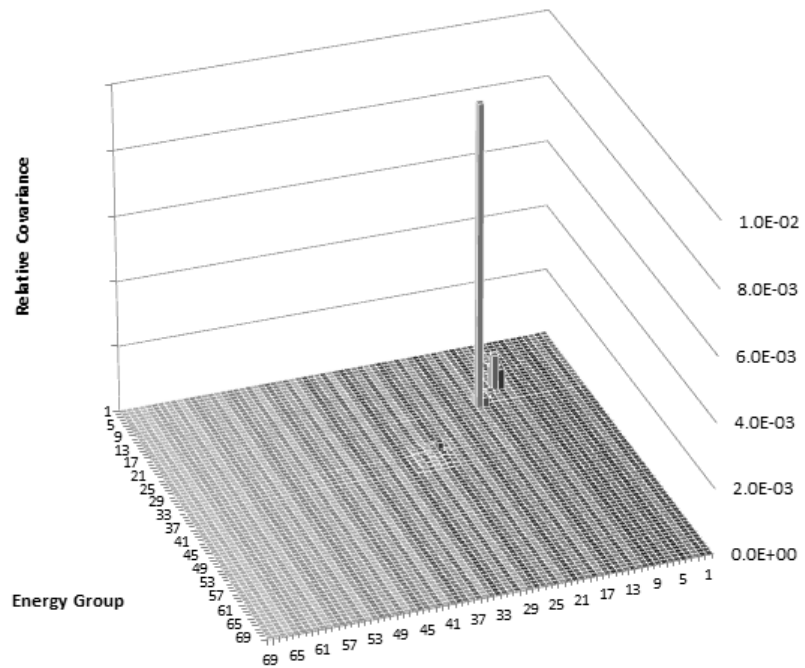


Figure B.11 – 69 Group Covariance for Reaction MT 18 in ENDF/B-VII

MT 102³²

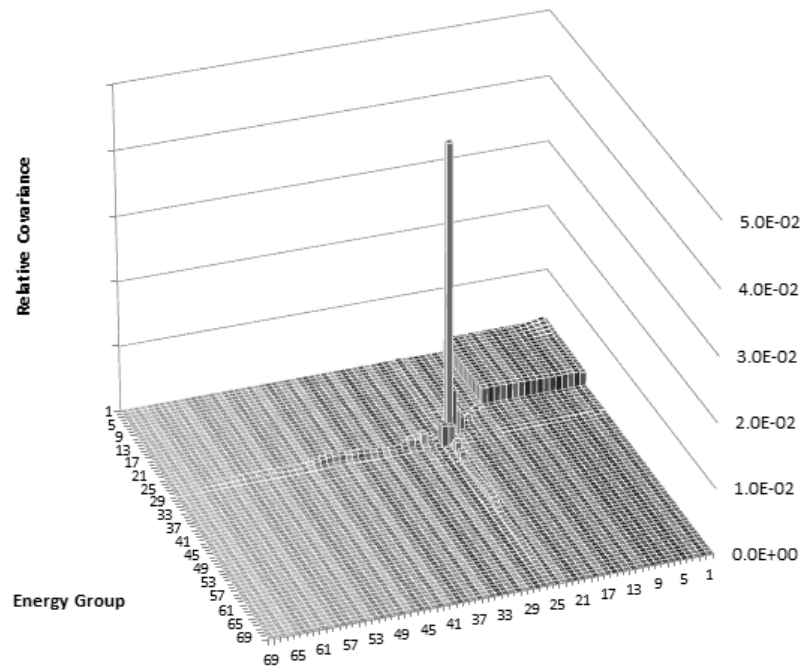


Figure B.12 – 69 Group Covariance for Reaction MT 102 in TENDL

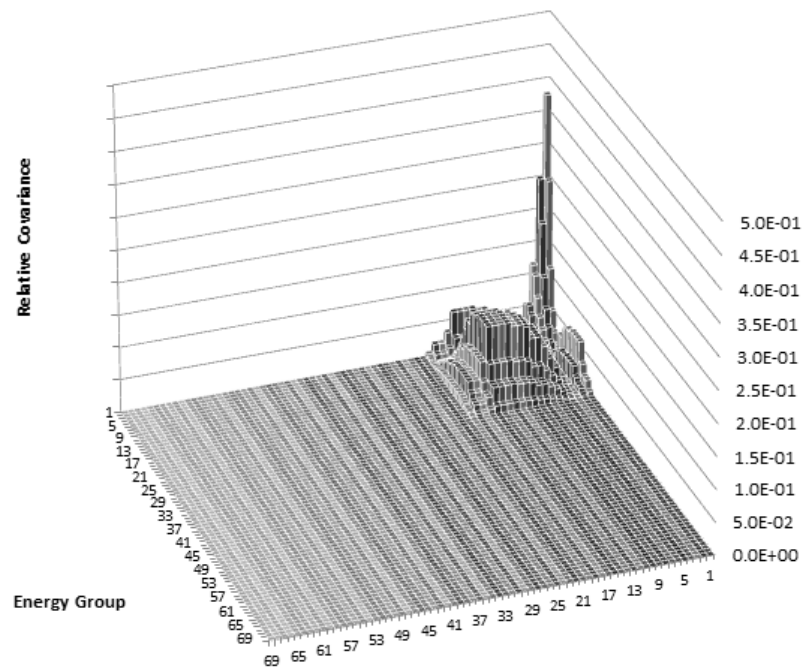


Figure B.13 – 69 Group Covariance for Reaction MT 102 in SCALE

³² Axes for TENDL covariances are not on the same scale as the other two.

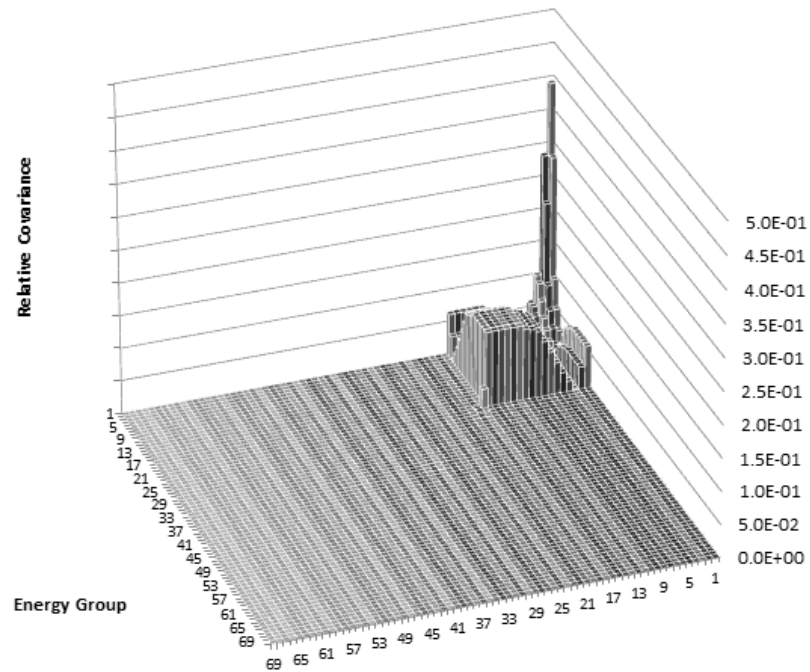


Figure B.14 – 69 Group Covariance for Reaction MT 102 in ENDF/B-VII

MT 107³³

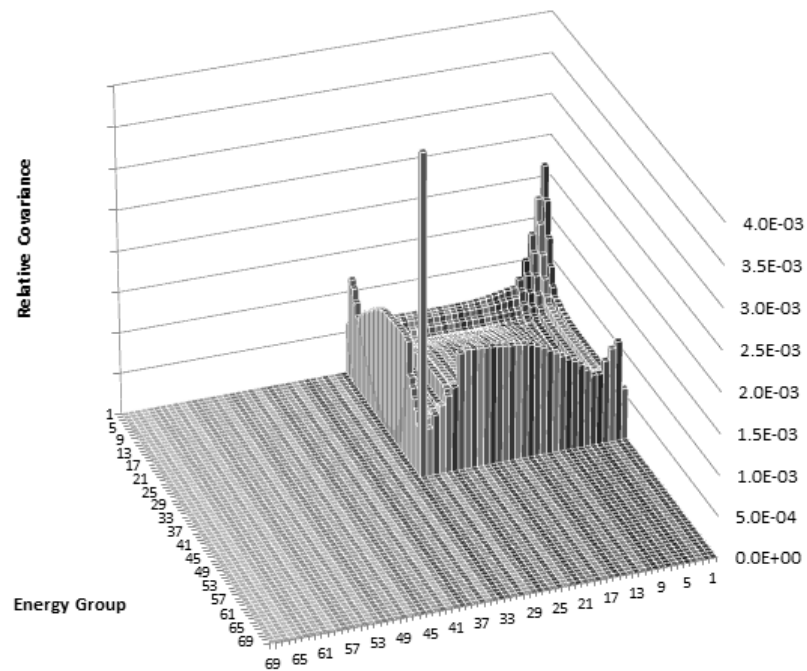


Figure B.15 – 69 Group Covariance for Reaction MT 107 in TENDL

³³ SCALE and ENDF/B-VII covariance not available.

MT 452 - Fission Neutron Yield ($\bar{\nu}$)³⁴

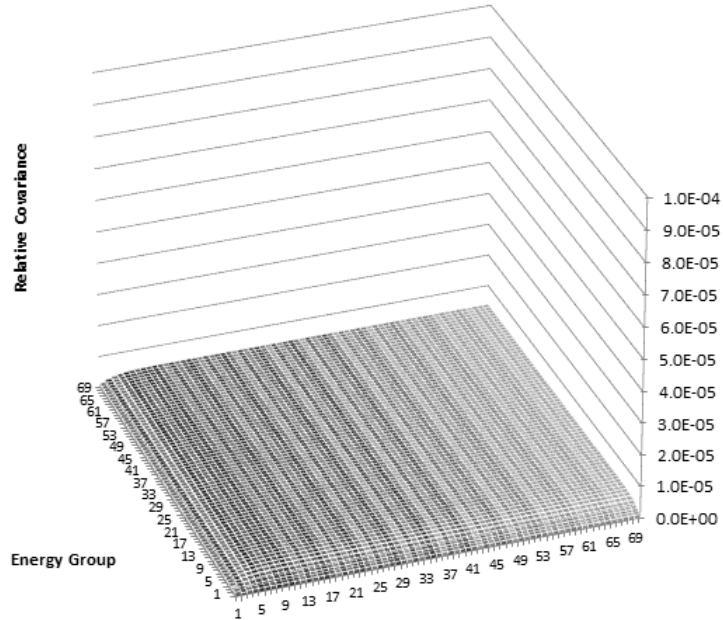


Figure B.16 – 69 Group Covariance for Reaction MT 452 in TENDL

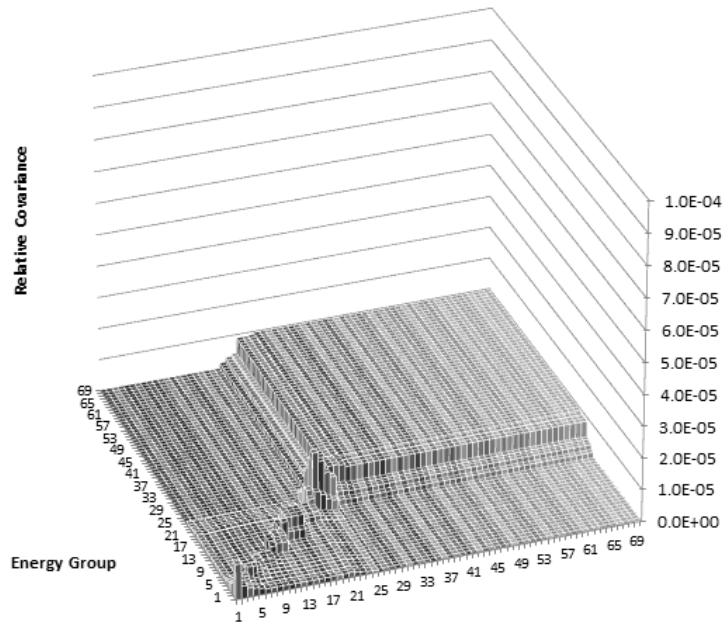


Figure B.17 – 69 Group Covariance for Reaction MT 452 in TENDL

³⁴ ENDF covariance not available.

Fission Spectrum (χ)³⁵

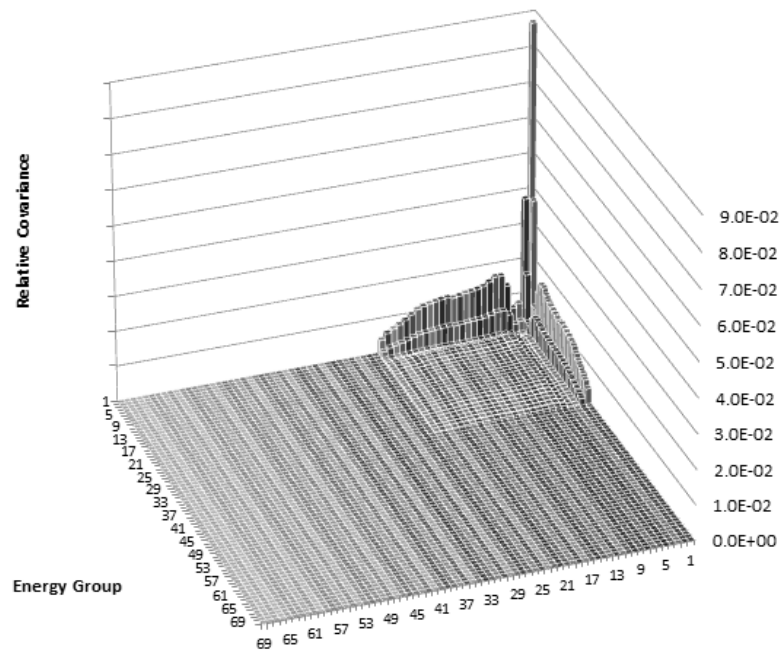


Figure B.18 – 69 Group Covariance for Fission Spectrum in TENDL

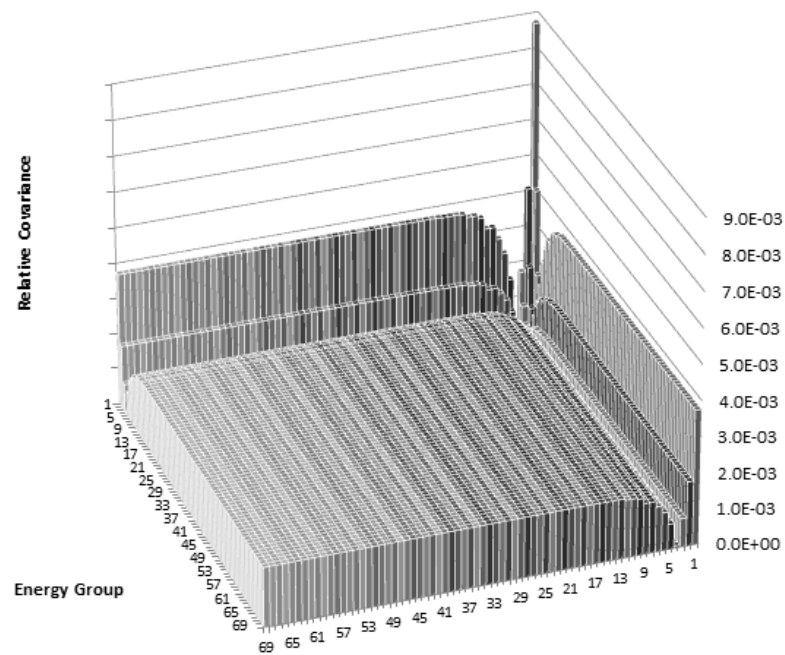


Figure B.19 – 69 Group Covariance for Fission Spectrum in SCALE

³⁵ ENDF covariance not available.

Appendix C – Dilution Dependence of U238 TENDL Covariance in 69 Groups

*All plots in this section are given as absolute values of the relative covariance.

MT 2

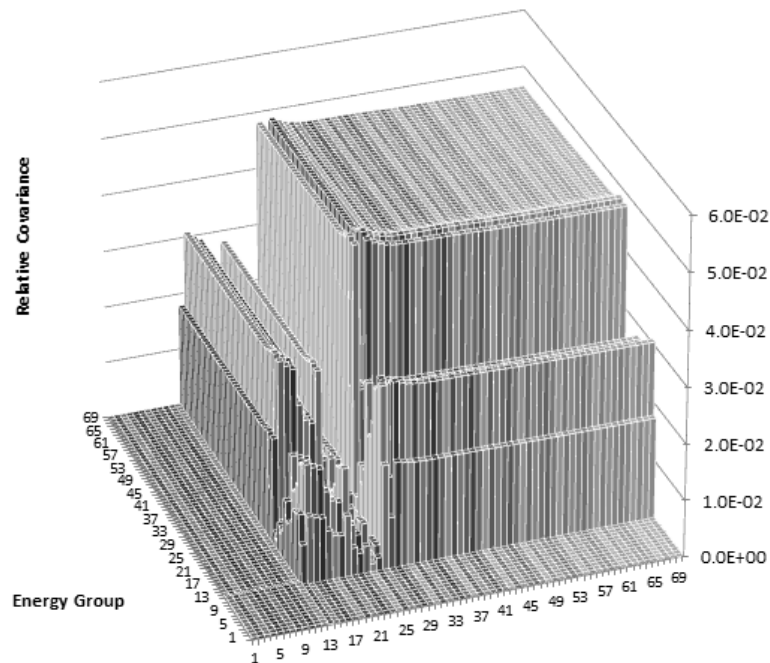


Figure C.1 – 69 Group TENDL Covariance for Reaction MT 2 at Infinite Dilution

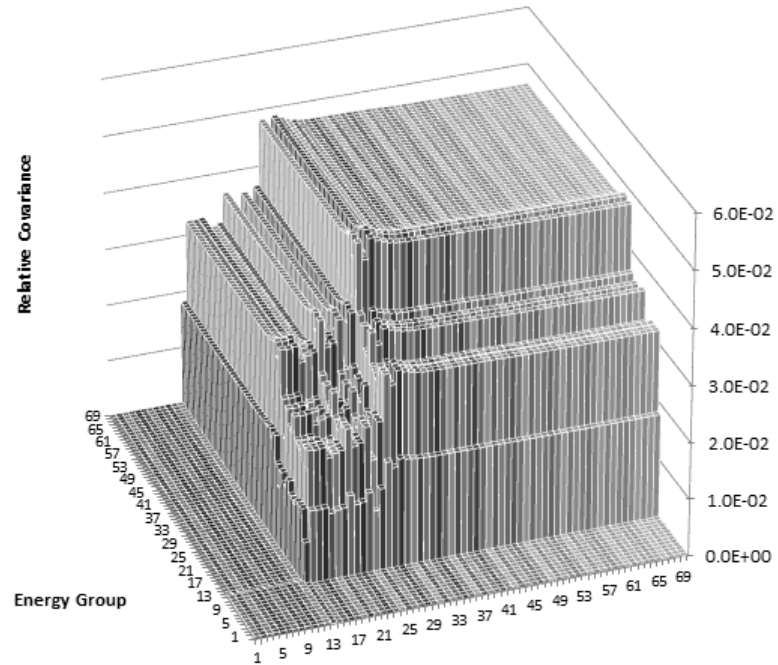


Figure C.2 – 69 Group TENDL Covariance for Reaction MT 2 at a Dilution of 52 Barns

MT 18

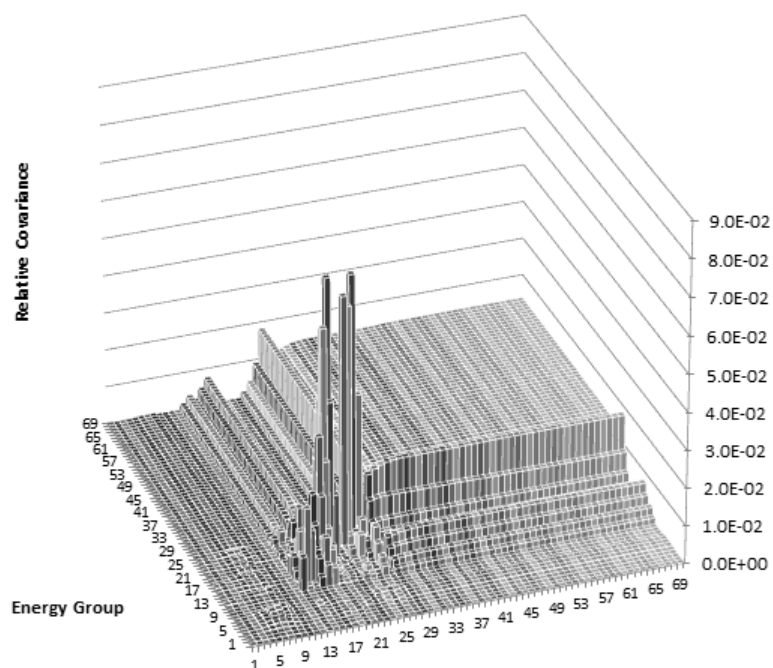


Figure C.3 – 69 Group TENDL Covariance for Reaction MT 18 at Infinite Dilution

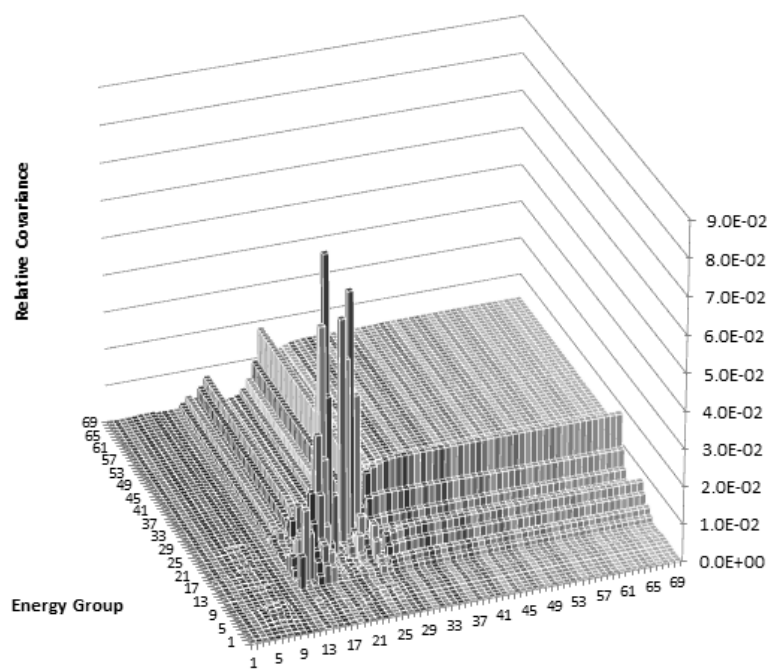


Figure C.4 – 69 Group TENDL Covariance for Reaction MT 18 at a Dilution of 52 Barns

MT 102

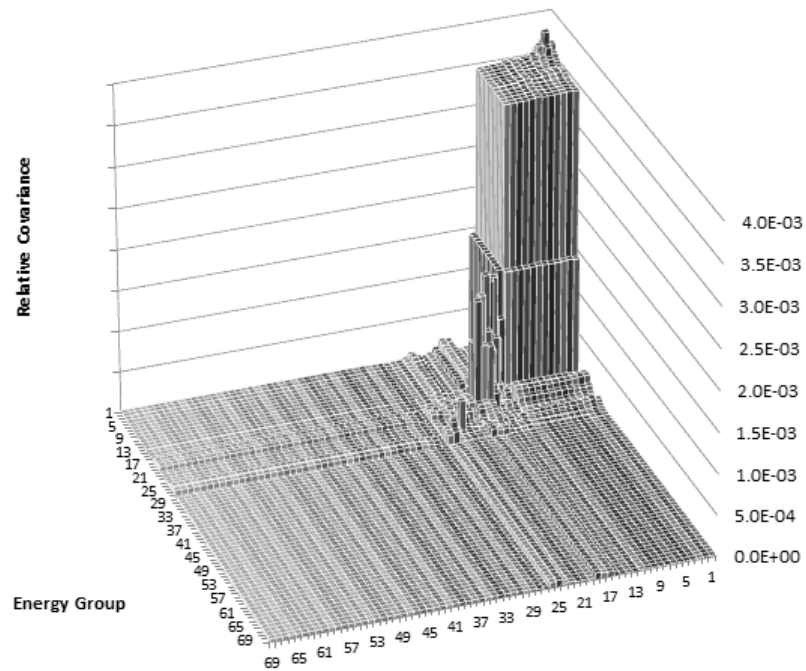


Figure C.5 – 69 Group TENDL Covariance for Reaction MT 102 at Infinite Dilution

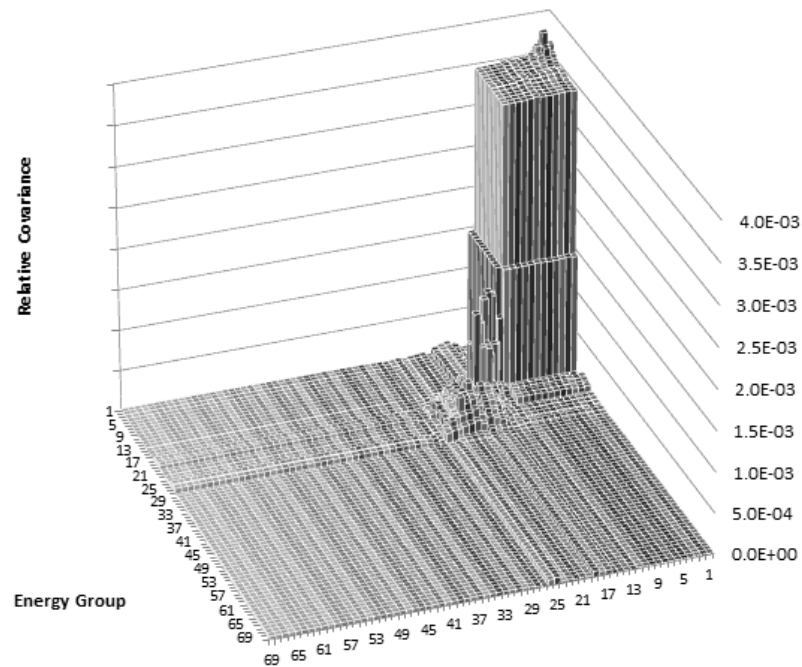


Figure C.6 – 69 Group TENDL Covariance for Reaction MT 102 at a Dilution of 52 Barns

Appendix D – Dilution Dependence of U235 TENDL Covariance in 69 Groups

*All plots in this section are given as absolute values of the relative covariance.

MT 2

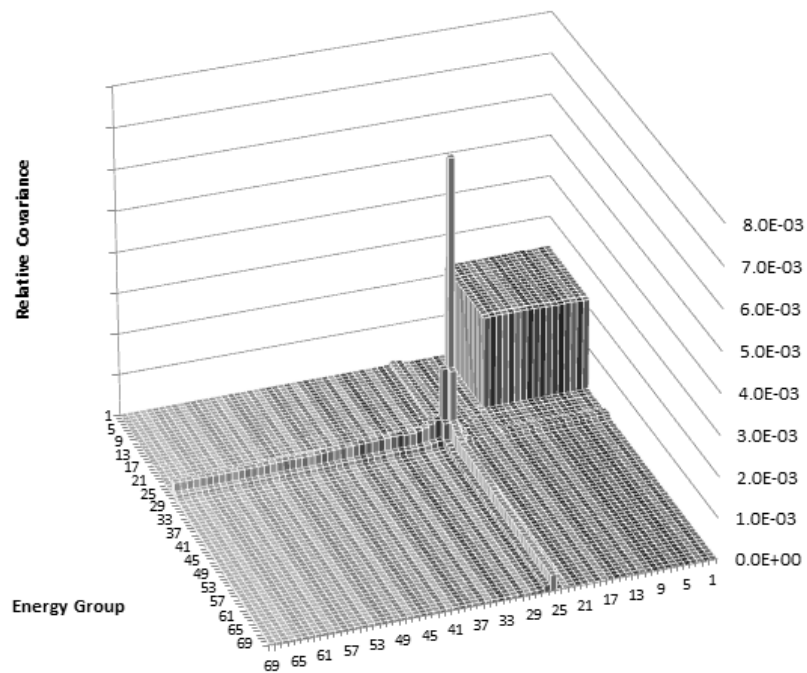


Figure D.1 – 69 Group TENDL Covariance for Reaction MT 2 at Infinite Dilution

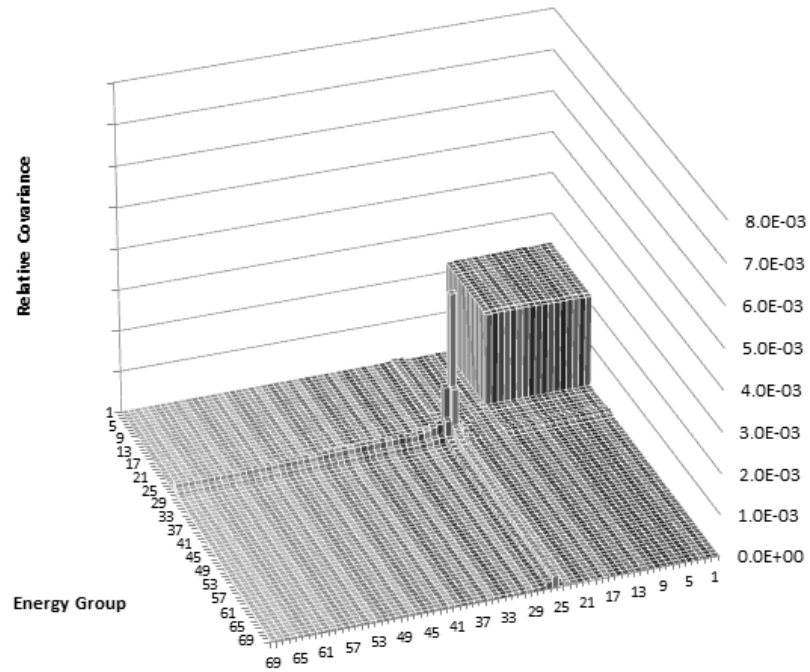


Figure D.2 – 69 Group TENDL Covariance for Reaction MT 2 at a Dilution of 800 Barns

MT 18

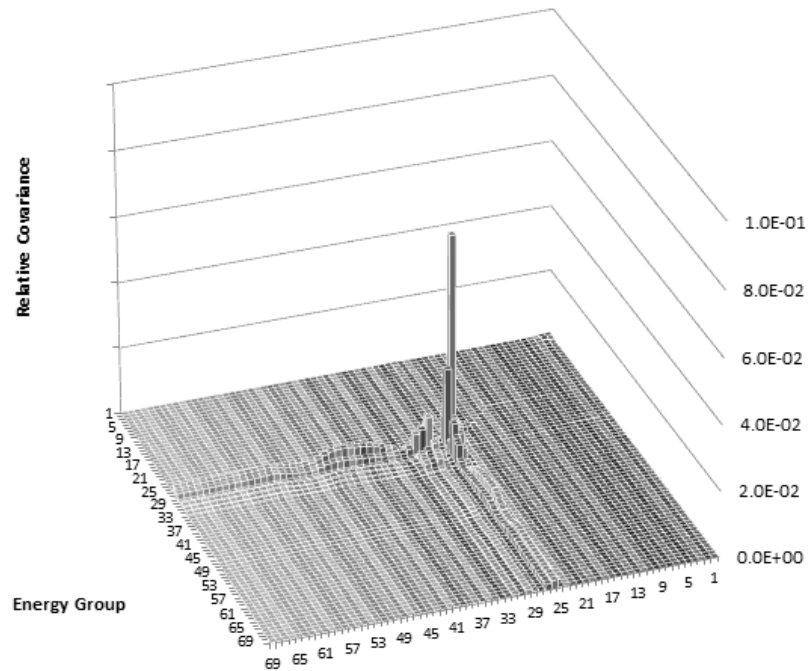


Figure D.3 – 69 Group TENDL Covariance for Reaction MT 18 at a Dilution of 800 Barns

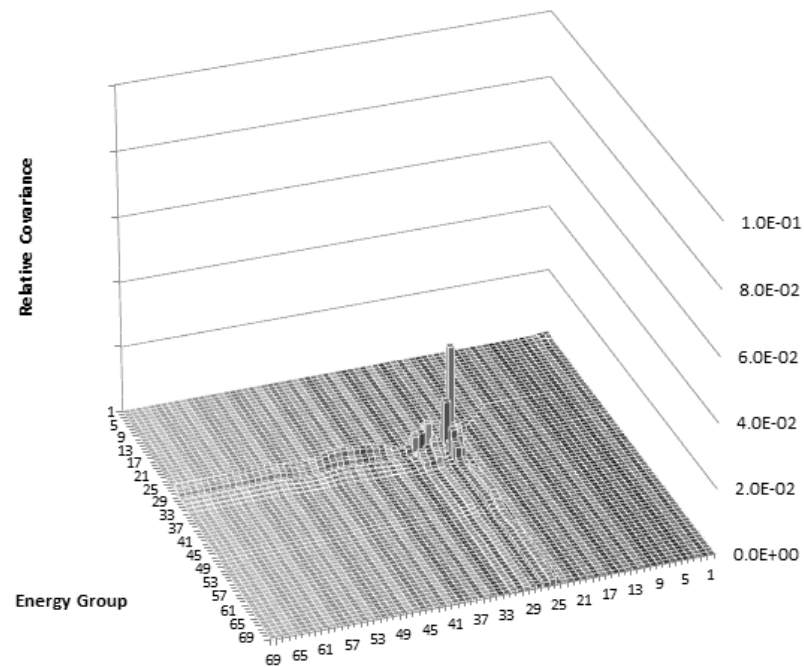


Figure D.4 – 69 Group TENDL Covariance for Reaction MT 18 at a Dilution of 800 Barns

MT 102

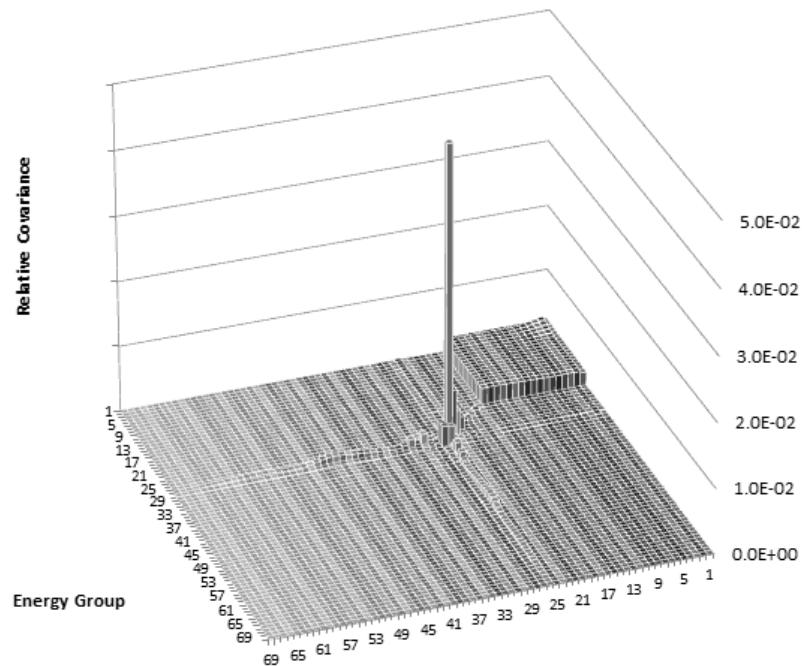


Figure D.5 – 69 Group TENDL Covariance for Reaction MT 102 at Infinite Dilution

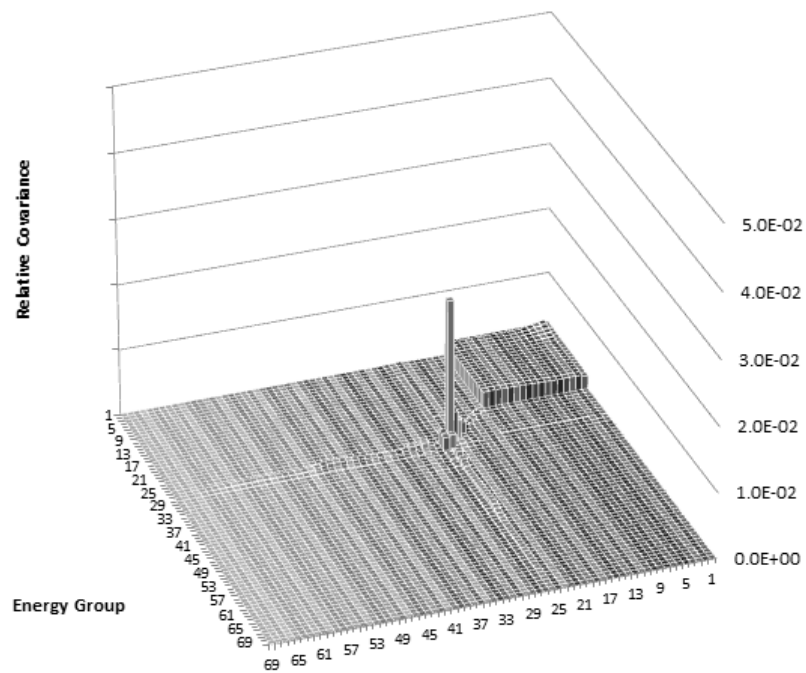


Figure D.6 – 69 Group TENDL Covariance for Reaction MT 102 at a Dilution of 800 Barns

Appendix E – Dilution Dependency of 2 Group Homogenized Cross Section Covariance

The plots in this section are identical to those in Figure 4.6 - Figure 4.9 with the exception that they have been colour coded to show which bars represent a negative covariance. In the figures that follow, bars highlighted in red are negative while the rest of the bars are positive.

109

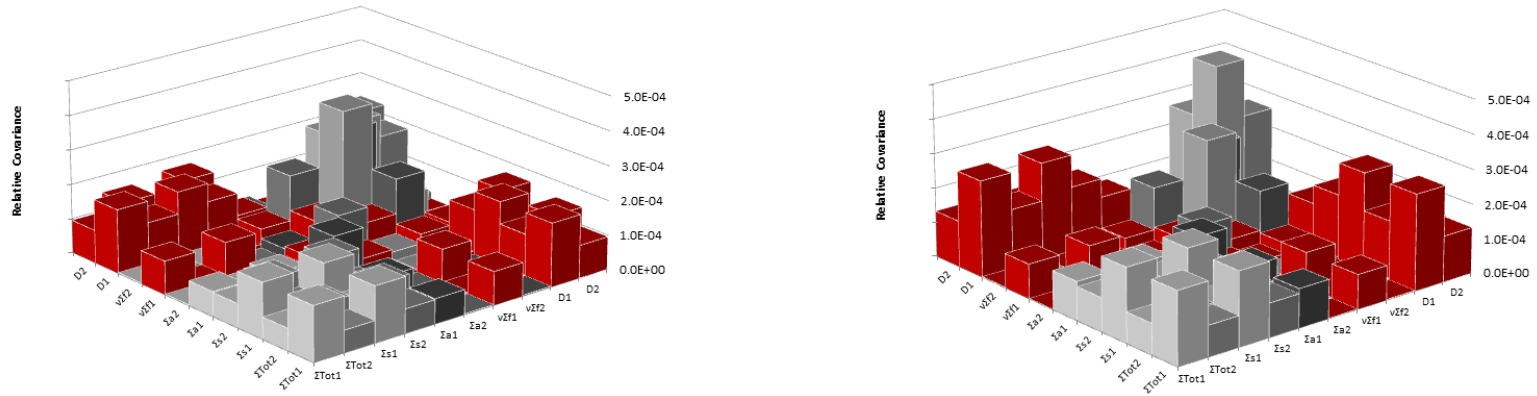


Figure E.3 - Homogenous 2 Group Covariance from Perturbation of the IAEA Library Using Infinite (left) and Finite (right) Dilution Covariance with Positive Covariances in Grey and Negative Covariances in Red

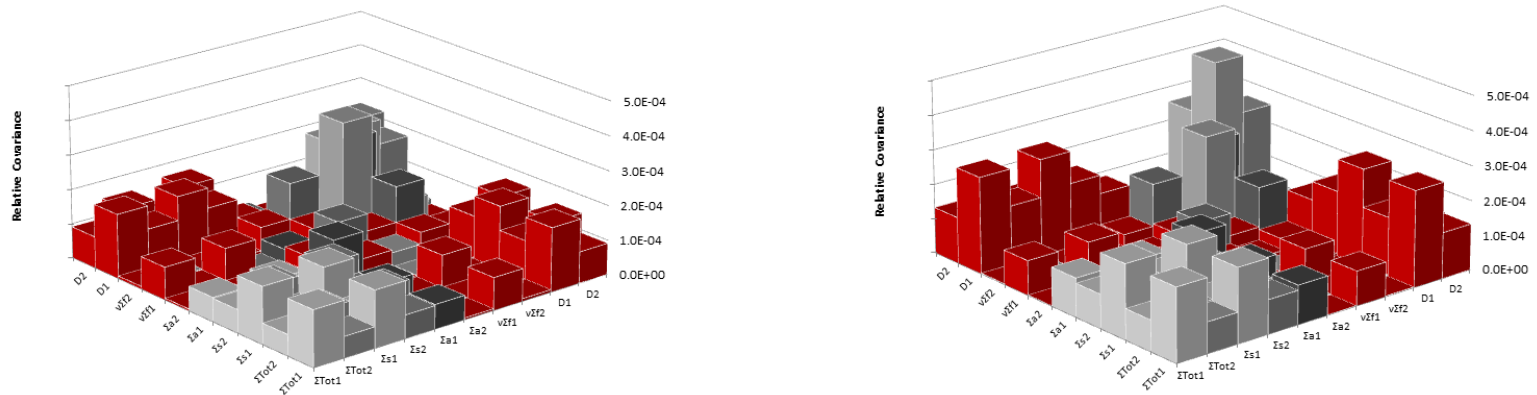
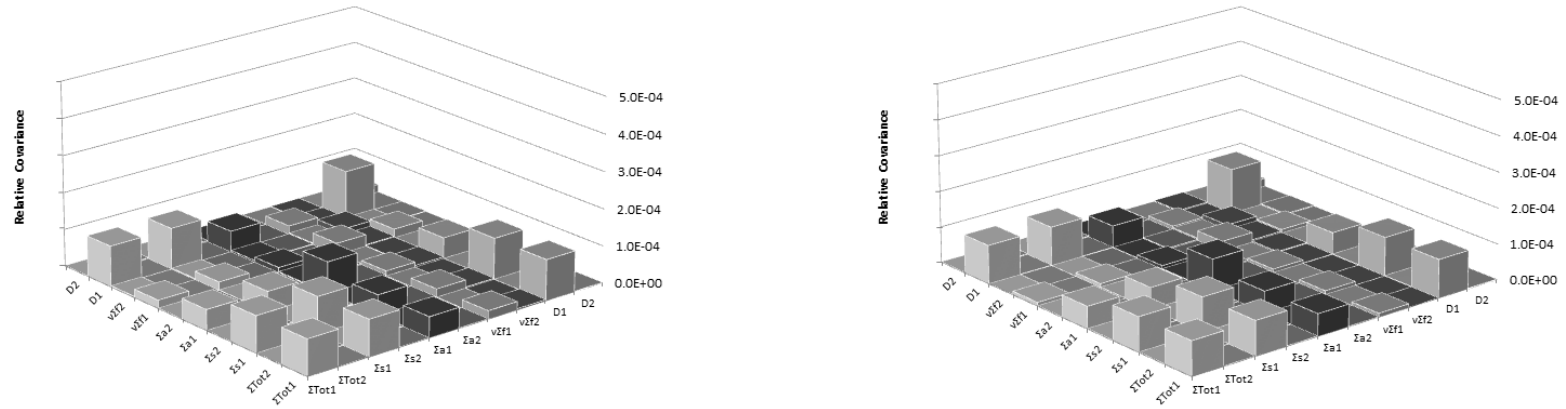


Figure E.4 - Homogenous 2 Group Covariance from Perturbation of the JEF22 Library Using Infinite (left) and Finite (right) Dilution Covariance with Positive Covariances in Grey and Negative Covariances in Red

Appendix F – Effect of Flux Solution Method on Homogenized 2 Group Cross Section Covariance

Given in this section are a set of 2 group homogenized cross section covariance plots which were calculated using a fixed buckling with k -infinite as the eigenvalue (type K) and using a fixed k -effective with the buckling as the eigenvalue (type B with a type B1 leakage model) to show the effect on the resulting uncertainty. The input files for each of these cases can be found in Appendix G. All of the perturbations were performed using the same set of SCALE covariances as well as the same fuel geometry and composition, thus the only difference is how the neutron transport equation was solved for the flux. The figures that follow are arranged vertically by perturbed library (ENDF/B-VI, ENDF/B-VII, IAEA, and JEFF 2.2) showing the results for a type B1 flux solution on the left and type K on the right. Almost no discernable difference was observed due to the flux solution method chosen and thus it is concluded that while the results in this work were obtained using a type B1 calculation, using a type K calculation would result in a very similar if not identical set of results.



Figurea F.1 – 2 Group Homogenized Cross Section Covariance Obtained by Perturbing the ENDF/B-VI Multigroup Library Using a Fixed K-Effective (left) and Fixed Buckling (right) Flux Solution

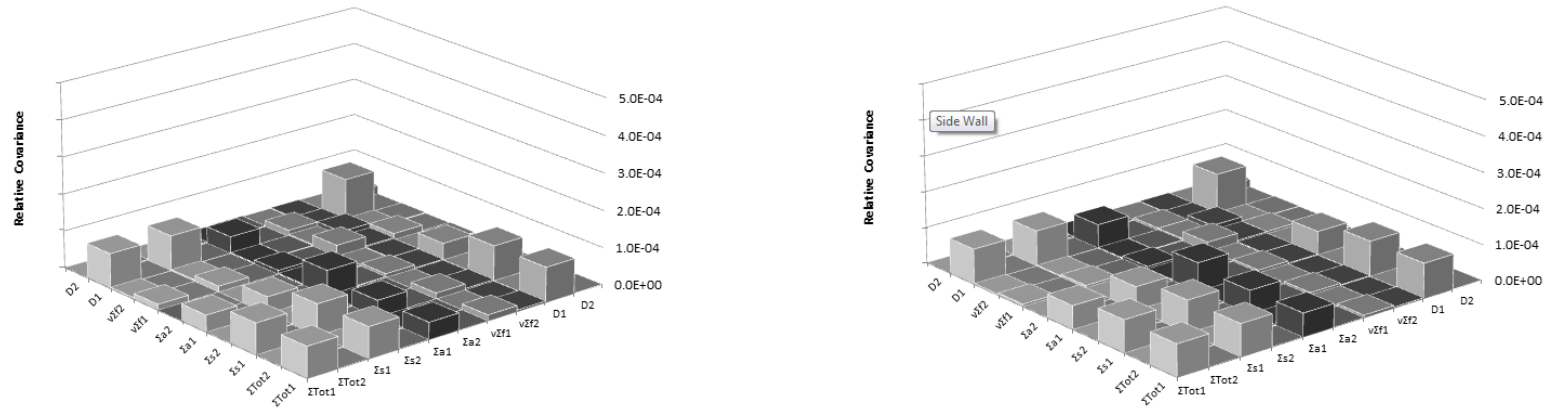


Figure F.2 - 2 Group Homogenized Cross Section Covariance Obtained by Perturbing the ENDF/B-VII Multigroup Library Using a Fixed K-Effective (left) and Fixed Buckling (right) Flux Solution

113

Appendix G – NJOY and DRAGON

Input Files

U235 NJOY Input File

*Input file is modified from the U-235 input file available on the WIMS Library Project Update (WLUP) website:

http://www-nds.iaea.org/wimsd/inputs/wlup69/u_235g.nji

The potential scattering cross section was changed depending on the value given in the evaluated nuclear library which was being processed. It has been underlined in the input file.

```
-- U_235g Process U-235 (run WIMSR with FP yields)
moder  /  Convert data to binary on Unit-21
1 -21
'TALYS U-235' /
20 9228
0 /
reconr / Reconstruct x-sect from resonance parameters on Unit-22
-21 -22
'PENDF TAPE FOR U-235 FROM TALYS  '/
9228 2 /
0.001 0. 0.005/ Reconstruction 0.1% (0.5% max)
'92-U-235 FROM TALYS  '/
' PROCESSED BY NJOY-99  '/
0 /
broadr / Doppler broaden to Unit-23
-21 -22 -23
9228 4 0 0 0 /
0.001 /
293. 600. 900. 1100.
0 /
purr / Doppler broaden /self-shield URP data to Unit-24
-21 -23 -24
9228 4 10 20 100 0 0 /
293. 600. 900. 1100.
1.E10 3.E4 8000. 4500. 2800. 1800. 1200. 800. 500. 200. /
0 /
thermr / Add thermal scattering data to Unit-26
0 -24 -26
0 9228 12 4 1 0 1 221 1
293. 600. 900. 1100.
0.001 4.0
```

```

groupnr / Generate group averaged data on Unit-25
-21 -26 0 -25
9228 9 0 -1 1 4 10 1
'92-U-235 FROM TALYS '/
293. 600. 900. 1100.
1.E10 3.E4 8000. 4500. 2800. 1800. 1200. 800. 500. 200. /
447.13 12.4437 20000 / Homog.Flux Calc.Param
      0.0000E+0 0.0000E+00 0 0 1 89
      89 5
      1.0000E-5 5.250E-04 9.0000E-3 3.550E-01 1.6000E-2 5.520E-01
      2.4000E-2 7.120E-01 2.9000E-2 7.850E-01 3.3000E-2 8.290E-01
      4.3000E-2 8.980E-01 5.0000E-2 9.180E-01 5.4000E-2 9.210E-01
      5.9000E-2 9.180E-01 7.0000E-2 8.920E-01 9.0000E-2 7.990E-01
      1.1200E-1 6.860E-01 1.4000E-1 5.200E-01 1.7000E-1 3.830E-01
      2.1000E-1 2.520E-01 3.0000E-1 1.080E-01 4.0000E-1 6.870E-02
      4.9000E-1 5.100E-02 5.7000E-1 4.370E-02 6.0000E-1 4.130E-02
      1.0000E+0 2.491E-02 4.0000E+0 6.786E-03 9.1180E+3 2.977E-06
      2.0000E+4 1.413E-06 3.0700E+4 9.884E-07 6.0700E+4 5.814E-07
      1.2000E+5 3.677E-07 2.0100E+5 2.770E-07 2.8300E+5 2.432E-07
      3.5600E+5 2.344E-07 3.7700E+5 2.160E-07 3.9900E+5 1.738E-07
      4.4200E+5 6.395E-08 4.7400E+5 1.381E-07 5.0200E+5 1.672E-07
      5.4000E+5 1.936E-07 6.5000E+5 1.872E-07 7.7000E+5 1.587E-07
      9.0000E+5 1.363E-07 9.4100E+5 1.134E-07 1.0000E+6 7.268E-08
      1.0500E+6 9.139E-08 1.1200E+6 1.083E-07 1.1900E+6 1.228E-07
      1.2100E+6 1.192E-07 1.3100E+6 5.451E-08 1.4000E+6 9.666E-08
      2.2200E+6 4.684E-08 2.3500E+6 5.814E-08 2.6300E+6 3.807E-08
      3.0000E+6 2.965E-08 4.0000E+6 1.626E-08 5.0000E+6 8.634E-09
      6.0000E+6 4.490E-09 8.0000E+6 1.169E-09 1.0000E+7 2.947E-10
      1.2570E+7 2.304E-11 1.2600E+7 2.236E-11 1.2700E+7 2.024E-11
      1.2800E+7 1.832E-11 1.2900E+7 1.658E-11 1.3000E+7 1.501E-11
      1.3100E+7 1.358E-11 1.3200E+7 1.229E-11 1.3300E+7 1.112E-11
      1.3400E+7 1.006E-11 1.3500E+7 9.108E-12 1.3600E+7 8.242E-12
      1.3700E+7 7.458E-12 1.3800E+7 6.748E-12 1.3900E+7 6.106E-12
      1.4070E+7 5.151E-12 1.4200E+7 4.522E-12 1.4300E+7 4.091E-12
      1.4400E+7 3.702E-12 1.4500E+7 3.349E-12 1.4600E+7 3.030E-12
      1.4700E+7 2.741E-12 1.4800E+7 2.479E-12 1.4900E+7 2.243E-12
      1.5000E+7 2.029E-12 1.5100E+7 1.835E-12 1.5200E+7 1.660E-12
      1.5300E+7 1.501E-12 1.5400E+7 1.358E-12 1.5500E+7 1.228E-12
      1.5676E+7 1.029E-12 2.0000E+7 1.317E-14 /
3 / Temperature 293.K
3 221 /
3 252 /
3 452 /
3 455 /
5 455 /
6 /
6 221 /
0 /
3 / Temperature 600.K
3 221 /
3 252 /
3 452 /
3 455 /
5 455 /
6 /
6 221 /
0 /

```

```

3 /          Temperature 900.K
3 221 /
3 252 /
3 452 /
3 455 /
5 455 /
6 /
6 221 /
0 /
3 /          Temperature 1100.K
3 221 /
3 252 /
3 452 /
3 455 /
5 455 /
6 /
6 221 /
0 /
0 /
wimsr / Process U-235 data for WIMS
-25 27
2 4 9
69 14 13 10
9228 0 2235.0 1
0 0 800. 4 12.4437 221 0 1 0 0 0 27 / F2, J1, x-sect at
Sig0=800.
    78 1.9551E-11
    236 1.0000E+00
    0 3.1210E-17
4083 5.3558E-03
4095 6.5398E-02
4099 6.1426E-02
4101 5.1716E-02
5103 3.0351E-02
4106 4.0432E-03
4103 1.5506E-09
4105 9.7556E-03
5105 0.0000E+00
4107 1.4932E-03
4108 5.5612E-04
4109 3.2178E-04
4113 1.4335E-04
4115 1.2384E-04
4125 3.4699E-04
5127 2.8043E-04
4127 1.3220E-03
6135 6.2900E-02
4131 2.8973E-02
5134 7.8448E-02
4135 2.5761E-03
4136 6.0911E-02
4133 6.6967E-02
4134 7.6560E-08
5135 4.9265E-06
4137 6.3429E-02
4143 5.9626E-02
4145 3.9396E-02

```

```

4147 1.0549E-02
5147 1.1896E-02
5148 4.6130E-11
4148 8.6204E-11
5149 1.0816E-02
6147 0.0000E+00
6148 0.0000E+00
4149 0.0000E+00
4150 2.9912E-07
4151 4.1863E-03
4152 2.6699E-03
5151 0.0000E+00
5152 1.7894E-12
4153 1.5845E-03
4154 1.9134E-09
4155 3.2283E-04
2154 1.1041E-13
2155 2.9104E-11
2156 1.4961E-04
2157 6.2396E-05
2158 3.3495E-05
 160 2.8055E-10
 161 9.0263E-07
 162 1.6701E-07
 163 6.1723E-08
 164 1.9597E-08
 165 9.7865E-09
2166 4.0071E-10
2167 1.0779E-14
4902 1.0693E+00
 234 0.0000E+00
 927 0.0000E+00
4927 0.0000E+00
8238 0.0000E+00
 937 0.0000E+00
1939 0.0000E+00
 948 0.0000E+00
6239 0.0000E+00
1240 0.0000E+00
1241 0.0000E+00
1242 0.0000E+00
 951 0.0000E+00
 952 0.0000E+00
1952 0.0000E+00
 953 0.0000E+00
 962 0.0000E+00
 963 0.0000E+00
 964 0.0000E+00
.2 .2 .2 .2 .2 .2 .2 .2 .2 .2 .2 .2 .2 / Choose fixed
1.18 2.763 4.922 3.964 2.517 2.121 1.199 .964 .7172 .5436
.4331 .3631 .3168 .2871 .2677 .231 .2214 .2143 .2105 .4124
.4056 .3008 .2002 .2432 .2416 .2094 .3891 / British current
wimsr / Process U-235 data for with the spectrum
-25 28
2 4 9
69 14 13 10
9228 0 2235.0 -1

```

```
0 0 800. 4 12.4437 221 0 1 0 1 0 27 / Print fission spectrum
.2 .2 .2 .2 .2 .2 .2 .2 .2 .2 .2 .2 / Choose fixed
1.18 2.763 4.922 3.964 2.517 2.121 1.199 .964 .7172 .5436
.4331 .3631 .3168 .2871 .2677 .231 .2214 .2143 .2105 .4124
.4056 .3008 .2002 .2432 .2416 .2094 .3891 / British current
stop
```

U238 NJOY Input File

*Input file is modified from the U-238 input file available on the WIMS Library Project Update (WLUP) website:

http://www-nds.iaea.org/wimsd/inputs/wlup69/u_238g.nji

The potential scattering cross section was changed depending on the value given in the evaluated nuclear library which was being processed. It has been underlined in the input file.

```
-- U_238g Process U-238 (run WIMSR with FP yields)
moder / Convert data to binary to Unit-21
1 -21
'CENDL-2 U-238' /
20 2922
0 /
reconr / Reconstruct x-sect from resonance parameters to Unit-22
-21 -22
'PENDF TAPE FOR U-238 FROM CENDL-2' /
2922 2 /
0.001 0. 0.005/ Reconstruction 0.1% (0.5% max)
'92-U-238 FROM CENDL-2' /
' PROCESSED BY NJOY-99' /
0 /
broadr / Doppler broaden to Unit-23
-21 -22 -23
2922 4 0 0 0. /
0.001 /
293. 600. 900. 1100.
0 /
purr / Doppler broaden & self-shield URP data to Unit-24
-21 -23 -24
2922 4 10 20 100 0 0 /
293. 600. 900. 1100.
1.E10 2.E4 3600. 1000. 260. 140. 64. 52. 28. 10. /
0 /
thermr / Add thermal scattering data to Unit-26
0 -24 -26
0 2922 12 4 1 0 1 221 1
293. 600. 900. 1100.
0.001 4.0
groupr / Generate group averaged data on Unit-25
-21 -26 0 -25
2922 9 0 -1 1 4 10 1
'92-U-238 FROM CENDL-2' /
293. 600. 900. 1100.
1.E10 2.E4 3600. 1000. 260. 140. 64. 52. 28. 10. /
1785.0 11.8237 30000 / Homogeneous
0.0000E+0 0.000E+00 0 0 1 89
89 5
```

1.0000E-5	5.250E-04	9.0000E-3	3.550E-01	1.6000E-2	5.520E-01
2.4000E-2	7.120E-01	2.9000E-2	7.850E-01	3.3000E-2	8.290E-01
4.3000E-2	8.980E-01	5.0000E-2	9.180E-01	5.4000E-2	9.210E-01
5.9000E-2	9.180E-01	7.0000E-2	8.920E-01	9.0000E-2	7.990E-01
1.1200E-1	6.860E-01	1.4000E-1	5.200E-01	1.7000E-1	3.830E-01
2.1000E-1	2.520E-01	3.0000E-1	1.080E-01	4.0000E-1	6.870E-02
4.9000E-1	5.100E-02	5.7000E-1	4.370E-02	6.0000E-1	4.130E-02
1.0000E+0	2.491E-02	4.0000E+0	6.786E-03	9.1180E+3	2.977E-06
2.0000E+4	1.413E-06	3.0700E+4	9.884E-07	6.0700E+4	5.814E-07
1.2000E+5	3.677E-07	2.0100E+5	2.770E-07	2.8300E+5	2.432E-07
3.5600E+5	2.344E-07	3.7700E+5	2.160E-07	3.9900E+5	1.738E-07
4.4200E+5	6.395E-08	4.7400E+5	1.381E-07	5.0200E+5	1.672E-07
5.4000E+5	1.936E-07	6.5000E+5	1.872E-07	7.7000E+5	1.587E-07
9.0000E+5	1.363E-07	9.4100E+5	1.134E-07	1.0000E+6	7.268E-08
1.0500E+6	9.139E-08	1.1200E+6	1.083E-07	1.1900E+6	1.228E-07
1.2100E+6	1.192E-07	1.3100E+6	5.451E-08	1.4000E+6	9.666E-08
2.2200E+6	4.684E-08	2.3500E+6	5.814E-08	2.6300E+6	3.807E-08
3.0000E+6	2.965E-08	4.0000E+6	1.626E-08	5.0000E+6	8.634E-09
6.0000E+6	4.490E-09	8.0000E+6	1.169E-09	1.0000E+7	2.947E-10
1.2570E+7	2.304E-11	1.2600E+7	2.236E-11	1.2700E+7	2.024E-11
1.2800E+7	1.832E-11	1.2900E+7	1.658E-11	1.3000E+7	1.501E-11
1.3100E+7	1.358E-11	1.3200E+7	1.229E-11	1.3300E+7	1.112E-11
1.3400E+7	1.006E-11	1.3500E+7	9.108E-12	1.3600E+7	8.242E-12
1.3700E+7	7.458E-12	1.3800E+7	6.748E-12	1.3900E+7	6.106E-12
1.4070E+7	5.151E-12	1.4200E+7	4.522E-12	1.4300E+7	4.091E-12
1.4400E+7	3.702E-12	1.4500E+7	3.349E-12	1.4600E+7	3.030E-12
1.4700E+7	2.741E-12	1.4800E+7	2.479E-12	1.4900E+7	2.243E-12
1.5000E+7	2.029E-12	1.5100E+7	1.835E-12	1.5200E+7	1.660E-12
1.5300E+7	1.501E-12	1.5400E+7	1.358E-12	1.5500E+7	1.228E-12
1.5676E+7	1.029E-12	2.0000E+7	1.317E-14	/	
3 /	Temperature 293.K				
3 221 /					
3 252 /					
3 452 /					
3 455 /					
6 /					
6 221 /					
0 /					
3 /	Temperature 600.K				
3 221 /					
3 252 /					
3 452 /					
3 455 /					
6 /					
6 221 /					
0 /					
3 /	Temperature 900.K				
3 221 /					
3 252 /					
3 452 /					
3 455 /					
6 /					
6 221 /					
0 /					
3 /	Temperature 1100.K				
3 221 /					
3 252 /					

```

3 452 /
3 455 /
6 /
6 221 /
0 /
0 /
wimsr / Process U-238 data for WIMS
-25 27
2 4 9
69 14 13 10
2922 0 8238.0 1
0 0 28. 4 11.8237 221 0 1 1 0 0 27 / J1, x-sect at Sig0=28 b
    78 2.0471E-11
    1939 1.0000E+00
    0 0.0000E+00
    4083 3.9366E-03
    4095 5.1293E-02
    4099 6.2380E-02
    4101 6.2091E-02
    5103 6.2730E-02
    4106 2.4953E-02
    4103 0.0000E+00
    4105 4.0929E-02
    5105 3.7253E-09
    4107 1.4459E-02
    4108 6.0098E-03
    4109 2.5171E-03
    4113 4.5358E-04
    4115 3.5749E-04
    4125 4.8524E-04
    5127 2.3883E-04
    4127 1.1259E-03
    6135 7.0147E-02
    4131 3.2878E-02
    5134 7.4571E-02
    4135 2.6864E-04
    4136 6.6835E-02
    4133 6.7293E-02
    4134 6.4600E-09
    5135 3.7107E-07
    4137 6.2259E-02
    4143 4.6168E-02
    4145 3.8706E-02
    4147 1.2185E-02
    5147 1.3741E-02
    5148 6.1300E-12
    4148 1.6600E-11
    5149 1.6316E-02
    6147 0.0000E+00
    6148 0.0000E+00
    4149 0.0000E+00
    4150 3.2902E-08
    4151 7.9940E-03
    4152 5.3023E-03
    5151 0.0000E+00
    5152 2.9200E-14
    4153 4.1479E-03

```

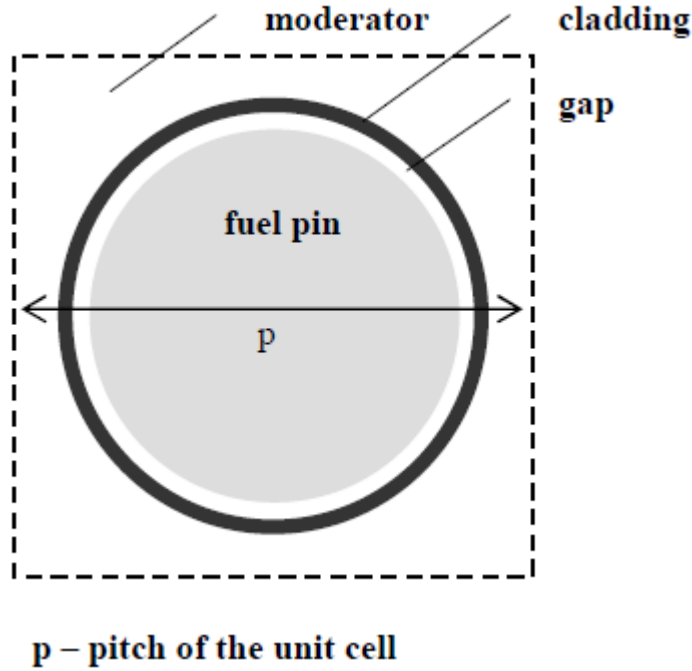


```

4154 8.2500E-11
4155 1.4152E-03
2154 0.0000E+00
2155 0.0000E+00
2156 7.6033E-04
2157 4.1375E-04
2158 1.8487E-04
160 1.8900E-11
161 1.2154E-05
162 3.4052E-06
163 2.0314E-06
164 1.2469E-06
165 7.6671E-07
2166 2.6124E-09
2167 0.0000E+00
4902 9.5590E-01
234 0.0000E+00
2235 0.0000E+00
236 0.0000E+00
927 0.0000E+00
4927 6.0000E-02
937 0.0000E+00
948 0.0000E+00
6239 0.0000E+00
1240 0.0000E+00
1241 0.0000E+00
1242 0.0000E+00
951 0.0000E+00
952 0.0000E+00
1952 0.0000E+00
953 0.0000E+00
962 0.0000E+00
963 0.0000E+00
964 0.0000E+00
.2 .2 .2 .2 .2 .2 .2 .2 .2 .2 .2 .2 .2 /
1.18 2.763 4.922 3.964 2.517 2.121 1.199 .964 .7172 .5436
.4331 .3631 .3168 .2871 .2677 .231 .2214 .2143 .2105 .4124
.4056 .3008 .2002 .2432 .2416 .2094 .3891 / British current
wimsr / Process U-238 data to print fission spectrum
-25 28
2 4 9
69 14 13 10
2922 0 8238.0 -1
0 0 28. 4 11.8237 221 0 1 1 1 0 27 / Print fission spectrum
.2 .2 .2 .2 .2 .2 .2 .2 .2 .2 .2 .2 .2 /
1.18 2.763 4.922 3.964 2.517 2.121 1.199 .964 .7172 .5436
.4331 .3631 .3168 .2871 .2677 .231 .2214 .2143 .2105 .4124
.4056 .3008 .2002 .2432 .2416 .2094 .3891 / British current
stop

```

TMI-1 PWR Pin Cell at Hot Full Power (HFP)



Parameter	Value
Unit cell pitch, mm	14.427
Fuel pellet diameter, mm	9.391
Fuel pellet material	UO ₂
Fuel density (95% TD), g/cm ³	10.283
Fuel enrichment, w/o	4.85
Cladding outside diameter, mm	10.928
Cladding thickness, mm	0.673
Cladding material	Zircaloy-4
Gap material	He
Moderator material	H ₂ O

Figure G.1 – TMI1 PWR Pin Cell Specifications [15]

TMI1 PWR DRAGON Input File (Multiplication Factor Search with Fixed Buckling)

```
*-----
* TEST CASE tmi1PWR HOT FULL POWER
* OECD BENCHMARK: Exercise I-1 (b)
*
*
*-----
* Define STRUCTURES and MODULES used
*-----
LINKED_LIST
  PWRPIN PWRPIN_SHI DISCR1 DISCRSHI LIBRARY CALC CP OUT1
  OUT2 OUT69 OUT172 ;
SEQ_BINARY
  TRKSPC1 TRKSPCSHI PERTLIB ;
SEQ_ASCII
  OUTASCII_1 OUTASCII_2 OUTASCII_69 OUTASCII_172 ;
MODULE
  LIB: GEO: EXCELT: SHI: ASM: FLU: EDI:
  DELETE: END: ;
*-----
* Microscopic cross sections from file iaea [format WIMSD4]
*-----
LIBRARY := LIB: ::
  NMIX 4 CTRA WIMS
  MIXS LIB: WIMSD4 FIL: iaea
  MIX 1 900.0
* //////////////////////////////////////////////////
* These atom densities are taken from SCALE/Geewhiz
* //////////////////////////////////////////////////
  O16_f   = '6016' 4.58889E-02 1
  U234_f   = '234'  1.26128E-06 1
  U235_f   = '2235' 1.12634E-03 1
  U238_f   = '8238' 2.18168E-02 1
* //////////////////////////////////////////////////
* This atom density is taken from SCALE/Geewhiz
* //////////////////////////////////////////////////
  MIX 2 600.0
  He_g     = '4'    2.68714E-05
```

```

MIX 3 600.0 6.55
* //////////////////////////////////////
* These weight percentages are taken from SCALE/Geewhiz
* //////////////////////////////////////
Zr_s   = '91'   98.230
Sn_s   = '118'  1.450
Fe_s   = '2056' 0.210
Cr_s   = '52'   0.100
Hf_s   = '178'  0.010

MIX 4 562.0 0.7480
H_m    = '3001' 1.11111E+1
O16_m  = '6016' 8.88889E+1
;

*----
* Geometry PWRPIN_SHE : Cartesian region geometry for self-shielding
* Reflective Boundary Conditions on every edge
*----

PWRPIN_SHI := GEO: :: CARCEL 4
X- REFL X+ REFL MESHX 0.0 1.4427
Y- REFL Y+ REFL MESHY 0.0 1.4427
RADIUS 0.0 0.46955 0.4791 0.5464 0.7
MIX 1 2 3 4 4
SPLITR 4 1 1 4
SPLITX 3
SPLITY 3
;
PWRPIN := GEO: :: CARCEL 4
X- REFL X+ REFL MESHX 0.0 1.4427
Y- REFL Y+ REFL MESHY 0.0 1.4427
RADIUS 0.0 0.46955 0.4791 0.5464 0.7
MIX 1 2 3 4 4
SPLITR 20 2 4 12
SPLITX 6
SPLITY 6
;

DISCRSHI TRKSPCSHI := EXCELT: PWRPIN_SHI ::
  TITL 'TMI2PWR: BALL BENCHMARK (EXCELT)'
  RENM
  MAXR 100 TRAK TISO 12 20.0 ;

LIBRARY := SHI: LIBRARY DISCRSHI TRKSPCSHI :: ;

```

```
DISCR1 TRKSPC1 := EXCEL: PWRPIN ::  
  TITL 'TMI2PWR: BALL BENCHMARK (EXCEL)'  
  RENM  
  MAXR 550 TRAK TISO 30 60.0 ;  
  
CP := ASM: LIBRARY DISCR1 TRKSPC1 :: ;  
CALC := FLU: CP LIBRARY DISCR1 ::  
  TYPE K ;  
  
OUT1 := EDI: CALC LIBRARY DISCR1 ::  
  EDIT 4 SAVE MERG MIX 1 1 1 1 COND ;  
OUTASCII_1 := OUT1 ;  
  
OUT2 := EDI: CALC LIBRARY DISCR1 ::  
  EDIT 4 SAVE MERG MIX 1 1 1 1 COND 0.625 ;  
OUTASCII_2 := OUT2 ;  
  
OUT172 := EDI: CALC LIBRARY DISCR1 ::  
  EDIT 4 SAVE MERG MIX 1 1 1 1 ;  
OUTASCII_172 := OUT172 ;  
  
TRKSPC1 := DELETE: TRKSPC1 ;  
TRKSPCSHI := DELETE: TRKSPCSHI ;  
END: ;  
QUIT "LIST" .
```

TMI1 PWR DRAGON Input File (Buckling Search Using B_1 Model for Leakage Coefficients)

```
*-----
* TEST CASE tmi1PWR HOT FULL POWER
* OECD BENCHMARK: Exercise I-1 (b)
*
*
*-----
* Define STRUCTURES and MODULES used
*-----
LINKED_LIST
  PWRPIN PWRPIN_SHI DISCR1 DISCRSHI LIBRARY CALC CP OUT1
  OUT2 OUT69 OUT172 ;
SEQ_BINARY
  TRKSPC1 TRKSPCSHI PERTLIB ;
SEQ_ASCII
  OUTASCII_1 OUTASCII_2 OUTASCII_69 OUTASCII_172 ;
MODULE
  LIB: GEO: EXCELT: SHI: ASM: FLU: EDI:
  DELETE: END: ;
*-----
* Microscopic cross sections from file iaea [format WIMSD4]
*-----
LIBRARY := LIB: ::
  NMIX 4 CTRA WIMS
  MIXS LIB: WIMSD4 FIL: iaea
  MIX 1 900.0
* ////////////////////////////////////////////////////
* These atom densities are taken from SCALE/Geewhiz
* ////////////////////////////////////////////////////
  O16_f   = '6016' 4.58889E-02 1
  U234_f   = '234'  1.26128E-06 1
  U235_f   = '2235' 1.12634E-03 1
  U238_f   = '8238' 2.18168E-02 1
* ////////////////////////////////////////////////////
* This atom density is taken from SCALE/Geewhiz
* ////////////////////////////////////////////////////
  MIX 2 600.0
  He_g     = '4'    2.68714E-05
```

```

MIX 3 600.0 6.55
* //////////////////////////////////////
* These weight percentages are taken from SCALE/Geewhiz
* //////////////////////////////////////
Zr_s   = '91'   98.230
Sn_s   = '118'  1.450
Fe_s   = '2056' 0.210
Cr_s   = '52'   0.100
Hf_s   = '178'  0.010

MIX 4 562.0 0.7480
H_m    = '3001' 1.11111E+1
O16_m  = '6016' 8.88889E+1
;

*----
* Geometry PWRPIN_SHE : Cartesian region geometry for self-shielding
* Reflective Boundary Conditions on every edge
*----

PWRPIN_SHI := GEO: :: CARCEL 4
X- REFL X+ REFL MESHX 0.0 1.4427
Y- REFL Y+ REFL MESHY 0.0 1.4427
RADIUS 0.0 0.46955 0.4791 0.5464 0.7
MIX 1 2 3 4 4
SPLITR 4 1 1 4
SPLITX 3
SPLITY 3
;
PWRPIN := GEO: :: CARCEL 4
X- REFL X+ REFL MESHX 0.0 1.4427
Y- REFL Y+ REFL MESHY 0.0 1.4427
RADIUS 0.0 0.46955 0.4791 0.5464 0.7
MIX 1 2 3 4 4
SPLITR 20 2 4 12
SPLITX 6
SPLITY 6
;

DISCRSHI TRKSPCSHI := EXCELT: PWRPIN_SHI ::
  TITL 'TMI2PWR: BALL BENCHMARK (EXCELT)'
  RENM
  MAXR 100 TRAK TISO 12 20.0 ;

LIBRARY := SHI: LIBRARY DISCRSHI TRKSPCSHI :: ;

```

```
DISCR1 TRKSPC1 := EXCEL: PWRPIN ::  
  TITL 'TMI2PWR: BALL BENCHMARK (EXCEL)'  
  RENM  
  MAXR 550 TRAK TISO 30 60.0 ;  
  
CP := ASM: LIBRARY DISCR1 TRKSPC1 :: ;  
CALC := FLU: CP LIBRARY DISCR1 ::  
  TYPE B1 ;  
  
OUT1 := EDI: CALC LIBRARY DISCR1 ::  
  EDIT 4 SAVE MERG MIX 1 1 1 1 COND ;  
OUTASCII_1 := OUT1 ;  
  
OUT2 := EDI: CALC LIBRARY DISCR1 ::  
  EDIT 4 SAVE MERG MIX 1 1 1 1 COND 0.625 ;  
OUTASCII_2 := OUT2 ;  
  
OUT172 := EDI: CALC LIBRARY DISCR1 ::  
  EDIT 4 SAVE MERG MIX 1 1 1 1 ;  
OUTASCII_172 := OUT172 ;  
  
TRKSPC1 := DELETE: TRKSPC1 ;  
TRKSPCSHI := DELETE: TRKSPCSHI ;  
END: ;  
QUIT "LIST" .
```